ALGORITHM THEORETICAL BASIS DOCUMENT

AIRS-TEAM UNIFIED RETRIEVAL FOR CORE PRODUCTS

Level 2

M. T. Chahine

AIRS Team Leader

H. Aumann, M. Goldberg, E. Kalnay, L. McMillin,
P. Rosenkranz, D. Staelin, L. Strow, J. Susskind

AIRS Team Member Contributors

R. Haskins

Editor, AIRS Deputy Team Leader

Version 1.7 18-Sep-97

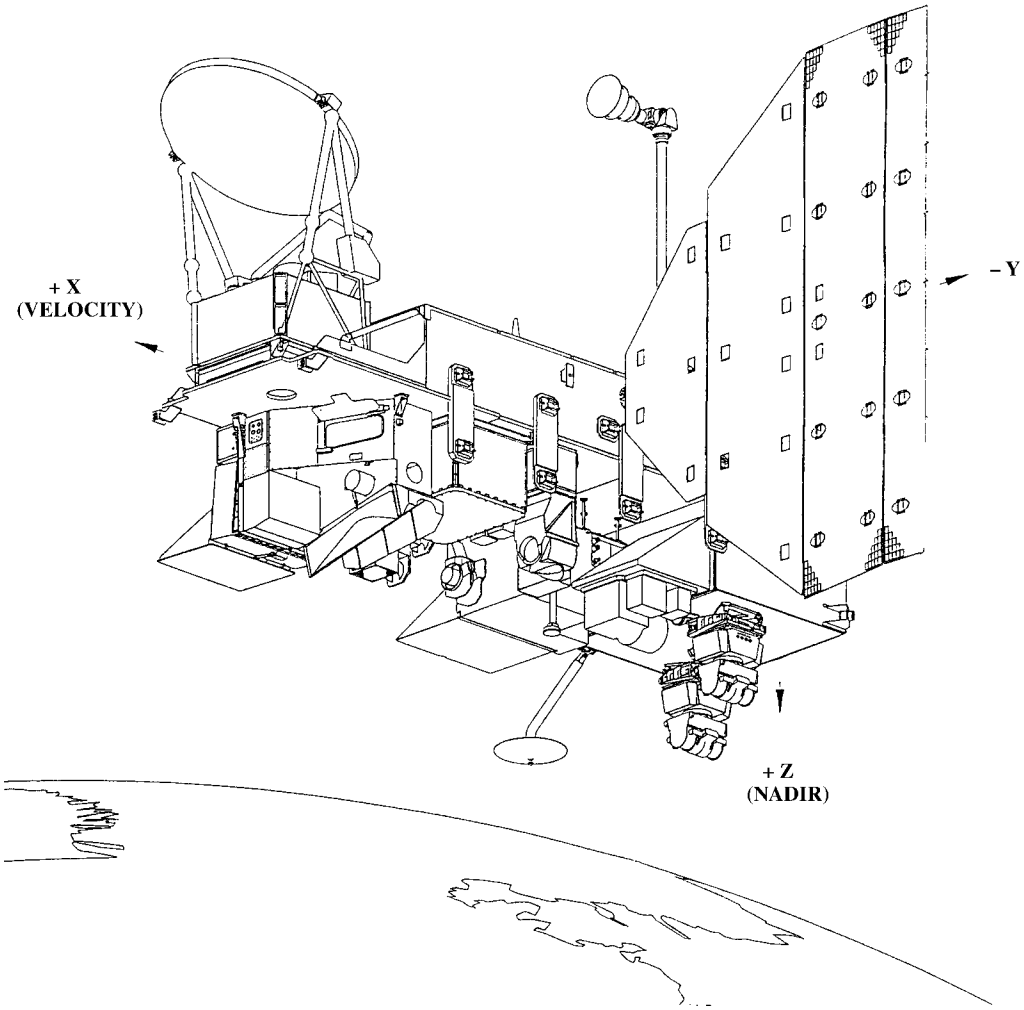

EOS-PM Platform

Table Of Contents

1. INTRODUCTION 1

2. OVERVIEW AND BACKGROUND INFORMATION..... 2

2.1 EXPERIMENTAL OBJECTIVES 2
2.2 HISTORICAL PERSPECTIVE 2
2.3 INSTRUMENT CHARACTERISTICS 3
2.4 MEASUREMENT STRATEGY 4
Infrared Measurements 6
Microwave Measurements 7
Visible and Near-infrared Measurements 9

3 THE FORWARD PROBLEM 10

3.1. RADIATIVE TRANSFER OF THE ATMOSPHERE IN THE MICROWAVE (ROSENKRANZ/STAELIN) 10
Oxygen 10
Water Vapor 11
Liquid Water 12
Rapid Transmittance Algorithm 12
3.2 RADIATIVE TRANSFER OF THE ATMOSPHERE IN THE INFRARED (STROW) 14
Basic Radiative Transfer and the Polychromatic Approximation 15
Spectroscopic Inputs 16
Spectroscopic Line Parameter Errors 16
Molecular Line Shape Effects 18
Line-by-Line Calculations 19
AIRS Atmospheric Layering Grid 20
Regression Profiles 21
FAST TRANSMITTANCE MODEL PARAMETERS 22

4. MATHEMATICAL DESCRIPTION OF THE CORE RETRIEVAL ALGORITHM..... 27

Overview 28
4.1 MICROWAVE INITIAL GUESS ALGORITHM (ROSENKRANZ/STAELIN) 30
Definition of the Initial Profiles 30
Cosmic Background Brightness Temperature 30
Estimation of Surface Brightness 31
Treatment of the Surface Temperature 31
Estimation of the Temperature Profile 32
Estimation of Relative Humidity and Clouds 33
4.2 FIRST PRODUCT -- (GOLDBERG/MCMILLIN) 37
Level 1 Cloud Clearing Algorithm 37
Fundamental Concepts of NOAA Cloud Clearing 37
Obtaining Clear Radiances for Driver Channels 39
Selecting Cloud Clearing Driver Channels 40
Determining Cloud Clearing Relationship 42
AIRS Cloudy Radiance Noise Reduction 43
Cloudy and Clearing Channels under Cloudy Conditions 43
First Guess Regression Procedure 44
Generating the Covariance Matrix and Regression Predictors 44
Generating the Regression Coefficients 45
Applying the Coefficients to Independent Data 46
Minimum Variance Physical Retrieval 46
Expressing the Retrieval Solution in more Computationally Efficient Form 49
Computation of the Kernel matrix 50
The Instrument Noise Covariance Matrix N 52
The Thermal and Moisture Covariance Matrix S 53
4.3 FINAL PRODUCT - (SUSSKIND LEAD, CHAHINE) 53
Introduction 53
Treatment of radiances in cloudy atmospheres 54
Single cloud formation with two fields-of-view 56

Channel selection for cloud filtering *57*
Determination of η *for a single cloud formation* *58*
Multiple Cloud Formations with Multiple Fields-of-view *60*
General Iterative Least Squares Solution *62*
Transformation of Variables *64*
Application of a Constraint *65*
Formulation of the background term *66*
Convergence Criteria *67*
The retrieval noise covariance matrix *68*
Computational noise covariance matrix N^c *70*
Variable and Channel Selection in the Application of Constrained Least Square Solution *71*
Product Error Estimates *80*

5. TUNING AND UNCERTAINTY ESTIMATES 82

5.1 TUNING (MCMILLIN) 82
Approach *82*
Use of coefficients *84*
5.2. SIMULATION SYSTEM (HASKINS, AUMANN) 84
Current Team Algorithm Simulation results (July 96) *87*
Data product Validation *90*

6. NUMERICAL COMPUTATIONAL CONSIDERATIONS (LEE) 91

6.1 PARAMETER DESCRIPTION 91
6.2 DATA STORAGE ESTIMATES 92
6.3 DATA PROCESSING REQUIREMENTS 92
6.4 REQUIRED INPUT DATA 93

7. QUALITY CONTROL, DIAGNOSTICS, AND EXCEPTION HANDLING (KALNAY / MCMILLIN / SUSSKIND / HASKINS /LEE) 95

7.1 PRE-RETRIEVAL QUALITY CONTROL (LEE) 95
Use of EOFs to Characterize Input Radiances (Haskins/McMillin) *96*
7.2 REJECTION CRITERION (SUSSKIND) 96
7.3 NCEP QUALITY CONTROL (KALNAY) 97
The 3-D variational assimilation of radiances and the present TOVS radiances QC *98*
Planned AIRS QC and monitoring *100*
7.4. STATISTICAL ERROR-BAR ASSESSMENT (HASKINS) 101
Use of EOFs to Characterize the Relation of Error to Residual *102*
Metric Verification *103*
7.5. SOFTWARE EXCEPTION HANDLING (LEE) 104

REFERENCES 105

Table Of Figures

FIGURE 2.1 AIRS/AMSU SCHEMATIC FOOTPRINT PATTERN 4
FIGURE 2.2 SCHEMATIC ILLUSTRATION OF A CONTRIBUTION FUNCTION AS A FUNCTION OF ATMOSPHERIC PRESSURE WHERE B IS THE PLANCK FUNCTION, τ IS THE TRANSMISSION TO SPACE, AND P IS THE PRESSURE 5
FIGURE 2.3 SIMULATED AIRS BRIGHTNESS TEMPERATURE SPECTRA FOR CLEAR CONDITIONS 6
FIGURE 3.1.1. ATTENUATION MEASUREMENTS OF TEST AIR AT 279K AND 7 PRESSURES, COMPARED WITH THE MPM 92 MODEL (FROM LIEBE *ET AL*, 1992). 11
FIGURE 3.1.2. BRIGHTNESS TEMPERATURE ERRORS (RAPID ALGORITHM MINUS LINE-BY-LINE ALGORITHM) FOR AMSU-A CHANNELS (1-15) AND AMSU-B CHANNELS (16-20). VERTICAL LINES INDICATE ± 1 STANDARD DEVIATION 14
FIG 3.2.1: TOP: A MEAN AIRS SPECTRUM IN A PORTION OF THE 15 μm CO_2 BAND. BOTTOM: THE MEAN BRIGHTNESS TEMPERATURE ERRORS DUE TO A +5% ERROR IN CO_2 LINE STRENGTHS, A +10% ERROR IN CO_2 LINE WIDTHS, AND A +20% ERROR IN THE CO_2 WIDTH TEMPERATURE DEPENDENCE. 17
FIG 3.2.2: TOP: A MEAN AIRS SPECTRUM IN A PORTION OF THE 7 μm H_2O BAND. BOTTOM: THE MEAN BRIGHTNESS TEMPERATURE ERRORS DUE TO A +5% ERROR IN H_2O LINE STRENGTHS, A +10% ERROR IN H_2O LINE WIDTHS, AND A +25% ERROR IN THE FOREIGN BROADENED H_2O CONTINUUM. 18
FIGURE 3.2.3: AIRS PFAAST MODEL PRESSURE LAYER STRUCTURE 21
FIG 3.2.4: RMS FITTING ERRORS OF THE AIRS PFAAST MODEL 24
FIG 3.2.5: HISTOGRAM OF THE AIRS PFAAST MODEL FITTING ERRORS FOR ALL CHANNELS 25
FIG 3.2.6: AIRS PFAAST MODEL RMS ERRORS OVER THE 1761 TIGR PROFILES IN THE 15 μm TEMPERATURE SOUNDING REGION. 25
FIG 3.2.7: AIRS PFAAST MODEL RMS ERRORS OVER THE 1761 TIGR PROFILES IN A REGION SENSING TROPOSPHERIC H_2O, NEAR 7 μm. 26
FIGURE 4.1 SIMPLIFIED ALGORITHM FLOW CHART 29
FIGURE 4.1.1. MICROWAVE INITIAL-GUESS ALGORITHM. 36
FIGURE 4.2.1 CLOUD CLEAR DRIVER CHANNEL SELECTIONS 41
FIGURE 5.2.1: AIRS SIMULATION SYSTEM 84
FIG 5.2.2: SIMULATION TRACKS 86
FIGURE 5.2.3: TRACK B CLOUD FRACTION FIGURE 5.2.4: TRACK B CLOUD LIQUID WATER 86
FIGURE 5.2.5A: TEAM ALGORITHM RETRIEVAL ERROR FOR ATMOSPHERIC TEMPERATURE) 88
FIGURE 5.2.5B: TEAM ALGORITHM RETRIEVAL ERROR FOR ATMOSPHERIC WATER VAPOR) 89
FIG 7.3.1: EVOLUTION OF THE 5-DAY FORECAST SKILL (ANOMALY CORRELATION) FOR THE NOAA/NCEP OPERATIONAL FORECASTS FOR THE JUNE-AUGUST SEASON FOR THE LAST DECADE USING TOVS RETRIEVALS (MRF). FOR THE YEAR 1995 AN EXPERIMENTAL SYSTEM IN WHICH THE RADIANCES WERE DIRECTLY ASSIMILATED IS ALSO SHOWN (RAD) TOP: NH; BOTTOM:SH. 99
FIGURE 7.4.1: RESIDUAL TO ERROR MAPPING 102

Table Of Tables

TABLE 2.1 CONTRIBUTION FUNCTION HALF WIDTH AS A FUNCTION OF SPECTRAL RESOLUTION 5
TABLE 2.2 AIRS 17 DETECTOR ARRAY CUTOFF WAVELENGTHS (AS MEASURED IN A VACUUM) 7
TABLE 2.3 AMSU-A CHANNEL SET (3.3 DEGREE BEAM DIAMETER) 8
TABLE 2.4 HSB (AMSU-B) CHANNEL SET (1.1 DEGREE BEAM DIAMETER) 8
TABLE 2.5 VISIBLE CHANNEL SET 9
TABLE 4.2.1 SELECTED AIRS CLOUD CLEARING DRIVER CHANNELS 42
TABLE 4.3.1. VARIABLES AND CHANNELS 55
TABLE 4.3.2. TRAPEZOID OR LAYER ENDPOINTS 74
TABLE 5.2.1: SUMMARY STATISTICS FOR THE AIRS TEAM ALGORITHM 87
TABLE 6.1.1 RETRIEVED PARAMETERS 91
TABLE 6.2.1 DATA STORAGE ESTIMATE 92
TABLE 6.3.1 DATA PROCESSING REQUIREMENT 92
TABLE 6.4.1 STATIC INPUT DATA SETS (LEVEL 2 PROCESSING) 93
TABLE 6.4.2 DYNAMIC INPUT DATA SETS (LEVEL 2 PROCESSING) 94
TABLE 7.1.1 INTERNAL INPUT DATA QUALITY CHECK FAILURE ACTIONS 95
TABLE 7.5.1 EXCEPTION HANDLING ON LEVEL 2 RETRIEVAL FAILURE 104

AIRS Team Member Contributions

Team Member	Role	Section
Aumann	Introduction	2.1, 2.2, 2.3,5.2
Chahine	Cloud Properties	1, 2.4, 4.3
Goldberg	NOAA Operational Algorithm Development Lead	4.2
Kalnay	Model based quality checks, Validation	7.3
McMillin	Tuning, Cloud Clearing	4.2, 5.1, 7.1
Rosenkranz/ Staelin	Microwave Radiative Transfer and Algorithm Development	3.1, 4.1
Strow	IR Radiative Transfer	3.2
Susskind	Final Product Algorithm Development, Lead	4.3, 7.2

1. INTRODUCTION

The Atmospheric Infrared Sounder (AIRS) is a facility instrument selected by NASA to fly on the second Earth Observing System polar orbiting platform, EOS-PM 1. The same platform will also carry the NOAA operational Advanced Microwave Sounding Unit, AMSU-A, and the Microwave Humidity Sounder of Brazil (HSB). AIRS is designed to meet the requirements of the NASA Earth science research programs and the NOAA operational plans.

The AIRS/AMSU system will provide both new and improved measurements of clouds, atmosphere, and land and oceans, with the accuracy, resolution and coverage required by future weather and climate models. Such data will be used to validate climate models, study geophysical processes, and monitor trends. The purpose of this document is to give an overview of the important climate data sets that AIRS/AMSU will produce:

- atmospheric temperature profiles with an average layer accuracy of 1K in 1 km thick layers in the troposphere and 1K in 4 km layers in the stratosphere
- sea surface temperature
- land surface temperature and infrared spectral surface emissivity
- humidity profiles and total precipitable water vapor
- fractional cloud cover, cloud spectral infrared emissivity, and cloud-top pressure and temperature
- total ozone column density and column density in three layers of ozone of the atmosphere

In this document we present the theoretical basis of the AIRS Core Algorithm. Many products are presented in one document because of the basic structure and approach of the Core Algorithm. In order to achieve the basic requirement of temperature profile accuracy of 1K in 1 km thick tropospheric layers, a multi-spectral simultaneous retrieval of the atmospheric thermodynamic state is attempted. Hence the Core Products refer to the basic thermodynamic variables that control the outgoing infrared radiance.

Furthermore, we consider this document as a snapshot of current status of the AIRS software development effort. We fully expect that many refinements will be made to the algorithms and to the simulation data we use to test the algorithms. The refinements will reflect added algorithm robustness and parameter retrieval improvements.

2. OVERVIEW AND BACKGROUND INFORMATION

2.1 Experimental objectives

The Earth's climate is a complex system with many components and feedback processes that operate on different time scales. The slow components involve the deep oceans, and permanent and semi-permanent ice and snow covers. Their response sets the pace for long-term climate trends and may introduce a delay of 50 years or more in the response of the climate system to external forcing. The fast components, whose scales range from hours to multiple seasons, encompass the atmosphere, upper ocean layers, and include the biosphere as well as air-land and air-sea interactions. The fast components are coupled and are controlled by the atmosphere, which drives the whole Earth environment and determines the amplitude and geographical patterns of climate change. The atmosphere controls many feedback processes that involve the interaction of radiation with clouds, water vapor, precipitation and temperature. Thus, a knowledge of the properties of the atmosphere is important not only for understanding processes that occur within the atmosphere itself; but also for understanding the feedback mechanisms among the various components of the entire climate system. Atmospheric and surface measurements from AIRS will provide data about these interactions with unprecedented accuracy.

The ability of AIRS/AMSU to provide simultaneous observations of the Earth's atmospheric temperature, ocean surface temperature, and land surface temperature, as well as humidity, clouds, albedo, and the distribution of greenhouse gases, makes AIRS the primary EOS instrument for investigating several interdisciplinary issues to be addressed in Earth science. Among these issues are:

- Improving numerical weather prediction.
- Demonstrating seasonal to interannual predictions of the effects of El-Nino and other transient climate anomalies.
- Characterizing the optical properties of atmospheric constituents, cloud and aerosols, in order to compute radiation fluxes.
- Monitoring variations and trends in the global energy and water cycles.

2.2 Historical perspective

The basic physics involved in the design of a temperature sounder from earth orbit was published in the late 1950's (Kaplan 1959). Ten years later, and shortly after Chahine (1968) published the relaxation algorithm to invert spectral radiances to obtain temperature profiles, the first experimental temperature soundings from space were achieved using the Satellite Infrared Radiation Spectrometer (SIRS), a seven channel grating spectrometer on NIMBUS-4 with a spectral resolution ($\lambda/\Delta\lambda$) of 100 in the 15 μm CO_2 band (Wark and Hilleary 1969). The presence of clouds in the field-of-view posed a major challenge. Smith (1968) published a monograph on this topic and proposed a numerical technique, the N* parameter, for "cloud-clearing". Clouds become optically thick much quicker in the infrared (15 μm = 0.0015 cm) than at 57 GHz (0.5 cm) microwave sounding frequencies. Staelin *et al.* (1975a) demonstrated the capability to sense atmospheric temperature within and below clouds in the microwave with the Nimbus-E Microwave Sounder (NEMS). Unfortunately, the mid to lower

tropospheric vertical resolution achievable in the microwave is inferior to that achievable in the 4.3 μm CO_2 band (see Table 2.1). A physical basis for "cloud-clearing" infrared radiances was proposed by Chahine (1974). Smith *et al.* (1978) demonstrated the N* technique using the ITPR on the NIMBUS-5 satellite. Aumann and Chahine (1976) and Chahine *et al.* (1977) demonstrated temperature sounding of partly cloudy atmospheres using 4.3 μm CO_2 and 11 μm window channels. A cloud-clearing technique, which combines the use of infrared and microwave data, is now routinely applied in the NOAA operational sounding system as well as at NASA Goddard Space Flight Center (Susskind *et al.* 1984). This method takes advantage of the fact that, to first order, the microwave data are not affected by most types of clouds and makes the assumption that the horizontal inhomogeneity in the scene due to clouds is much larger than the inhomogeneity due to temperature profile changes on a scale of a microwave field-of-view. By 1978 the HIRS-2 sounder (Smith, *et al.*, 1979), a radiometer with 19 channels between 3.7 μm and 15 μm and a spatial resolution of about 75 kilometers, plus the Microwave Sounding Unit, MSU (a follow-up to NEMS), with 4 channels near the 57 GHz oxygen band, became the first of the TIROS Operational Vertical Sounders (TOVS). This system is the current operational NOAA sounding system. The NOAA Polar Orbiting Sounding System will soon be upgraded with the HIRS3, AMSU-A and AMSU-B, to be launched on NOAA-K in 1997.

2.3 Instrument characteristics

AIRS is a continuously operating cross-track scanning sounder, consisting of a telescope that feeds an echelle spectrometer. The spectrometer analyzes thermal infrared radiation between the wavenumbers of 650 cm^{-1} - 2700 cm^{-1}, with an average resolving power of 1200. This spectral region includes the important temperature sounding regions in the 4.2 and 15μm CO_2 bands, water vapor sounding in the 6.3 μm water band and ozone sounding in the 9.6 μm region. AIRS has about 2400 detector elements at the focal plane, arranged in several linear arrays. Each detector has a noise-equivalent difference temperature on the order of 0.2K (at 250K) seen in each 1.1° Instantaneous Field Of View (IFOV) -- see Figure 2.1.

During each scan, the rotating external mirror scans the underlying Earth from 49° on one side of the nadir to 49° on the other side, in 90 integration periods, and provides two views of dark space, one view of an internal radiometric calibration target, and one view of an internal spectral calibration target. Thus each scan produces 94 sets of measurements (90 Earth scenes and 4 calibrations). The scan is repeated every 8/3 seconds. The downlink data rate from the AIRS instrument is 1.2 Mbit/sec.

Proper interpretation of AIRS data requires the use of co-located temperature and humidity data from a passive microwave sounder. Therefore, the Advanced Microwave Sounding Unit (AMSU) instrument will fly as part of the AIRS instrument complement on EOS. This instrument (which will fly on the NOAA-K, -L, -M, and -N weather satellites) is composed of two subsystems, AMSU-A and the Humidity Sounder of Brazil (HSB) (formerly the Microwave Humidity Sounder, MHS).

AMSU-A is a cross-track scanning multispectral microwave radiometer, with a 3.3° IFOV and 15 spectral channels (23 GHz - 90 GHz). Each cross-track scan produces 32 sets of measurements (30 Earth looks, 1 dark space calibration, and 1 internal blackbody radiometric calibration). The scan repeats every 8 seconds, being synchronized with every 3 AIRS scans (via the spacecraft master clock).

HSB is a cross-track scanning multispectral microwave radiometer, with a 1.1° IFOV and 4 spectral channels (150 GHz - 183 GHz). One channel was eliminated from those of AMSU-B by our Brazilian partners as a cost saving measure. Each cross-track scan produces 92 sets of measurements (90 Earth looks, 1 dark space calibration, and 1 blackbody calibration). The scan repeats every 8/3 seconds, being synchronized every third scan line.

The overlap between AIRS and AMSU-A footprints in the cross-track direction is illustrated in Figure 2-1. Note that HSB and AIRS will share approximately the same footprints. The current retrieval system produces one set of core products per AMSU-A footprint.

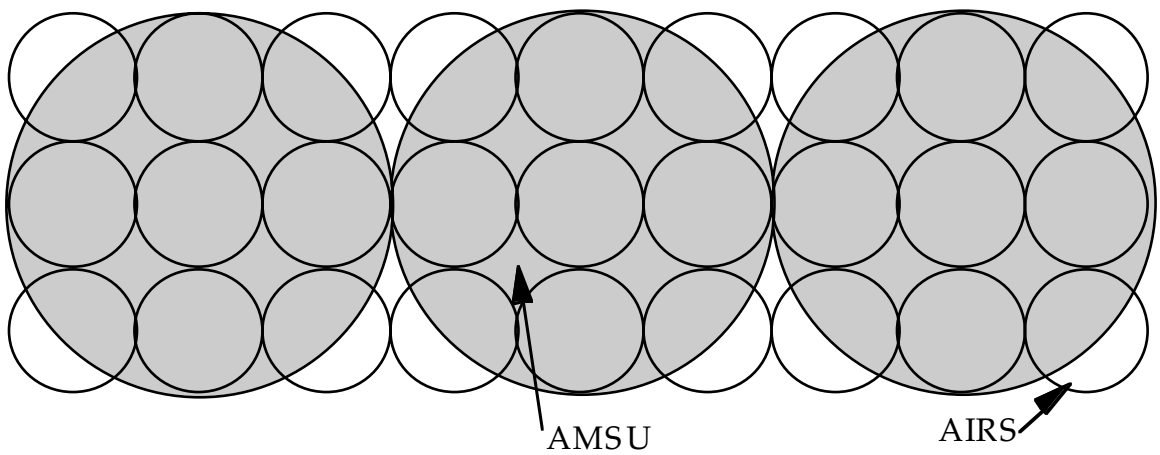

FIGURE 2.1 AIRS/AMSU SCHEMATIC FOOTPRINT PATTERN

2.4 Measurement Strategy

During the past 20 years, considerable progress has been made in passive infrared remote sensing of temperature profiles. Currently, the combination of the High Resolution Infrared Sounder (HIRS) and the Microwave Sounding Unit (MSU) provides atmospheric temperature profiles with an average RMS error of approximately 2.0 K, with a vertical resolution of 3 to 5 km in the troposphere. This accuracy, however, falls short of the requirements for numerical weather prediction models. At present the need for improved sounding is accentuated by the fact that, during the past decade, models have evolved more rapidly than the capabilities of satellite-borne temperature sounders to supply accurate data. The inability of current sounders to match the vertical and horizontal resolution of general circulation models and difficulties in correcting for the effects of clouds are the major deficiencies to be improved upon.

The limitation in vertical resolution is caused mainly by the broadness of the contribution functions (i.e., the weighting function multiplied by the Planck function - see Figure 2.2) of current instruments. When the contribution functions are broad, emitted energy reaching the satellite in each channel will have components originating from a thick layer of the atmosphere, thereby making the discrimination of fine-scale vertical details practically impossible. This problem is compounded by the limited number of HIRS channels. Furthermore, because of the broadness of the contribution functions (see Table 2.1) and difficulties in eliminating cloud contamination effects, as well as surface

emissivity, O_3, H_2O, and other minor constituents, the RMS errors in the retrieved temperature profiles remain high. AIRS takes advantage of the temperature dependence in the high-J lines in the 4.18 μm CO_2 band to sharpen the weighting functions.

	Band	$\lambda/\Delta\lambda$	Half-width in scale heights	Remarks
Stratosphere	14.5 μm	100	2.4	VTPR/HIRS
	15.0 μm	1200	1.6	AIRS
	15.0 μm	10000	1.4	Wings of lines
	60 GHz	1000	1.3	AMSU
Troposphere	15.0 μm	100	1.6	VTPR
	60 GHz	1000	1.5	AMSU
	4.46 μm	100	1.3	HIRS
	4.18 μm	1200	0.69	AIRS
	4.18 μm	10000	0.60	Wings of lines

TABLE 2.1 CONTRIBUTION FUNCTION HALF WIDTH AS A FUNCTION OF SPECTRAL RESOLUTION

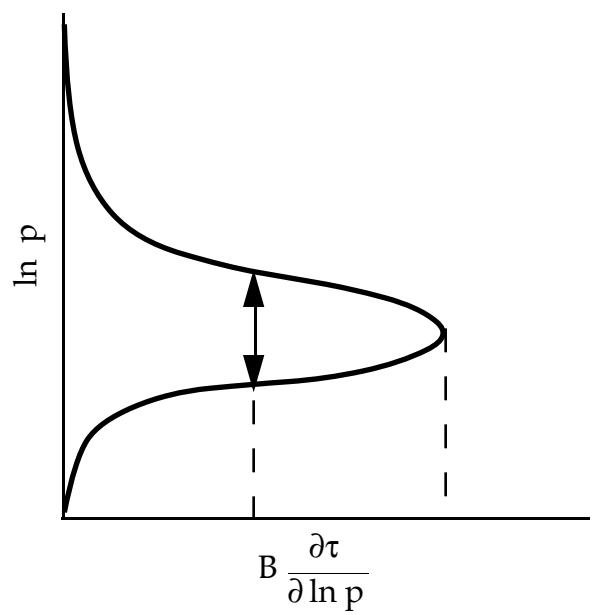

FIGURE 2.2 SCHEMATIC ILLUSTRATION OF A CONTRIBUTION FUNCTION AS A FUNCTION OF ATMOSPHERIC PRESSURE WHERE B IS THE PLANCK FUNCTION, τ IS THE TRANSMISSION TO SPACE, AND P IS THE PRESSURE

Experience with the current generation of sounders has shown that amalgamation of microwave and infrared data is a very useful combination for accurate elimination of most effects of clouds. Microwave observations in the 50 GHz region are not affected by most types of clouds, which allows them to be used as an accurate filter to retrieve a variety of clear-column parameters. Some microwave channels are affected slightly by the surface, especially over land, and are less effective for filtering out low clouds. Visible

channels are needed here as a diagnostic to discriminate between low-level clouds and different types of terrain.

All AIRS/AMSU sounding channels, including the visible channels, must observe the same field-of-view at approximately the same time. This simultaneity requirement will insure that all the channels observe the same clouds and, consequently, the same cloud correction applies to all the frequencies.

Infrared Measurements

High spectral resolution in the infrared is key to achieving high vertical resolution. In the troposphere, the ability of microwave channels to provide high vertical discrimination is inherently weak. High J-lines in the R-branch of the 4.18 μm region, in which the CO_2 absorption coefficient increases rapidly with increasing temperature, provide the highest possible lower tropospheric vertical resolution of any part of the infrared spectrum and this resolution enhancement can be captured only through high spectral resolution measurements. In addition, a sufficiently large number of 15 μm infrared channels are required in the upper troposphere and adjacent lower stratosphere; and this requirement can also be satisfied as a consequence of high spectral resolution. High spectral resolution also permits selection of sounding channels not contaminated by water vapor lines or by emission from other active gases, and provides spectrally clean window-channels for surface measurements. The effect of the surface emission must be separated from the emission of the lower troposphere to provide accurate temperature profiles near the surface.

The infrared channels to be used for retrieving such parameters as temperature and humidity profiles, ocean and land surface temperature, clouds and O_3, must be selected carefully. This is aided by the availability of a number of narrow band-pass channels that are located away from unwanted absorption lines, while taking advantage of the unique spectral properties of several regions such as the high J-lines in the R-branch of the 4.3 μm CO_2 band and very clear window channels near 3.7 μm. A typical AIRS spectra is presented in Figure 2.3 and Table 2.2 presents the precise AIRS array specifications.

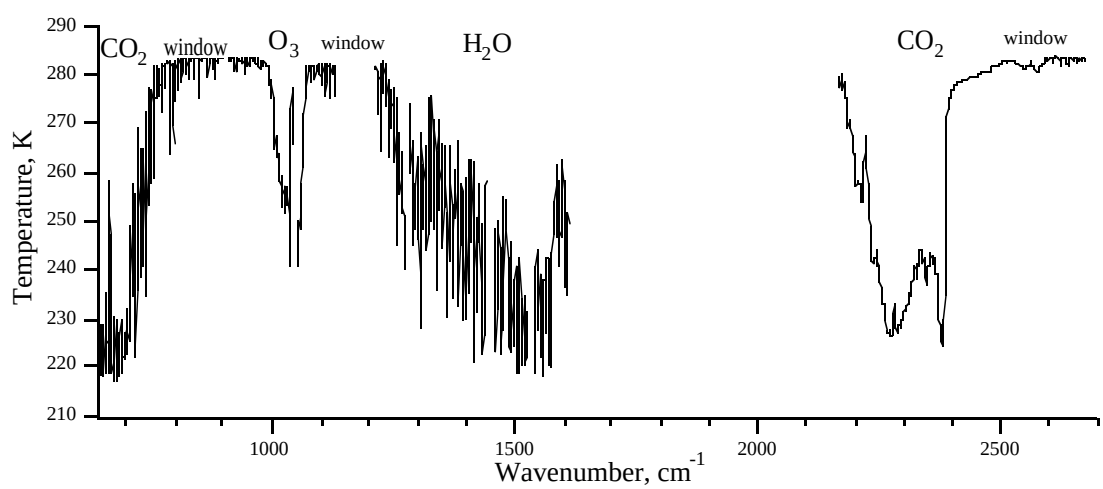

FIGURE 2.3 SIMULATED AIRS BRIGHTNESS TEMPERATURE SPECTRA FOR CLEAR CONDITIONS

Beginning wavelength $\lambda 1$	Ending wavelength $\lambda 2$	Beginning wavenumber μ_1	Beginning wavenumber μ_2
3.736	3.917	2676.37	2553.04
3.915	4.110	2554.34	2433.09
4.110	4.329	2433.09	2309.95
4.327	4.609	2311.02	2169.90
6.200	6.493	1612.83	1540.03
6.550	6.850	1526.62	1459.85
6.936	7.477	1441.84	1337.45
7.475	7.792	1337.88	1283.35
7.861	8.220	1272.18	1216.55
8.807	9.480	1135.42	1054.90
9.565	10.275	1045.48	973.24
10.275	10.985	973.24	910.33
11.070	11.751	903.31	850.98
11.743	12.685	851.56	788.33
12.799	13.746	781.32	727.50
13.738	14.553	727.92	687.13
14.667	15.400	681.79	649.35

TABLE 2.2 AIRS 17 DETECTOR ARRAY CUTOFF WAVELENGTHS (AS MEASURED IN A VACUUM)

Microwave Measurements

AMSU-A consists of 12 channels within the 50-60 GHz portion of the oxygen band to provide temperature and precipitation information. In addition, AMSU-A contains three window-channels at 24, 31 and 89 GHz to provide total precipitable water, cloud liquid water content and precipitation measurements. These channels will also be used to provide information on sea-ice concentration and snow cover. The 3-dB beam diameter of AMSU-A is 3.3°, corresponding to about 50x50 km at nadir. The set of 15 microwave channels is given in Table 2.3.

A second microwave instrument package will also be provided. The Microwave Humidity Sounder of Brazil (HSB), formerly AMSU-B, contains one window-channel at 150 GHz to obtain high resolution measurements of precipitation, snow cover and sea-ice with the same spatial footprint as AIRS. Three additional channels in the 183 GHz water vapor line will be used to improve the accuracy of atmospheric humidity profiles and total precipitable water vapor. The 3-dB beam diameter of HSB is 1.1°, corresponding to about 16 km at nadir. The full set of HSB (AMSU-B) channels and their specifications is given in Table 2.4.

Channel No.	Center Frequency	Bandwidth (MHz)	Function
1	23.800 GHz	270	Water Vapor Burden
2	31.400 GHz	180	Surface Temperature
3	50.30 GHz	180	Surface Temperature
4	52.800 GHz	400	Surface Temperature
5	53.596 ±0.115 GHz	2x170	Tropospheric Temp
6	54.400 GHz	400	Tropospheric Temp
7	54.940 GHz	400	Tropospheric Temp
8	55.500 GHz	330	Tropospheric Temp
9	57,290.344 MHz (= f9)	330	Stratospheric Temp
10	f9 ±217 MHz	2x78	Stratospheric Temp
11	f9 ±322.2±48 MHz	4x36	Stratospheric Temp
12	f9 ±322.2±22 MHz	4x16	Stratospheric Temp
13	f9 ±322.2±10 MHz	4x8	Stratospheric Temp
14	f9 ±322.2±4.5 MHz	4x3	Stratospheric Temp
15	89.0 GHz	6000	Cloud Top/Snow

TABLE 2.3 AMSU-A CHANNEL SET (3.3 DEGREE BEAM DIAMETER)

Channel No.	Center Frequency (GHz)	Bandwidth (GHz)	Function
1*			
2	150.0	4000	Water vapor
3	183.31 ± 1.0	2x500	Water vapor
4	183.31 ± 3.0	2x1000	Water vapor
5	183.31 ± 7.0	2x2000	Water vapor

TABLE 2.4 HSB (AMSU-B) CHANNEL SET (1.1 DEGREE BEAM DIAMETER)
*Channel 1 (89 GHz) has been deleted for the HSB

Visible and Near-infrared Measurements

AIRS will also carry a small set of visible channels as a diagnostic aid in accounting for low-level clouds. In addition, the visible channels are needed to diagnose land surface inhomogeneities for the determination of surface temperature and emissivities and enhance the synergism with the Moderate Resolution Imaging Spectroradiometer (MODIS) on EOS. A set of visible and near-infrared channels between 0.4 and 1.1 μm is presented in Table 2.5. There are 36 spots within one AIRS infrared footprint.

Channel No.	**Frequency Range (μm)**	**IFOV**
1	0.40 - 0.44	1.1°/6
2	0.58 - 0.68	1.1°/6
3	0.71 - 0.98	1.1°/6
4	0.40 - 1.06*	1.1°/6

* warm Si-diode cutoff

TABLE 2.5 VISIBLE CHANNEL SET

3 The Forward Problem

In the following, atmospheric radiative transfer or the 'forward problem' will be discussed. Because the retrieval methodology utilized by the AIRS team depends on the ability to accurately determine the outgoing radiance, particular attention will be paid to errors in the spectroscopy and errors in modeling the outgoing radiation -- the rapid forward model. To overcome these error sources, a process known as tuning is used to remove systematic effects and is described in section 5.1.

3.1. Radiative Transfer of the Atmosphere in the Microwave (Rosenkranz/Staelin)

At the frequencies measured by AMSU-A and HSB, the most important absorbing gases in the atmosphere are oxygen and water vapor. The oxygen molecule has only a magnetic dipole moment, and its lines are intrinsically much weaker than those which result from the electric dipole of water vapor; however, the much greater abundance of oxygen in the atmosphere more than compensates for this difference. When clouds are present, liquid water also plays a role in radiative transfer. However, fair-weather cirrus composed of ice particles small compared to the wavelength are effectively transparent to microwave radiation.

Oxygen

The dipole moment of O_2 is due to two unpaired electron spins and thus it can be expressed in terms of fundamental constants. Hence, the intensities of the O_2 spin-rotation transitions are among the most precisely calculable of any molecule. The values used are from the JPL line catalog (Poynter and Pickett, 1985). These transitions comprise approximately 30 lines between 50 and 70 GHz and an isolated line at 118.75 GHz (which is not observed by AMSU-A or HSB). The pressure-broadened widths of the lines in the 50-70 GHz band have been measured by several groups. The most accurate measurements are probably those of Liebe *et al.*, (1977) and Liebe and Gimmestad (1978), where the errors were estimated to be ≤ 1% for most of the stronger lines.

The characteristic of oxygen's microwave spectrum that introduces difficulty for construction of models is the significant degree of line mixing. In the Millimeter-wave Propagation Model (MPM92) (Liebe, *et al.*, 1992), line mixing was treated by a first-order expansion in pressure, and the coefficients of the expansion were fitted by a constrained linear method to laboratory measurements made on an O_2 - N_2 mixture over the frequency range of 49-67 GHz and the temperature range 279-327 K, with a noise level of approximately 0.06 dB/km. Within that range, the model represents the measurements to ≤ 0.2 dB/km (see for example, Figure 3.1.1). It is possible, however, that extrapolation to colder temperatures introduces larger errors. (Recent measurements from the NASA ER-2 may answer this question.) There is also some indication from aircraft and ground-based atmospheric measurements that model errors in oxygen zenith opacity may reach 10-20% near 30 and 90 GHz. However, the main absorber at those frequencies is water.

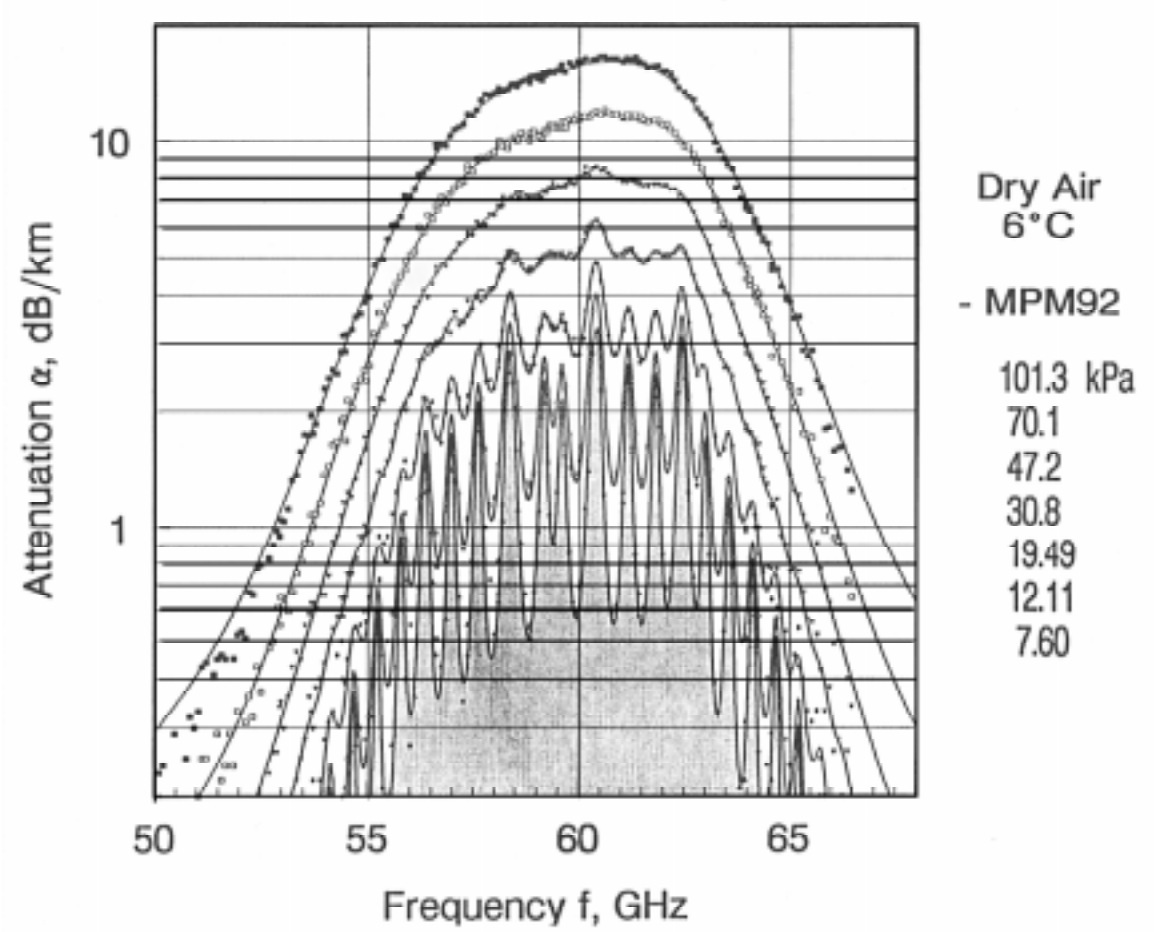

FIGURE 3.1.1. ATTENUATION MEASUREMENTS OF TEST AIR AT 279K AND 7 PRESSURES, COMPARED WITH THE MPM 92 MODEL (FROM LIEBE *ET AL*, 1992).

Water Vapor

Water has a weak rotational line at 22.23 GHz that is semi-transparent at normal atmospheric humidities, and a much stronger, opaque line at 183.31 GHz. Intensities of these lines have been calculated and tabulated by Poynter and Pickett (1985 -- JPL line catalog) and Rothman *et al.*, (1992) (HITRAN), among others. For the 22-GHz line, the JPL intensity, which is used here, is lower than the HITRAN value by 3%. There is also a measurement by Liebe *et al.*, (1969) (estimated error 0.3%) which is 0.5% lower than the JPL value. At 183 GHz, the JPL line intensity is 0.8% lower than HITRAN. Widths have been measured by Liebe *et al.*, (1969) and Liebe and Dillon (1969) at 22 GHz with estimated uncertainty of 1% for both self and foreign-gas broadening; and by Bauer *et al.*, (1989) at 183 GHz, with uncertainties of 0.5% for self-broadening and 1.6% for foreign-gas broadening.

At frequencies away from these two lines, microwave absorption by water vapor is predominantly from the continuum, which is attributed to the low-frequency wing of the intense infrared and submillimeter rotational spectrum. In the microwave part of the spectrum, the foreign-broadened component of the continuum is stronger than the self-broadened component, for atmospheric mixing ratios. Measurements of continuum absorption as a function of temperature have been made at various frequencies by Liebe and Layton (1987) and by Bauer's group (Godon, *et al.*, 1992; Bauer *et al.*, 1993, 1995). There are also numerous measurements at single temperatures and frequencies in the laboratory, and in the atmosphere where temperature and mixing ratio are variable. The

measurements do not present a consistent picture. With respect to the foreign-broadened component, measurements by different experimenters differ by as much as 80% after adjustments for frequency are made. The MPM 89 H_2O continuum model (Liebe, 1989), which is based on the Liebe and Layton (1987) measurements, is used here because it yields the most satisfactory overall agreement with atmospheric measurements.

Liquid Water

It is useful to distinguish between precipitating and nonprecipitating clouds with respect to their interactions with microwaves. Over the range of wavelengths measured by AMSU-A and HSB, nonprecipitating droplets (with diameters of 50 μm or less) can be treated using the Rayleigh small-droplet approximation. In this regime, absorption is proportional to the liquid water content of the air, and scattering can be neglected. The accuracy of calculations is basically determined by the water dielectric constant model. The double-Debye model of Liebe *et al.*, (1991) is used here; it has an estimated maximum prediction error of 3% between 5 and 100 GHz, and 10% up to 1 THz. Precipitation, on the other hand, requires Mie theory to calculate both absorption and scattering. The latter is generally not negligible, and at some wavelengths is predominant. In the case of convective storms, scattering from ice at high altitudes is often the most important process. In simulations so far we have not considered scattering, and the rapid transmittance algorithm uses only the small-droplet approximation for cloud liquid water.

Rapid Transmittance Algorithm

The physical retrieval algorithms used for AIRS/AMSU/HSB do radiative transfer calculations for each profile and hence need a computationally efficient transmittance algorithm. The microwave algorithm computes an effective channel transmittance between two adjacent pressure levels as

$$\left\langle \tau(P_1, P_2) \right\rangle = \exp\left[-(\alpha + \beta\rho_V + \gamma\rho_L)\right], \tag{3.1.1}$$

where ρ_V is the water vapor column density of the (P_1, P_2) layer, ρ_L is its liquid water column density, and the coefficients α, β, γ, are calculated for each layer and channel. They implicitly depend on temperature, pressure, and the angle of observation; β also depends implicitly on ρ_V. For AMSU channel 14, α has a weak dependence on the local geomagnetic field. The magnetic field is currently calculated by a fifth-order spherical-harmonic representation that has an accuracy of a few microteslas. α includes the opacity due to O_2 and a small contribution from pressure-induced absorption by N_2. Parameterization of the coefficients uses approximations described by Rosenkranz (1995) for oxygen-band or window-type channels. The oxygen-band-channel coefficients are computed on a set of fixed pressure levels and then linearly interpolated to the pressure levels of the present retrieval, which can be variable (as is the case for the surface pressure). Window-channel coefficients use analytic approximations for far-wing line and continuum absorption. Channels near the two water lines (AMSU-A channel 1 and HSB channels 3-5) use a Lorentzian-line calculation for the nearby line, with the contributions of other lines treated in the same way as for a window channel. The local water-line parameters, the water continuum, and the liquid-water absorption are interpolated from a table as functions of temperature.

The retrieval algorithm described in Sec. 4.1 also makes use of the derivative $d\beta/d\rho_V$, which is computed in the rapid algorithm by appropriate analytic expressions corresponding to the local-line and continuum components.

The transmittance of multiple layers is calculated by taking the product of the transmittances for each layer. This transmittance is then used in the radiative transfer equation to compute brightness temperature:

$$\Theta = \int_0^{P_s} T(P) < d\tau(0,P) > + \varepsilon T_s < \tau(0,P_s) >$$
$$+ (1-\varepsilon) < \tau(0,P_s) > \int_0^{P_s} T(P) < d\tau(P_s,P) > + (1-\varepsilon)\Theta_c < \tau(0,P_s) >^2 \qquad (3.1.2)$$

where T(P) is atmospheric temperature at level P, T_s and P_s are the surface temperature and pressure, Θ_c is the cosmic background brightness temperature (see eq. 4.1.2), and ε is the emissivity of the surface, assumed to be smooth here.

The ability of the rapid algorithm to approximate a line-by-line calculation was tested on a set of 300 profiles from the TOVS Initial Guess Retrieval (TIGR) (Chedin *et al.*, 1985) ensemble. The first 100 profiles from each of the tropical, midlatitude, and polar groups were used. The line-by-line calculation followed Rosenkranz (1993). Figure 3.1.2 shows brightness temperature errors (mean ± 1 standard deviation) at nadir, with surface emissivity = 0.7. For the channels that are not opaque (1-5, 15-17, 19 and 20), these brightness temperature errors depend on surface emissivity. The value ε = 0.7 is typical of ocean at the highest frequencies, and intermediate between ocean and land at the lowest frequencies. Errors for higher-emissivity land surfaces are smaller than in Figure 3.1.2. The errors for ch. 14 include the consequences of the magnetic field approximation.

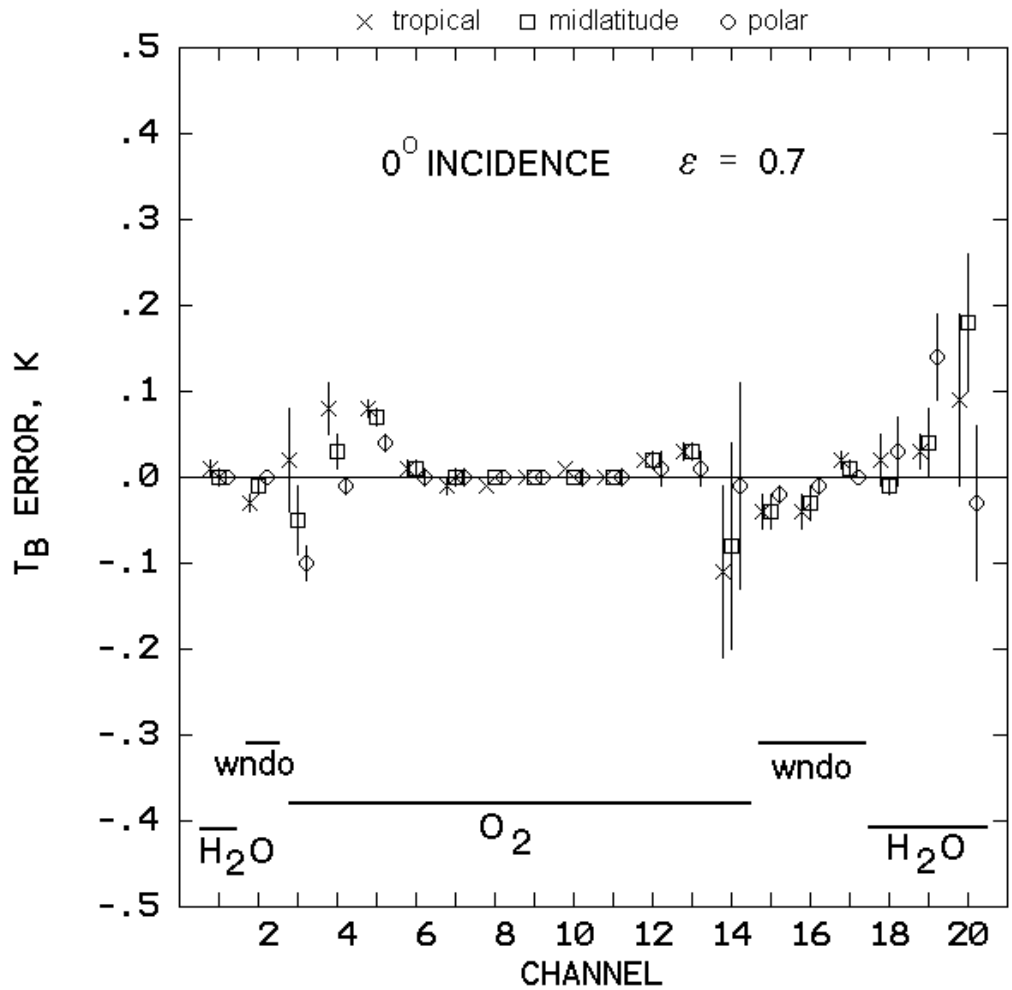

FIGURE 3.1.2. BRIGHTNESS TEMPERATURE ERRORS (RAPID ALGORITHM MINUS LINE-BY-LINE ALGORITHM) FOR AMSU-A CHANNELS (1-15) AND AMSU-B CHANNELS (16-20). VERTICAL LINES INDICATE ± 1 STANDARD DEVIATION.

3.2 Radiative Transfer of the Atmosphere in the Infrared (Strow)

Physical retrievals of atmospheric parameters from infrared spectra require accurate radiative transfer models, known as forward models, relating the atmospheric parameters to the observed channel radiances. The forward model described in this sub-section relates atmospheric parameters to the layer transmittances required for AIRS radiative transfer calculations. In order to keep up with the high data rate of AIRS, such a forward model must quickly calculate these transmittances, and thus is termed a 'fast transmittance model.' Furthermore, the high spectral resolution of AIRS requires highly accurate modeling of the molecular spectroscopy of the infrared active gases, especially spectral line shapes. Outgoing atmospheric radiances contain emission lines at the higher altitudes with widths as small as 0.001 cm^{-1}. Performing radiative transfer at this spectral resolution, and then convolving the resultant radiances with the AIRS spectral response function would be many orders of magnitude too slow for EOSDIS. For this reason, the forward model provides transmittances suitably convolved with the AIRS spectral response

function so radiative transfer computations need only be performed for each AIRS channel. We have developed the Pressure layer Fast Algorithm for AtmoSpheric Transmittances (PFAAST) for the AIRS forward model.

The PFAAST model actually produces equivalent channel averaged optical depths, k's, which are related to the layer transmittances, τ 's, by $\tau = \exp(-k)$. The optical depth is the product of the absorption coefficient and the optical path. For AIRS, a fast model for k is much more accurate than a model that directly returns layer τ 's. k's are computed for each of the 100 atmospheric layers used for AIRS radiative transfer (the layering scheme is discussed in more detail later in this sub-section). The current PFAAST model allows water, ozone, methane, carbon monoxide, the temperature, and local scan angle to vary. All other gases are treated as 'fixed gases.' Tentatively, N_2O amounts may be allowed to vary. In addition, some variation in CO_2 amounts will be required, but this may be done 'off-line' as a semi-continuous adjustment of the 'fixed gas' transmittances. It may also be necessary to let some of the minor gases vary, such as the chlorofluorocarbons (CFC's). Although the observed radiances are primarily sensitive to temperature via the Planck function, the temperature dependence of the transmittances is also important.

Over the years, a number of fast transmittance models have been developed for various satellite instruments [McMillin and Fleming, 1976; Fleming and McMillin, 1977; McMillin *et al.*, 1979, 1995; Scott and Chedin, 1981; Susskind *et al.*, 1983; Erye and Woolf, 1988; Chéruy *et al.*, 1995]. However, some of these models only have been applied to the model microwave region where the measured radiances are essentially monochromatic and easier to model. PFAAST most closely follows Susskind *et al.* [1983] by parameterizing the optical depths rather than transmittances. Preliminary work has been performed with the new Optical Path TRANsmittance (OPTRAN) algorithm developed by McMillin *et al.* [1979, 1995]. Both PFAAST and OPTRAN appear adequate for AIRS with similar computational requirements [Hannon, *et al.*, 1996].

Basic Radiative Transfer and the Polychromatic Approximation

The monochromatic radiance leaving the top of the atmosphere, excluding any scattering and clouds, and assuming a Lambertian surface is approximated by

$$R(\nu,\theta) = \varepsilon_s B[\nu,T_s]\tau(\nu,p_s,\theta) + \int_{\ln p_s}^{\ln p_\infty} B[\nu,T(p)]\frac{\partial\tau(\nu,p,\theta)}{\partial \ln p}\,d\ln p +$$

$$(1-\varepsilon_s)\tau(\nu,p_s,\theta)\int_{\ln p_s}^{\ln p_\infty} B[\nu,T(p)]\frac{\partial\tau(\nu,p,\theta)}{\partial \ln p}\,d\ln p + \rho_s H(T_{sun})\tau(\nu,p_s,\theta)\tau(\nu,p_s,\theta_{sun})\cos(\vartheta_{sun}) \tag{3.2.1}$$

where $B[\nu,T(p)]$ is the Planck function emission for layer p at temperature T(p), $\tau(\nu,p,\theta)$ is the layer-to-space transmittance at viewing angle θ, $\tau_s(\nu,p,\theta)$ is the surface-to-space transmittance, and T_s, ε_s, and ρ_s refer to the Earth's surface temperature, emissivity, and reflectivity respectively. Also, the solar term is represented by $H(\nu)=2.16\text{x}10^{-5}\,\pi\,B(\nu,T_{sun})$. The polychromatic approximation replaces the monochromatic layer-to-space transmittances with transmittances convolved with the AIRS spectral response function (SRF). In most cases, the AIRS channel radiances calculated from the above equation using convolved layer-to-space transmittances differ from the convolved monochromatic AIRS channel radiances by ≤ 0.1 K. This difference is generally less than the nominal 0.2 K RMS noise of AIRS, and thus does not introduce any serious inaccuracies. PFAAST produces effective layer transmittances since they can be modeled more accurately and because the AIRS retrieval algorithms perform radiative transfer using layer transmittances. However, if polychromatic radiative transfer is performed using layer

transmittances that have been directly convolved from the monochromatic layer transmittances, large radiance errors will result due to the breakdown of Beer's law. For this reason, PFAAST uses layer transmittances derived from ratios of convolved layer-to-space transmittances, thus preserving Beer's law to a much higher degree. Although an exponentiation is required to produce transmittances, PFAAST provides a relatively simple relationship between optical depths and atmospheric variables. Scattering is negligible for long wavelength IR but will be modeled for the short wavelength AIRS channels.

Spectroscopic Inputs

The ultimate goal is to produce a forward model that does not introduce significant errors in AIRS computed radiances. In the past, this has not been possible given the state-of-the-art in atmospheric spectroscopy. However, advances in laboratory measurements of line parameters and advances in phenomenological spectral lineshape models make an accurate AIRS forward model a real possibility. This is especially important for water vapor, H_2O. Radiosonde humidity errors coupled with always present errors in the time and space co-location of the radiosonde and AIRS measurements make tuning of the AIRS H_2O radiances quite suspect. Consequently, the forward model is of fundamental importance for AIRS data products. The sensitivity of the AIRS forward model to errors in spectroscopic line parameters and the development of improved spectral lineshape models for CO_2 and H_2O are summarized in the following subsections.

Spectroscopic Line Parameter Errors

Due to the dominance of either CO_2 or H_2O absorption in the majority of AIRS channels, the most important spectroscopy errors are associated with errors in the line parameters and line shapes of these two gases. The line center frequencies are well known, and thus should not be a noticeable source of error. Although there is a shift in the line center frequency with pressure, these shifts are too small to be of concern for AIRS. The line parameters most likely to introduce spectroscopy errors into the fast forward model for AIRS are the line strengths, line widths, and the temperature dependence of the line widths. However, errors in spectral lineshapes and continuum absorption probably will be more troublesome than line parameter errors.

Currently, the HITRAN92 [Rothman *et al.*, 1992] database is used for most atmospheric line parameters, supplemented by more recent water linewidths measured by Toth [private communication]. The AIRS forward model will be regularly updated with the latest available line parameters using databases such as HITRAN96 and GEISA [Husson *et al.*, 1992]. Because there are so many bands and molecules that contribute to the observed radiances, the accuracy of the existing line parameters is difficult to judge in detail. Fortunately for AIRS, most of the important lines of both CO_2 and H_2O have been measured in the laboratory .

In general the CO_2 line parameters are better known than those for H_2O. The line strengths for the stronger CO_2 lines are good to 5% or better, while the H_2O line strengths may only be good to 10%. The H_2O line strengths are also more likely to have different errors for different bands and isotopes. The effects of these potential errors in line strengths for CO_2 and H_2O are shown in Figures 3.2.1 and 3.2.2, respectively. Note, these figures assume systematic errors in the line strengths and widths. While it is reasonable to expect some level of systematic error, at least over 20-50 cm^{-1}, there will also be random components to these errors.

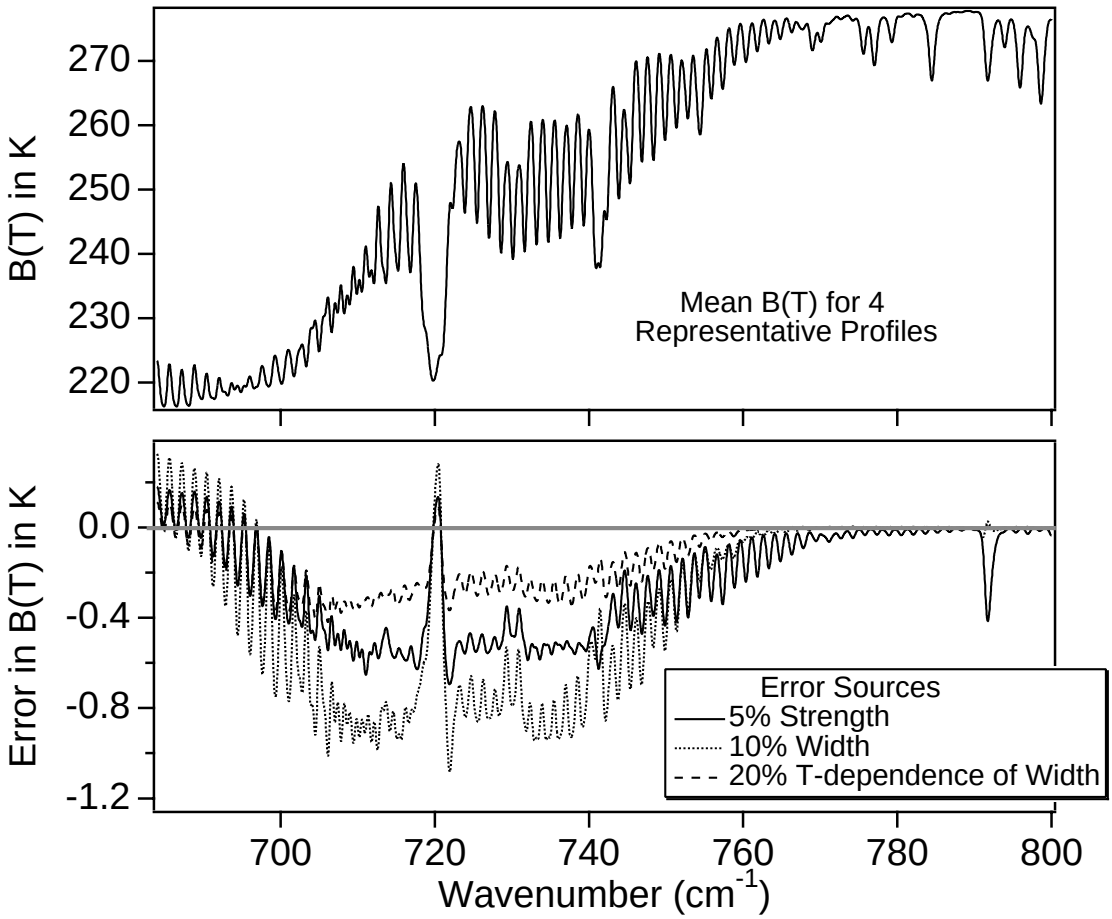

FIG 3.2.1: TOP: A MEAN AIRS SPECTRUM IN A PORTION OF THE 15 μm CO_2 BAND. BOTTOM: THE MEAN BRIGHTNESS TEMPERATURE ERRORS DUE TO A +5% ERROR IN CO_2 LINE STRENGTHS, A +10% ERROR IN CO_2 LINE WIDTHS, AND A +20% ERROR IN THE CO_2 WIDTH TEMPERATURE DEPENDENCE.

The estimated uncertainty in the line widths are 10% for CO_2 and 20% for H_2O. Again, the H_2O widths are more likely to have both larger random and systematic errors between bands and isotopes. Line width errors will probably be the dominant source of spectroscopy errors for water, while line strength and width errors will probably be of approximately equal importance for CO_2. The effects of these errors in line widths for CO_2 and H_2O are shown in Figures 3.2.1 and 3.2.2, respectively.

The temperature dependence of the line widths is the least well known, with an uncertainty of perhaps 20% and sometimes more. However, of the four sources of errors discussed here, it is the least important. A plot of the effects of a +20% error in the temperature dependence of the CO_2 line widths is shown in Figure 3.2.1. The similar error for H_2O is much smaller than those that are shown in Figure 3.2.2.

The uncertainty in the H_2O foreign continuum may be as large as 25% in portions of the 7 μm band. For AIRS, the maximum errors due to this fall in the 1400 cm^{-1} region. A plot of the impact of a +25% error in the H_2O foreign continuum is shown in Figure 3.2.2. In other portions of the 7 μm band these uncertainties are likely smaller.

All of the errors quoted here are somewhat conservative. Over the next several years, continuing laboratory spectroscopy efforts, especially in Europe, should lower the errors quoted here by a factor of two.

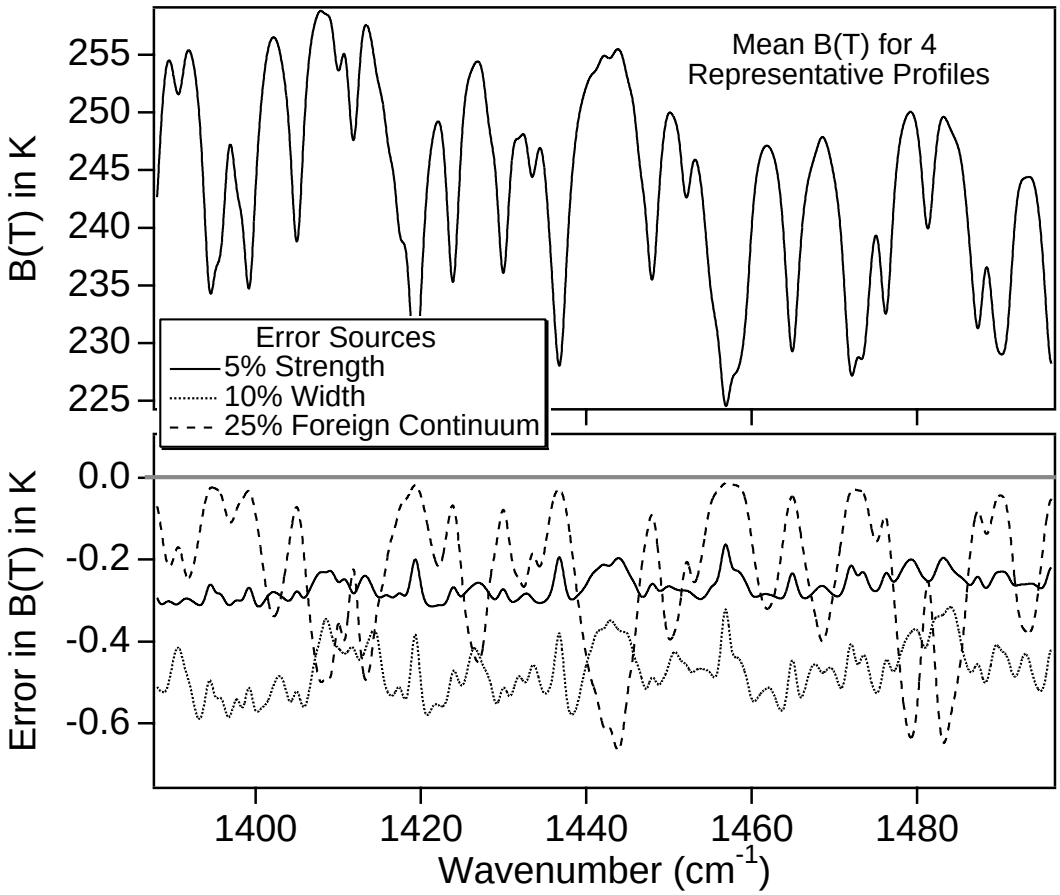

FIG 3.2.2: TOP: A MEAN AIRS SPECTRUM IN A PORTION OF THE 7 μm H_2O BAND. BOTTOM: THE MEAN BRIGHTNESS TEMPERATURE ERRORS DUE TO A +5% ERROR IN H_2O LINE STRENGTHS, A +10% ERROR IN H_2O LINE WIDTHS, AND A +25% ERROR IN THE FOREIGN BROADENED H_2O CONTINUUM.

Molecular Line Shape Effects

Errors in the spectral lineshapes of CO_2 and H_2O are much more problematic than line parameter errors. Because of the large optical depths of CO_2 and H_2O in the atmosphere, their spectral line wings can be quite important, especially for remote sensing of temperature and humidity. For example, AIRS channels with the sharpest weighting functions are located in between lines or in the line wings where knowledge of the spectral line shape is most important. Moreover, accurate measurements of the line wing absorption are exceedingly difficult due to problems simulating atmospheric optical depths in a laboratory cell, especially for H_2O. It is also tedious and expensive to make these large optical depth measurements at the low temperatures found in the upper troposphere.

AIRS will require better CO_2 spectral line shapes than are presently available in the literature. Recent theoretical developments in line mixing for CO_2 Q-branches can affect AIRS brightness temperature by more than 10K. These effects are already well characterized in the line-by-line code used to generate the AIRS PFAAST model, a specialized version of GENLN2 [Edwards, 1992]. What is presently missing in GENLN2 is an accurate far-wing model for CO_2, especially in the 15 μm region. L. Strow (UMBC) and D. Tobin (Univ. Wisc.) are presently developing a phenomenological far wing line shape model for the 15 μm region of CO_2 that includes both P- and R-branch line mixing and duration of collision effects. These enhancements to GENLN2 should reduce many existing errors from the mostly empirical models currently used in line-by-line

forward models. A CO_2 line shape model for the important 4.3 μm channels is also under development.

Recent laboratory work has greatly improved our knowledge of the H_2O line shape within the strong part of the H_2O band [Tobin *et al.* 1996a, 1996b], a region important for the determination of mid- to upper-tropospheric H_2O. In addition, recent measurements with the Atmospheric Emitted Radiance Interferometer (AERI) at the Department of Energy's Atmospheric Radiation Measurement program Cloud And Radiation Testbed site in Oklahoma should lead to an improved H_2O continuum in the AIRS window channels near 10 μm. However, there are still considerable gaps in our knowledge of the H_2O vapor line shape. Of particular concern is the 1250 to 1400 cm^{-1} region used to sense lower tropospheric H_2O. This spectral region is difficult to study in the laboratory because of the long pathlengths required and is often too opaque in the atmosphere for good measurements by AERI. Moreover, the H_2O continuum switches from primarily a quadratic dependence to primarily a linear dependence on H_2O amount somewhere in this spectral region. Continued field measurements, as discussed in Section 8, are needed to improve our knowledge of the continuum in this region. If a long enough cell can be identified, laboratory measurements in the region would also greatly benefit the AIRS forward model.

Line-by-Line Calculations

The monochromatic layer-to-space transmittances used to determine the parameters of the AIRS PFAAST model are indirectly generated from the GENLN2 [Edwards, 1992] line-by-line radiative transfer model. Over the next several years, we will incorporate the spectroscopic advances discussed in the preceding section into GENLN2 in collaboration with David Edwards at NCAR. These improved line-by-line models will undergo continual validation and refinement using data acquired in the field campaigns discussed in Section 8 of this ATBD.

Currently, 36 profiles are used in the regressions for the fast transmittance parameters. However, 36 line-by-line calculations for each of the 100 AIRS pressure layers are not performed directly with GENLN2. Instead, GENLN2 is used to compute a very large look-up table of monochromatic layer optical depths for a set of 11 reference atmospheric profiles. Such a look-up table is similar to the approach of Scott and Chedin [1981]. Transmittances for the 36 regression profiles are easily calculated from this look-up table. Layer optical depths scale linearly with gas amount since the look-up table is monochromatic. In addition, the layer optical depths vary quite slowly and smoothly with temperature, allowing accurate interpolations in temperature.

A look-up table with 11 evenly spaced temperatures is sufficient to accurately interpolate the layer optical depths in temperature. This saves substantial computational time versus the same calculations for the 36 regression profiles. Inclusion of an additional regression profile simply requires an interpolation. Note, any change in physics in the line-by-line codes requires recalculation of the entire monochromatic look-up table. The current look-up table neglects effects of water vapor self-broadening, thus introducing small errors in water vapor transmittances. However, for the AIRS channel widths of ≈ 0.5 to 2 cm^{-1} this is a reasonably small error, generally < 0.2 K. Unfortunately, due to its large size, ≈ 35 GByte, the monochromatic look-up table is quite cumbersome to use.

Each file in the look-up table covers a 25 cm^{-1} interval with 10,000 points (0.0025 cm^{-1} spacing) for 100 pressure layers (0.009492 to 1085 mb). The pressure layer structure, described in more detail in the following sub-section, was chosen to produce errors < 0.2 K in observed brightness temperatures for AIRS. For each infrared active gas

and 25 wavenumber region from 605 cm^{-1} to 2830 cm^{-1}, 11 tables are computed differing only by the temperature profile. The 11 profiles are the U.S. Standard profile, and 10 profiles offset from it in ±10K increments. On average, 7 gases must be included per 25 cm^{-1} region. The continua due to gases such as N_2 and O_2 also are included in these tables. Because their optical depths are easily computed for any profile, water vapor continuum absorption and gases provided by HITRAN as cross sections, such as CFC's, are not included in the look-up tables. Optical depths are computed using GENLN2 at a 0.0005 cm^{-1} grid and then averaged to the database grid spacing of 0.0025 cm^{-1}. Consequently, the highest altitude optical depths are not truly monochromatic, but exhibit good integrated optical depths. The relatively large width of the AIRS Spectral Response Function (SRF) results in negligible errors due to this averaging. Optical depths for all the HITRAN gases, except CO_2 and H_2O, are computed using the Voigt lineshape. As discussed earlier, the CO_2 and H_2O lineshapes are modified from the Voigt lineshape.

AIRS Atmospheric Layering Grid

The atmospheric pressure layering grid for the AIRS PFAAST model was selected to keep radiative transfer errors well below the instrument noise. Grid characteristics are a function of the spectral region(s) of observation, the instrument resolution, and instrument noise. The speed of the final fast transmittance model will depend on the number of layers, so excessive layering should be avoided.

GENLN2 simulations indicate some channels need a top layer with pressures as small as 0.01 mb, an altitude of ~ 80 km. The region of primary importance to AIRS is the troposphere and lower stratosphere, where layers on the order of 1/3 the nominal 1 km vertical resolution of AIRS retrievals are desired. Smoothly varying layers facilitate interpolation and avoid large changes in layer effective transmittances. The following relation defines the pressure layer boundaries selected for AIRS:

$$P_i = (ai^2 + bi + c)^{7/2} \qquad (3.2.2)$$

where P is the pressure in mb; i is the layer boundary index and ranges from 1 to 101; and the parameters a, b, and c were determined by solving this equation with the following fixed values: P_1 = 1100 mb, P_{38} = 300 mb, and P_{101} = 5×10^{-3} mb. The 101 pressure layer boundaries in turn define the 100 AIRS layers. These layers vary smoothly in thickness from several tenths of a kilometer near the surface to several kilometers at the highest altitudes. Figure 3.2.3 displays a plot of this atmospheric layer structure.

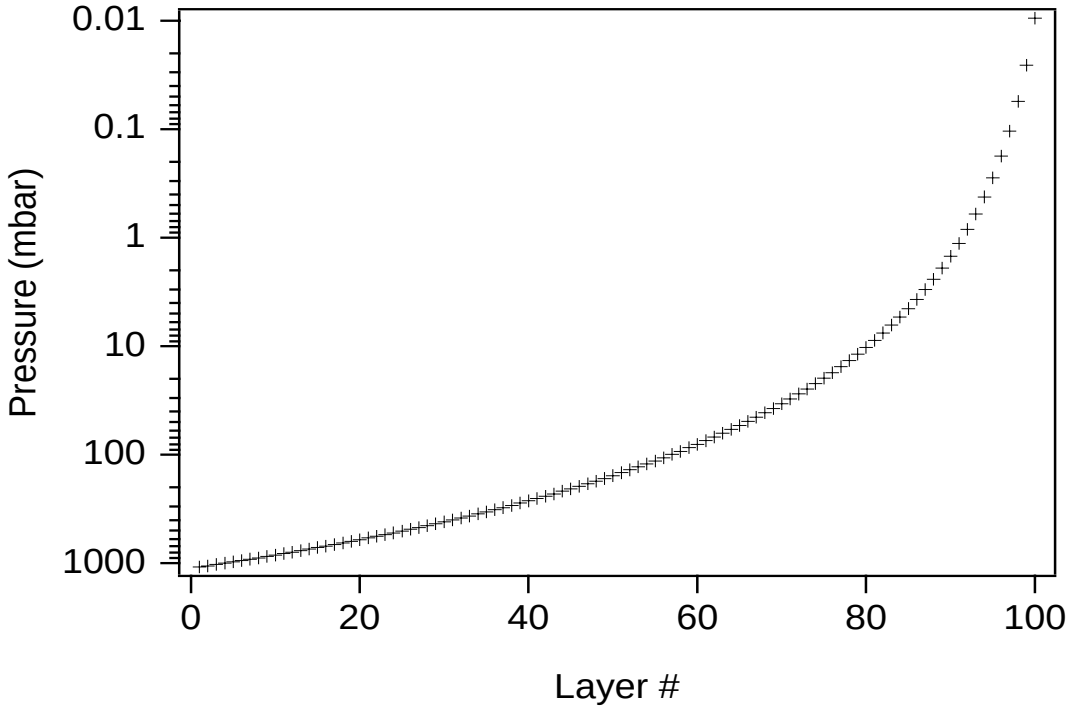

FIGURE 3.2.3: AIRS PFAAST MODEL PRESSURE LAYER STRUCTURE.

Regression Profiles

One other necessary pre-processing step is the selection of a set of profiles for calculation of the layer-to-space transmittances. The transmittances for these profiles become the regression data for the fast transmittance coefficients. These profiles should span the range of atmospheric variation, but, on the whole, should be weighted towards the more typical cases. The range of variation provides the regression with data points covering the range of possible atmospheric behavior, while the weighting of the mix of profiles towards more typical cases produces a transmittance model that works best on more statistically common profiles.

The process of calculating and convolving monochromatic layer-to-space transmittances is generally computationally intensive, thus imposing a practical limit on the number of profiles one can calculate for use in the regression. As discussed earlier, 36 regression profiles (at 5 viewing angles each) are sufficient to cover most of the profile behavior. This number is a compromise between the available time and computing resources and the need to cover a wide range of profile behavior in the regression. Choosing too few profiles leads to accuracy problems for profiles outside the range of behaviors considered. Choosing more profiles than necessary does not hurt the fast model, but does consume extra time and computer resources in the creation of the model.

Each profile should cover the necessary pressure (altitude) range with data for temperature as well as absorber amount for each of the gases allowed to vary. The fixed gases include all those whose spatial and temporal concentration variations have a negligible impact on the observed radiances. As previously mentioned, the variable gases include H_2O, O_3, CO, CH_4, and N_2O. At present, transmittance models for H_2O, O_3, CO, and CH_4 have been developed; all other gases are included in the 'fixed gas' category. In the future, N_2O and possibly CO_2 will be allowed to vary.

For those satellite viewing angles relevant to the AIRS instrument (0 to 49 degrees), the effects of viewing angle can be approximated fairly well by multiplying the nadir optical depth by the secant of the local path angle. This approximation neglects the

minor refractive effect at large angles. Local atmospheric path angles of 0, 38, 49, 56, and 63 degrees are used in the regression profiles to cover the 0-49 degree satellite view angle range.

Fast Transmittance Model Parameters

All the steps leading up to the generation of the accurate layer-to-space monochromatic transmittances have been described in the preceding sub-sections. They are the inputs to the regressions that determine the fast transmittance coefficients used in the AIRS PFAAST model as described below.

Breakout of Gases

With the layering grid and regression profiles selected, the monochromatic layer-to-space transmittance can be calculated. The gases are distributed into sub-groups that are either fixed or variable. The details of how the transmittance model simultaneously handles several variable gases is somewhat complicated and beyond the scope of this document. For simplicity, this discussion is restricted to fixed gases (*F*), water vapor (*W*), and ozone (*O*). The breakout of the other variable gases is similar. The monochromatic layer-to-space transmittances for the 36 regression profiles are calculated for each pressure layer, grouped into the following three sets, and convolved with the AIRS SRF,

$$\begin{aligned} F_{\infty,l} &= \tau_{\infty,l}(fixed) \\ FW_{\infty,l} &= \tau_{\infty,l}(fixed + water) \\ FWO_{\infty,l} &= \tau_{\infty,l}(fixed + water + ozone) \end{aligned} \tag{3.2.3}$$

The shape of each of the channel spectral responses functions will be measured carefully on the ground. The centered frequencies will be determined on orbit by spectral calibration. The accuracy of this is discussed in the L1B AIRS ATBD.

Water continuum absorption is excluded since it varies slowly with wavenumber and does not need to be convolved with the AIRS SRF. Later, the water continuum is factored into the total transmittance as a separate term.

For each layer *l*, the convolved layer-to-space (∞,*l*) transmittances are ratioed with transmittances in the layer above, *l* - 1, to form effective layer transmittances for fixed (*F*), water (*W*), and ozone (*O*) as follows:

$$\begin{aligned} F_l^{eff} &= \frac{F_{\infty,l}}{F_{\infty,l-1}} \\ W_l^{eff} &= \frac{FW_{\infty,l}}{FW_{\infty,l-1}} \div \frac{F_{\infty,l}}{F_{\infty,l-1}} \\ O_l^{eff} &= \frac{FWO_{\infty,l}}{FWO_{\infty,l-1}} \div \frac{FW_{\infty,l}}{FW_{\infty,l-1}} \end{aligned} \tag{3.2.4}$$

The exact form of these ratios reduce the errors inherent in separating the gas transmittances after the convolution with the instrument spectral response function. The total effective layer transmittance can be regenerated as follows:

$$FWO_l^{eff} = F_l^{eff} * W_l^{eff} * O_l^{eff} = \frac{FWO_{\infty,l}}{FWO_{\infty,l-1}} \tag{3.2.5}$$

The convolution of a product of terms is in general not the same as the product of the terms convolved individually. However, the above formulation guarantees the product of all the layer transmittances from layer l to ∞ *exactly* returns $FWO_{\infty,l}$.

The zeroth layer transmittance (*i.e.* when l - 1 = 0) is taken to be exactly 1.0. The negative logarithm of these layer effective transmittances is taken to get effective layer optical depths,

$$\begin{aligned} k_{fixed} &= -\ln(F_{eff}) \\ k_{water} &= -\ln(W_{eff}) \\ k_{ozone} &= -\ln(O_{eff}) \end{aligned} \tag{3.2.6}$$

which are fit with the layer transmittance model.

Predictors

The effective layer optical depths become the dependent variables in a regression to calculate the fast transmittance coefficients relating a set of profile dependent predictors to the layer effective optical depth. Care must be used to restrict the regression to k values that are significant for radiative transfer.

The optimal set of predictors used to parameterize the effective layer optical depth depends upon the gas, the instrument's spectral response function, the range of viewing angles, the spectral region, and even the layer thicknesses. In short, no one set of predictors is likely to work well in every case. Finding the set of predictors which gives the best results is, in part, a matter of trial and error. However, there are some general trends.

For an instrument such as AIRS with thousands of channels, it is difficult to develop individual optimal predictors for each channel. At this point, one set of predictors for each gas has been developed that works sufficiently well for all channels. These sets of predictors were determined by extensive trial and error testing of a few representative channels estimated to span the range of behaviors present in the entire channel set. The most difficult channels to model appear to be ones with low altitude emission by water lines and those covering the strong ozone band.

The regression is prone to numerical instabilities if the values of the predictors vary too greatly. Consequently, we follow the usual practice of defining the predictors with respect to the values of a reference profile, either by taking a ratio or an offset. There is also a danger of numerical instability in the results of the regression due to the interaction of some of the predictors. Sensitivity of the output to small perturbations in the predictors is avoided by systematic testing. There are practical difficulties in detecting small problems since we are performing on the order of 1 million regressions. We hope to regularize these regressions in the future in a way that might allow automatic trimming of unnecessary predictors on a channel by channel basis.

For simplicity, only the predictors for the fixed gases are shown:

$$\begin{array}{lll} 1)a & 2)a^2 & 3)aT_r \\ 4)aT_r^2 & 5)T_r & 6)T_r^2 \\ 7)aT_z & 8)a\,T_z/T_r & \end{array} \tag{3.2.7}$$

where *a* is the *secant* of the local path angle, T_r is the temperature ratio $T_{profile}/T_{reference}$, and T_z is the pressure weighted temperature ratio above the layer

$$T_z(l) = \sum_{i=2}^{l} P(i)\big(P(i) - P(i-1)\big)T_r(i-1) \qquad (3.2.8)$$

where *P(i)* is the average layer pressure for layer *l*. The predictors for the variable gases can involve more complicated dependencies on the gas and the pressure weighted gas ratios above the layer, similar to the temperature terms defined above. Note, terms like T_z (or W_z, *etc*. for the variable gases) makes the layer *l* transmittance dependent on the temperature (or gas amounts) in the layers above *l*.

Regressions for Fast Transmittance Parameters

The accuracy of radiative transfer calculations made with the AIRS PFAAST model improve significantly if the data is weighted prior to performing the regression. Radiative transfer is insensitive to layers for which the change in layer-to-space transmittance across the layer is ~ zero. This occurs when either the layer effective transmittance is ~ unity, or when the layer-to-space transmittance above the layer is ~ zero. Therefore, the data going into the regression is not all of equal importance to the final accuracy of radiative transfer calculations made with the model. We found it useful to weight the data in terms of both its effective layer optical depth as well as the total optical depth of all the layers above the layer under consideration.

The spectral dependence of the fitting errors are shown in Fig 3.2.4 and a histogram of these errors in Fig 3.2.5. The errors are calculated with respect to the regression profile set, comparing the RMS errors between the brightness temperatures of input data and the AIRS PFAAST model calculated values.

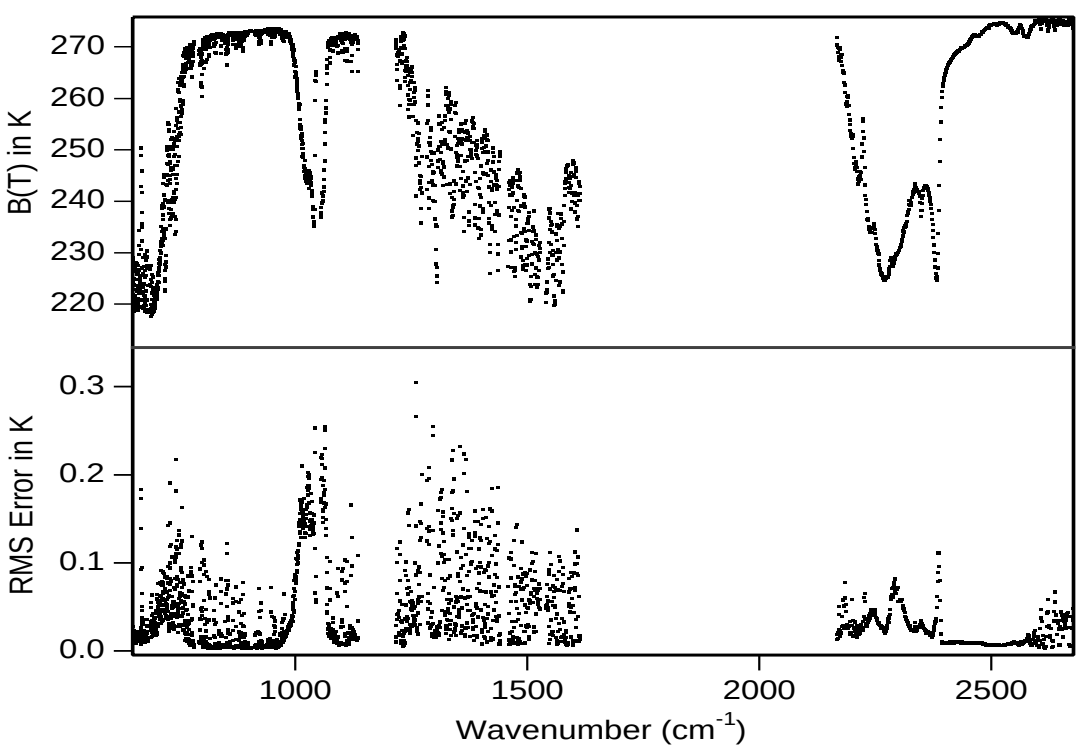

FIG 3.2.4: RMS FITTING ERRORS OF THE AIRS PFAAST MODEL.

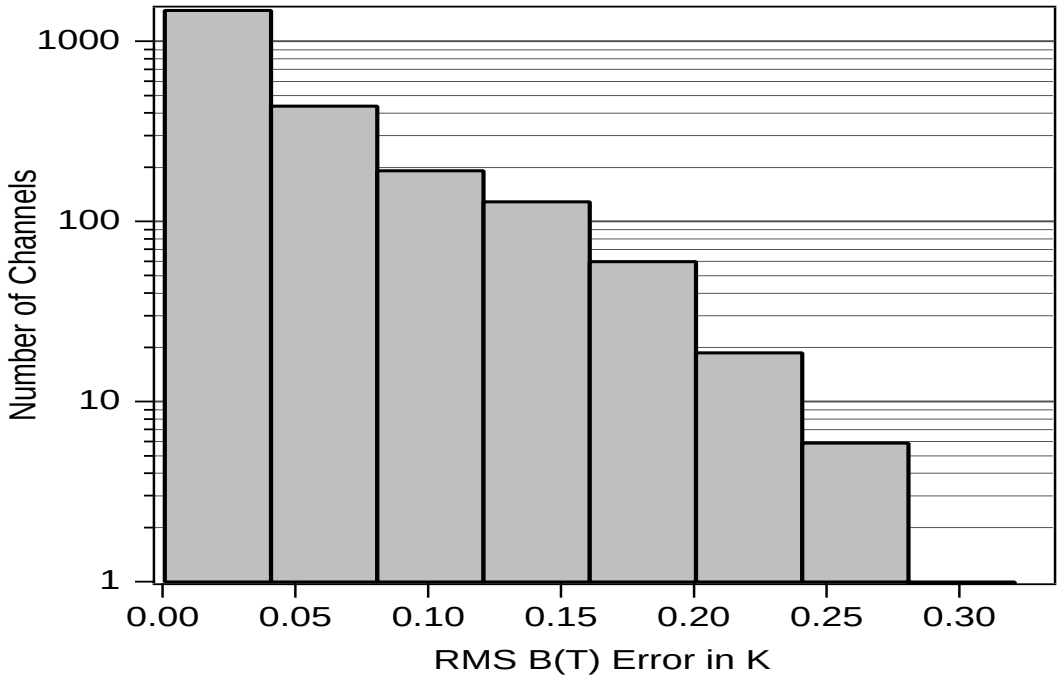

FIG 3.2.5: HISTOGRAM OF THE AIRS PFAAST MODEL FITTING ERRORS FOR ALL CHANNELS.

Errors in the AIRS PFAAST Model calculated for TIGR, a large independent profile set, are shown in Figures 3.2.6 and 3.2.7 and are very similar to those shown in Figures 3.2.4 and 3.2.5. In general the RMS errors are at or below the estimated signal noise for AIRS and spectroscopic errors. As previously mentioned, the largest errors are generally associated with either low altitude water or are inside the strong ozone band near 1100 cm^{-1}.

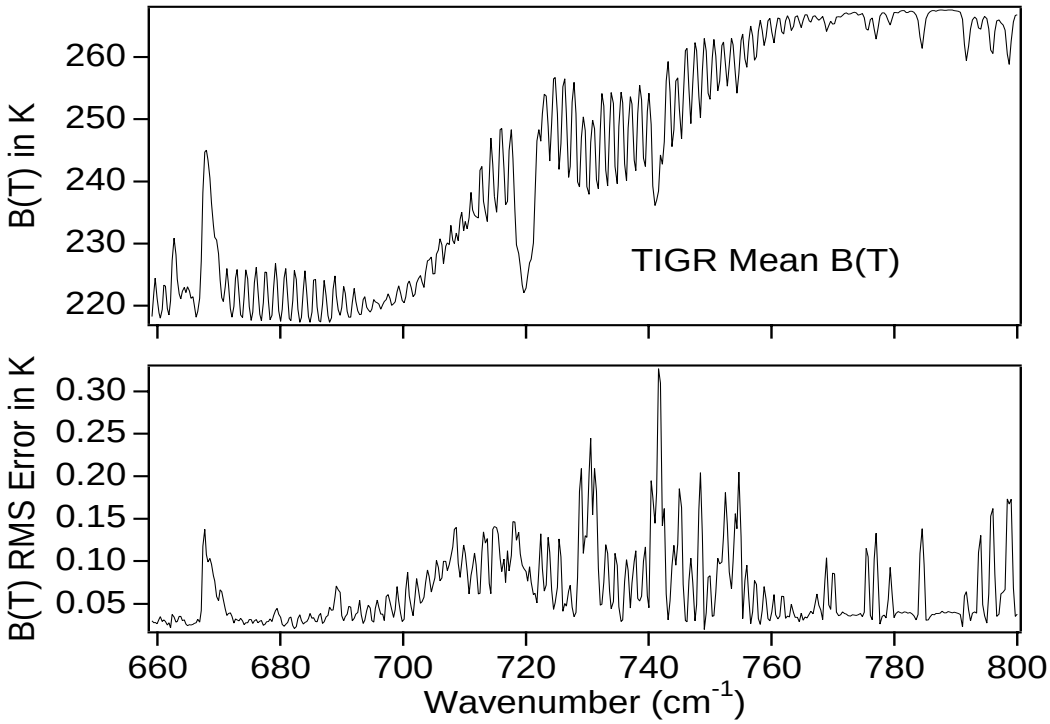

FIG 3.2.6: AIRS PFAAST MODEL RMS ERRORS OVER THE 1761 TIGR PROFILES IN THE 15 μm TEMPERATURE SOUNDING REGION.

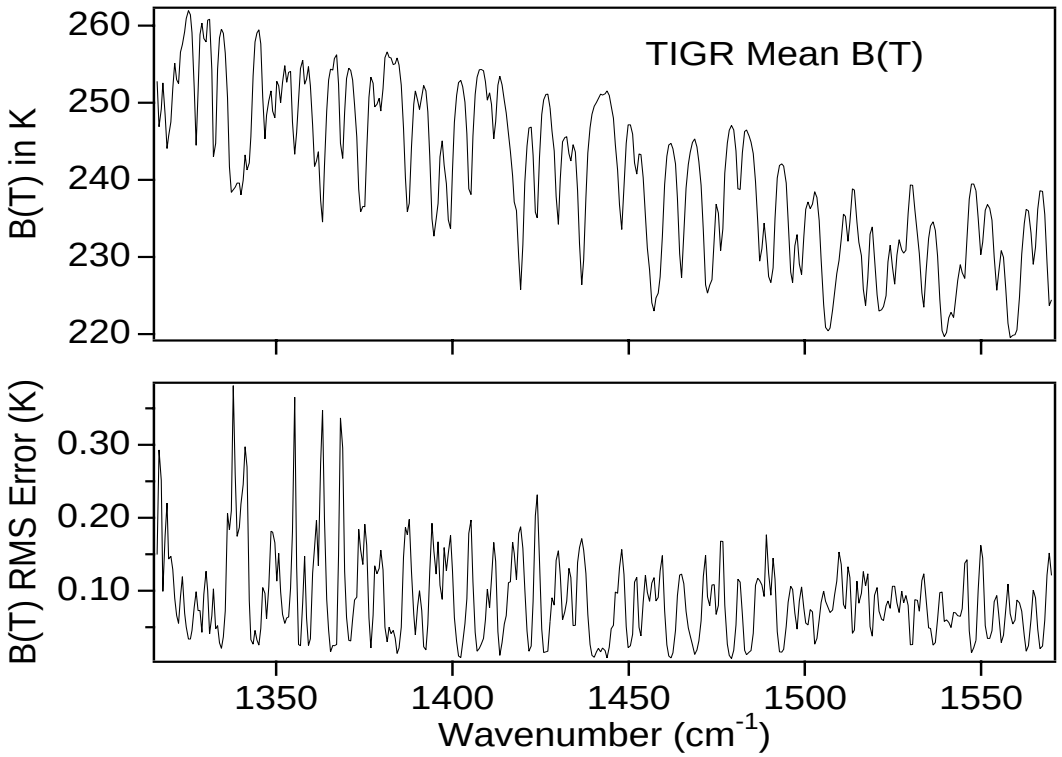

FIG 3.2.7: AIRS PFAAST MODEL RMS ERRORS OVER THE 1761 TIGR PROFILES IN A REGION SENSING TROPOSPHERIC H_2O, NEAR 7 μm.

4. Mathematical description of the Core retrieval algorithm

The AIRS Team Core Algorithm has two major goals:

- Meet the NOAA operational requirements.
- Meet the EOS science requirements.

The NOAA operational requirements are met by the first three algorithm steps: microwave first guess, first pass cloud clearing, and the NOAA first product see (figure 4.1). The EOS requirements are met by the second pass cloud clearing and the final retrieval, as illustrated in figure 4.1.

In this section both the underlying physics and the algorithms used to deconvolve the measurements into geophysical parameters will be described. Many different types of retrieval methodologies can be applied to this problem with advantages belonging to each type. In general we can classify the approaches into two types: 1) pre-computed Empirical Orthogonal Function (EOF) or regression methods and 2) physically-based techniques which match measured and calculated radiances and iterate until the match is within the expected signal-to-noise. Approach 1 is the fastest methodology because all the radiative transfer calculations are done off-line. The first approach is used by NOAA to produce a rapid and accurate estimate of the geophysical parameters which they subsequently refine by a rapid physical retrieval step to meet NOAA operational time constraints. To produce the final product, a more sophisticated physical retrieval, which includes the use of a scene dependent noise covariance matrix, that allows for further refinement of the products and predicted error estimates on a case by case basis.

There are also two approaches to the infrared cloud clearing problem: 1) account for the effects of clouds in the observed radiances and 2) eliminate the effects of clouds from the observed radiances. The method chosen for the AIRS Team algorithm is approach 2 which has had a long and successful application to current and previous generations of temperature sounder measurements. (Approach 1 will be examined as a research product and is not described in this document.

The cloud clearing methodology assumes very little about the radiative properties of the clouds. The only assumption is that for a given channel, a given cloud formation behaves the same in all fields of view. To the extent that a cloud formation behaves differently in different fields of view, it is in reality more than a single cloud formation. The cloud clearing methodology can handle many cloud formations in principle, and has been tested for two cloud formations. Should the assumption of cloud homogeneity (between fields of view) for a given number of cloud formations break down, a satisfactory solution will not be found and the profile will be rejected.

The final product algorithm does not attempt to solve for cloud properties simultaneously with the temperature and moisture profile because errors in the cloud properties (radiative properties of clouds can behave in a very complex way) will propagate into errors in the other retrieved properties. We first obtain clear column radiances in a way that does not require knowledge of the detailed radiative properties of the clouds, then obtain solutions for other geophysical parameters, and then retrieve cloud properties.

Overview

The approach the AIRS team has taken to meet the very stringent temperature accuracy constraint of 1K RMS Tropospheric error in 1 km increments is to provide multiple retrieval strategies, designated as products. A simplified chart is presented in figure 4.1 that describes the basic flow of the AIRS Team Algorithm design.

- The main objective of the microwave initial guess algorithm (section 4.1) is to characterize the atmospheric column in terms of precipitation and cloud liquid water which are used in the cloud-clearing process throughout the core algorithm retrieval.
- The NOAA first product algorithm (section 4.2) has two objectives: (1) delivers the initial guess using in the final product algorithm and (2) within three hours of observations, deliver to NOAA the retrieved surface and atmospheric data required for operational weather forecasts.
- The final product algorithm (section 4.3) delivers all the AIRS/AMSU/HSB Core Products as defined in this document. The final product algorithm is a totally new state of the art algorithm developed for a high signal to noise instrument with many channels. The algorithm takes great care to describe all sources of channel noise (defined as the error in the difference between observed and computed brightness temperatures), especially errors due to cloud clearing. The algorithm then finds solutions which best match these radiances, given the noise covariance matrix, with no explicit consideration given to the estimated accuracy of the first guess, or the extent of deviation of the solution for the first guess. The algorithm has been shown to have only a very weak first guess dependence, and does not require considerations or coefficients which depend on location or season. In addition, the algorithm produces error estimates for all products, including clear column radiances, on a profile by profile basis. The final product algorithm is not dependent on the NOAA product, but can use either the microwave product, the NOAA product, or the NOAA regression guess, as its first guess. The final retrieval is only weakly dependent on the first guess used.

During the simulation testing (described in Section 5.2) and during the first phase of instrument checkout the algorithm will be streamlined into its most robust and efficient form. The mainstay of the algorithm design process is the use of simulated data.

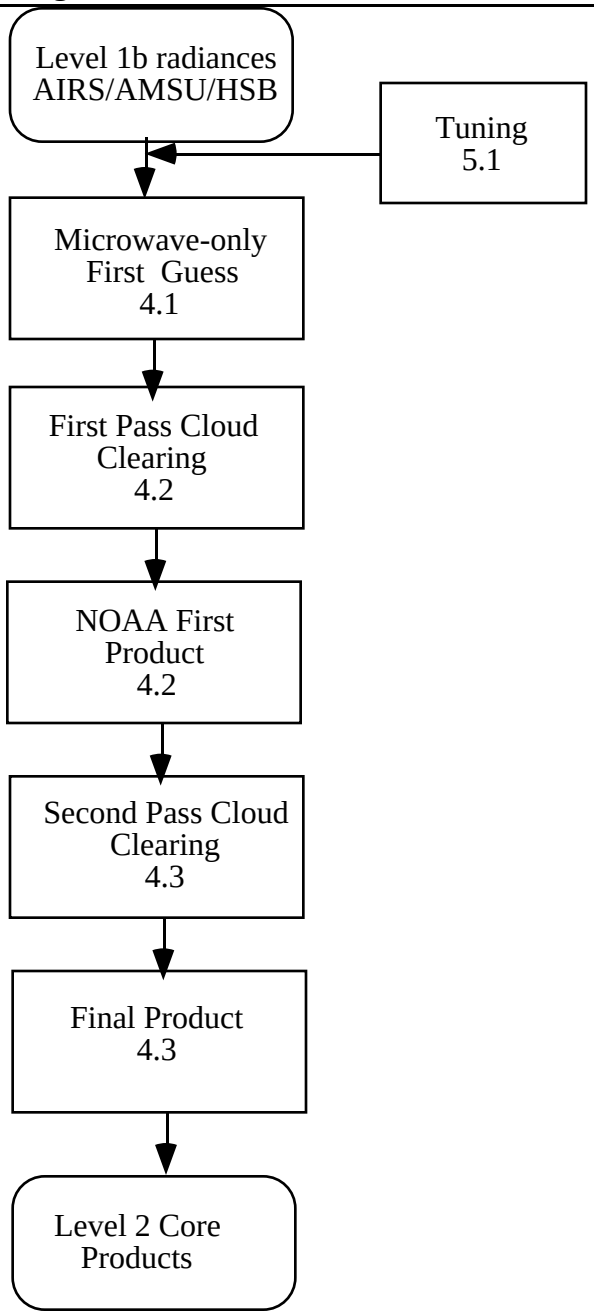

FIGURE 4.1 SIMPLIFIED ALGORITHM FLOW CHART

4.1 Microwave Initial Guess Algorithm (Rosenkranz/Staelin)

The microwave initial guess profile retrieval algorithm will derive temperature, water vapor and non-precipitating cloud liquid water profiles from AMSU/HSB brightness temperatures. It is intended to provide the starting point for the AIRS cloud-clearing and retrieval. This is an iterative algorithm in which the profile increments are obtained by the minimum-variance method, using weighting functions computed for the current temperature and moisture profiles with the rapid transmittance algorithm described in Section 3.1. A block diagram is shown in Figure 4.1.1.

The input vector of brightness temperatures is accompanied by an input validity vector whose elements are either one or zero. This provides a way of handling missing or bad data. Prior to the retrieval, the presence of rain in the field of view should be tested for, using the output of the precipitation algorithm. If the rain exceeded some threshold, the lower tropospheric channels could be excluded from use in the retrieval by setting their validity flags to zero.

Definition of the Initial Profiles

Two options are allowed for the initial guess; one is a climatological input and the other is a Kalman-type guess. The Kalman-type first guess uses a previously retrieved (from AIRS/AMSU/HSB) temperature profile $\hat{T}(d)$ at a distance d and a model for the horizontal temperature autocorrelation function $\rho(d)$; the minimum-variance initial profile at d = 0 is then

$$\tilde{T}(0) = (1-\alpha)\hat{T}(d) + \alpha\langle T\rangle \qquad (4.1.1)$$

where <T> is the global mean profile and $\alpha = 1-\rho(d)$. Previous studies (e.g. Briancon, 1986) have shown that for distances d less than a few hundred km, a reasonable model is $\rho(d) = \exp(-d/L)$, where L is a scale length that can vary with altitude, climate, season, and direction. However, L = 1000 km is a typical value for temperature. With the spacing d = 85 km in a previous AIRS simulated data set (see section 3.1.3.a), the value of α was set to 0.08 for temperature. Currently $\alpha = 1$ is used for relative humidity (i.e., no correlation). These values have not been optimized.

Cosmic Background Brightness Temperature

Planck's equation for radiant intensity is a nonlinear function of temperature. However, at microwave frequencies, the physical temperatures encountered in the earth's atmosphere lie at the high-temperature asymptote of this function. Hence, as discussed by Janssen (1993), brightness temperature can be used as a surrogate for radiance in the equation of radiative transfer, within an accuracy of a few hundredths of a Kelvin. The only exception to this statement occurs with the cosmic background, which must be assigned an effective brightness temperature at frequency ν of

$$\Theta_C = (h\nu/2k)\,(e^{h\nu/kTc} + 1)\,(e^{h\nu/kTc} - 1)^{-1}, \qquad (4.1.2)$$

instead of its actual temperature $T_c = 2.73K$, in order to linearize Planck's function.

Estimation of Surface Brightness

From the window channels of AMSU-A, an estimate of the surface brightness Θ_S, which is the product of the surface emissivity and surface temperature, is obtained by correcting the measured brightness temperatures Θ^* for atmospheric attenuation and emission due to oxygen and water vapor. This correction is done by computing τ, the one-way transmittance of the atmosphere; Θ_{direct}, the component of brightness temperature emitted from the atmosphere on a direct path to space; and Θ_{sky}, the sky brightness temperature as observed from the surface. The 'measured' surface brightness is given by:

$$\Theta_S^* = [(\Theta^* - \Theta_{direct}) / \tau - \Theta_{sky}] / (1 - \Theta_{sky}/T_S) \qquad (4.1.3)$$

in which T_S is the surface temperature from the initial profile. The four-parameter model of Grody (1988):

$$\Theta_S = [T_o + (\nu/\nu_o)^s T_\infty] / [1 + (\nu/\nu_o)^s], \qquad (4.1.4)$$

is used to represent the surface brightness spectrum. If the slope of surface brightness between 31 and 50 GHz is positive, or if the surface brightness at 31 GHz is less than 180 K, then the surface is categorized as a wet scatterer. In this case, s = 1.2 and $T_\infty = 0.93\ T_S$. Otherwise, the surface is categorized as frozen; then $T_0 = 0.93\ T_S$ and $\nu_0 = 31.4$ GHz. The frequency ν_0 is typically 31 - 33 GHz for ice and snow (Grody, 1988) but the use of channel 2's frequency simplifies the equations. The model is based on aircraft and ground-based measurements and theoretical calculations for nadir view and may be revised after experience with AMSU-A and -B data from NOAA satellites.

With two of the four parameters fixed and Θ_S given at 31 and 50 GHz, Eq. (4.1.4) is solved for the remaining two parameters. The algorithm then computes Θ_S for the sounding frequencies that are sensitive to the surface. If Θ_S (31 GHz) < 250 K, an adjustment to the initial water vapor column density is computed as

$$R_{H2O} = 1 + \ln[(T_{H2O} - \Theta_{S1}) / (T_{H2O} - \Theta_{S1}^*)] / 2\beta_1 \qquad (4.1.5)$$

where Θ_{S1} is the surface brightness temperature at 24 GHz calculated from Eq. (4.1.4), Θ_{S1}^* is the "measured" value, β_1 is the one-way water vapor opacity at 24 GHz through the atmosphere, and T_{H2O} is the vapor-weighted mean atmospheric temperature. The atmospheric correction is then recomputed for 24 to 50 GHz with the water vapor profile multiplied by R_{H2O}. The equations are iterated until

$$\sum_{i=1}^{3} [(\Theta_{Si}^* - \Theta_{Si})\ \tau_i^2 / N_i]^2 < 3, \qquad (4.1.6)$$

where τ_i is the computed one-way atmospheric transmittance for channel i, and N_i is the RMS noise level of channel i. If the number of iterations exceeds a preset limit, an error code is returned.

Treatment of the Surface Temperature

If Θ_S were divided by surface temperature T_S to obtain emissivity for use in the temperature profile retrieval, then an error due to the variance of the *a priori* surface temperature would be introduced. Instead, the equation of radiative transfer is written in the form

$$\Theta = \Theta_{direct} + \tau\ (\Theta_S + \Theta_{sky} - \Theta_{sky}\ \Theta_S / T_S) \qquad (4.1.7)$$

where Θ is the brightness temperature emitted from the top of the atmosphere.

The atmospheric temperature vector is augmented by T_S, which is considered to be distinct from the air temperature near the surface. The measured Θ's used in the temperature profile retrieval are the 11 oxygen-band channels of AMSU-A, not including

the 50.3 GHz channel (which was used to obtain Θ_S). The sensitivities of the measured Θ's to the elements of the temperature profile vector constitute the observation matrix. The elements of this matrix corresponding to the atmospheric part of the temperature vector are given by the atmospheric weighting functions. The elements corresponding to T_S are obtained by partial differentiation of Eq. (4.1.7):

$$\partial\Theta/\partial T_S = \tau T_{sky}\,\Theta_S / T_S^{\,2} \qquad (4.1.8)$$

The dependence on T_S is nonlinear here, because Θ_S is considered to be a known input.

The covariance of the temperature vector is also required by the estimation algorithm described below. The atmospheric covariances were obtained from the TIGR data set (Chedin *et al.*, 1985). The difference between T_S and the air temperature near the surface (T_{1013}) is assumed to have zero mean and standard deviation of 4 K. Thus, T_S has a larger variance, by 16 K^2, than T_{1013}, but its covariances with other levels are equal to those of T_{1013}.

Estimation of the Temperature Profile

Given the initial profile $\tilde{T}$, the estimated profile is to be determined from a vector Θ^* of observed brightness temperatures, which for small difference profiles $T-\tilde{T}$ is related to the true profile T by

$$\Theta^* = \Theta(\tilde{T}) + \mathbf{W}(\tilde{T})[T - \tilde{T}] + e \qquad (4.1.9)$$

in which $\Theta(\tilde{T})$ is the brightness temperature vector that would theoretically be emitted from the atmospheric profile described by $\tilde{T}$ and the rows of the matrix $\mathbf{W}(\tilde{T})$ are weighting functions, whose elements are in general dependent on the profile; e represents unknown measurement errors. Although not explicit in equation (4.1.9), the weighting functions in the microwave band also depend on Θ_S, on surface pressure, on humidity, and at very low pressures on the magnetic field. If the validity of a channel is zero, then the row of **W** corresponding to that channel is set to zeros. The dimensions of the matrix remain the same.

The new, minimum-variance estimate of T is obtained by Newtonian iteration (Rodgers, 1976, Eq. 101)

$$\hat{T}_n = \tilde{T} + \tilde{\mathbf{R}}_{\mathbf{T}}\mathbf{W}^t(\hat{T}_{n-1})X \qquad (4.1.10)$$

where $\tilde{\mathbf{R}}_T$ is the covariance matrix of $T - \tilde{T}$, X is the solution vector to

$$\left[\mathbf{W}(\hat{T}_{n-1})\tilde{\mathbf{R}}_T\mathbf{W}^t(\hat{T}_{n-1}) + \mathbf{R}_e\right]X = \Theta^* - \Theta(\hat{T}_{n-1}) + \mathbf{W}\,(\hat{T}_{n-1})\left[\hat{T}_{n-1} - \tilde{T}\right] \qquad (4.1.11)$$

and $\mathbf{R}_e$ is the (normally diagonal) covariance matrix of *e*. Superscript t indicates transpose and $\hat{T}_0 = \tilde{T}$. $\mathbf{R}_e$ includes the effects of surface brightness uncertainty and instrument noise. Iteration of Eqs. (4.1.10) and (4.1.11) stops when one of the following conditions is met : (1) the estimate $\hat{T}_n$ meets the closure criterion

$$\sum_{i=1}^{N_B} [\Theta_i^* - \Theta_i(\hat{T}_n)]^2 / NE\Delta T_i^2 \le N_B, \qquad (4.1.12)$$

where $NE\Delta T_i$ is the instrument noise on channel i and N_B is the number of valid elements in Θ^*; or (2) when successive computations of the left side of (4.1.12) change by less than 1% of the right side; or (3) when the number of iterations exceeds a preset limit, currently 8.

Estimation of Relative Humidity and Clouds

This algorithm is based on retrieval methods described by Wilheit (1990) and Kuo *et al.* (1994). Retrieval of RH uses the four channels of HSB and the 89 GHz channel of AMSU-A. In the present algorithm, the HSB measurements are averages in 3 x 3 spatial arrays which aproximate the AMSU-A field of view. The measurements of brightness temperature are a result of the vertical profile of atmospheric opacity relative to temperature in the atmosphere. To distinguish between opacity, at a given altitude, due to water vapor and opacity due to liquid water, it is necessary to introduce some *a priori* information or constraint. For this purpose, cloud coverage is parameterized as in the stratiform condensation model of Sundqvist *et al.* (1989), where a relative humidity threshold determines the onset of condensation. If the instrument had infinitesimal horizontal resolution, an appropriate threshold would be 100% relative humidity. However, it is assumed that the condensation process is not spatially resolved, hence the threshold is less than 100%. Currently, the threshold is

$$RH_{cth} = \begin{cases} 75\% - \text{land} \\ 80\% - \text{water} \end{cases} \tag{4.1.13}$$

which is the same as in NCEP's Eta model, which was used to generate the simulation data. It is anticipated that these thresholds will be adjusted after experience with AMSU-B data.

The RH profile stored by the algorithm has a composite definition. When RH is less than 100%, it is interpreted as the relative humidity of the <u>clear</u> part of the field of view. (If $RH \le RH_{cth}$, this is the entire field.) Within the cloudy part of the field, the water vapor profile is saturated. Hence, the average vapor density in the field of view is

$$\rho_v = \begin{cases} \rho_s \, RH/100, & \text{if } RH \le RH_{cth}, \\ \rho_s \, [(1 - b)\, RH/100 + b] & \text{if } RH_{cth} < RH \le 100, \\ \rho_s & \text{if } RH \ge 100, \end{cases} \tag{4.1.14}$$

where ρ_s is the saturation value of vapor density, and

$$b = (RH - RH_{cth}) / (100 - RH_{cth}). \tag{4.1.15}$$

The liquid water density ρ_L averaged over the field of view is assumed to be given by

$$\rho_L = \begin{cases} 0 & \text{if } RH \le RH_{cth}, \\ C_L \, \rho_S \, b & \text{if } RH > RH_{cth}, \end{cases} \tag{4.1.16}$$

where C_L is a preset constant, currently 0.04. In this way, RH (combined with ρ_s, which depends only on the temperature profile) serves to define both the vapor and cloud liquid water density profiles. Note that RH can take values > 100 in cloudy regions.

The saturation vapor density is computed from the retrieved temperature profile. Saturation vapor density is calculated with respect to liquid water (by extrapolation) even when the temperature is below 273 K, because ice clouds are not considered within the

context of this algorithm. (Absorption from ice is much less than from liquid water, and scattering is not included in the radiative transfer formulation.) This algorithm therefore allows supercooled liquid water and water vapor greater than the saturation value over ice.

Measured brightness temperature Θ^* is related to the RH profile by

$$\Theta^* = \Theta(\tilde{\mathrm{RH}}, \hat{\mathrm{T}}) + \mathbf{W}_{\mathrm{RH}}(\tilde{\mathrm{RH}}, \hat{\mathrm{T}})\left[\mathrm{RH} - \tilde{\mathrm{RH}}\right] + e \tag{4.1.17}$$

where $\Theta(\tilde{\mathrm{RH}}, \hat{\mathrm{T}})$ is a computed brightness temperature vector and the matrix $\mathbf{W}_{\mathrm{RH}}(\tilde{\mathrm{RH}}, \hat{\mathrm{T}})$ has elements which for a given channel and pressure layer are equal to

$$\mathbf{W}_{\mathrm{RH}}(\mathrm{RH,T}) = \partial\Theta/\partial\kappa \bullet (\partial\kappa/\partial\rho_v \bullet \partial\rho_v/\partial\mathrm{RH} + \gamma\, \partial\rho_L/\partial\mathrm{RH}), \tag{4.1.18}$$

where κ represents the opacity of the layer and $\gamma = \partial\kappa/\partial\rho_L$. The rapid transmittance algorithm computes the coefficient γ in the small-droplet (Rayleigh) approximation. Hence, it is intended to be applied only to non-precipitating cloud situations. A quadratic model is used to compute the opacity of water vapor:

$$\kappa = \beta_1\, \rho_v + \beta_2\, \rho_v^2 + \text{other contributions}; \tag{4.1.19}$$

hence

$$\frac{\partial\kappa}{\partial\rho_v} = \beta_1 + 2\beta_2\rho_v, \tag{4.1.20}$$

where

$$\beta_1 = \beta\left(\tilde{\rho}_v, \hat{\mathrm{T}}\right) - \beta_2\tilde{\rho}_v, \tag{4.1.21}$$

$$\beta_2 = d\beta / d\rho_v. \tag{4.1.22}$$

The coefficients β and $d\beta/d\rho_v$ are computed by the rapid transmittance algorithm using the temperature profile retrieval and the initial moisture profile. Recomputation on each iteration is unnecessary. As a consequence of (4.1.14-16) $\partial\rho_v/\partial\mathrm{RH}$ and $\partial\rho_L/\partial\mathrm{RH}$ depend on RH as follows:

$$\frac{\partial\rho_v}{\partial\mathrm{RH}} = \begin{cases} \rho_S/100, & \text{if } \mathrm{RH} \le \mathrm{RH}_{cth}, \\ .02\,(100\text{-}\mathrm{RH})\,\rho_S / (100 - \mathrm{RH}_{cth}), & \text{if } \mathrm{RH}_{cth} < \mathrm{RH} \le 100, \\ 0 & \text{if } \mathrm{RH} > 100, \end{cases} \tag{4.1.23}$$

$$\frac{\partial\rho_L}{\partial\mathrm{RH}} = \begin{cases} 0, & \text{if } \mathrm{RH} < \mathrm{RH}_{cth}, \\ C_L\, \rho_S / (100 - \mathrm{RH}_{cth}), & \text{if } \mathrm{RH} \ge \mathrm{RH}_{cth}, \end{cases} \tag{4.1.24}$$

The estimate of the RH profile is obtained by iteration of equations similar to (4.1.10) and (4.1.11), except that Eyre's (1989a) method of damping is used to avoid large relative humidity increments, because of the nonlinearity of the problem:

$$\hat{\mathrm{RH}}_n = \hat{\mathrm{RH}}_{n-1} - \delta\left[\hat{\mathrm{RH}}_{n-1} - \tilde{\mathrm{RH}}\right] + \delta\, \tilde{\mathrm{R}}_{\mathrm{RH}}\, \mathrm{W}^t_{\mathrm{RH}}\left(\hat{\mathrm{RH}}_{n-1}, \hat{\mathrm{T}}\right) \mathrm{X}_{\mathrm{RH}} \tag{4.1.25}$$

in which $\tilde{R}_{RH}$ is the *a priori* covariance matrix of $RH - \tilde{R}H$, X_{RH} is the solution vector to

$$\left[W_{RH}\left(\hat{R}H_{n-1},\ \hat{T}\right)\delta\tilde{R}_{RH}\ W_{RH}^{t}\left(\hat{R}H_{n-1},\ \hat{T}\right) + R_e\right] X_{RH} = \Theta^* - \Theta\left(\hat{R}H_{n-1},\ \hat{T}\right) + W(\hat{R}H_{n-1},\ \hat{T})\ \delta\left[\hat{R}H_{n-1}\ -\ \tilde{R}H\right], \tag{4.1.26}$$

and

$$\delta = \begin{cases} 1 \text{ if } \Theta_i^* - \Theta_i\left(\hat{R}H_{n-1},\ \hat{T}\right) \le 10 \text{ K for all i,} \\ 0.1 \text{ otherwise.} \end{cases} \tag{4.1.27}$$

Here δ is a scalar rather than a matrix as in Eyre's paper. For the moisture channels, the measurement error covariance $\mathbf{R_e}$ is the sum of contributions due to surface brightness uncertainty, instrument noise, and a diagonal error of $(1.5\ K)^2$ which approximately represents errors in $\Theta(\tilde{R}H, \hat{T})$ resulting from errors in the temperature profile retrieval. The convergence criterion is similar to the temperature algorithm. Because convergence is determined from the brightness temperature residuals, which in turn are computed using the vapor and liquid column densities, the role of RH in this algorithm is only to introduce the *a priori* statistics and constraints.

There is a discontinuity in $W_{RH}(RH,T)$ at $RH = RH_{CTH}$ due to eqs. (4.1.23-24). To compensate in an approximate way for this effect, when RH crosses the RH_{CTH} threshold in the positive direction on any iteration, the increment of RH above RH_{CTH} is divided by 5. There is no discontinuity at RH = 100. After each iteration, the water vapor and liquid water profiles are computed from the new RH, using (4.1.14-16). Subsequent iterations then use the appropriate absorption coefficient for liquid or vapor. Finally, the estimated $\hat{R}H$ profile is limited by zero from below and from above by a value which converts to 0.01 g/cm^2 liquid column density, per layer. This latter value is intended to approximate non-precipitating cloud densities, and hence it will tend to leave large brightness temperature residuals in situations of precipitation, and expecially when scattering is occurring. If the left side of eq. 4.1.12, computed for the five moisture channels, is greater than a preset threshold value, then the ice scattering flag will be set at all altitudes for which clouds are present and the temperature estimate is below 273 K. On the basis of experience with SSM/T2 data, the scattering threshold is currently set at 500.

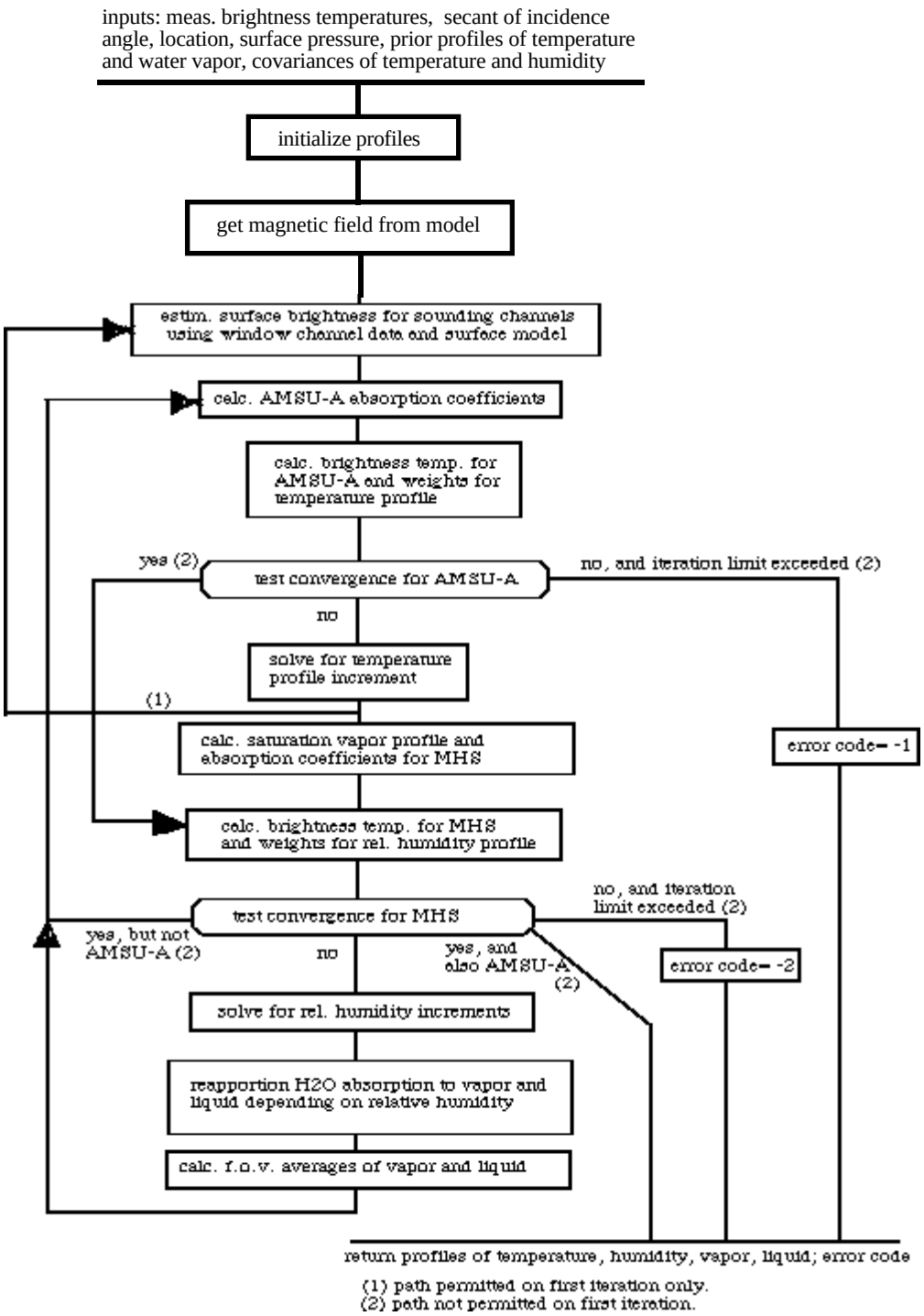

FIGURE 4.1.1. MICROWAVE INITIAL-GUESS ALGORITHM.

4.2 First Product -- (Goldberg/McMillin)

The cloud clearing/retrieval system supplied by NOAA provides a "first product" of level 1B radiance, and level 2 surface, temperature, and moisture parameters using combined InfraRed(IR) and MicroWave(MW) measurements from the AIRS/AMSU/HSB instrument suite. The system produces the following outputs: (i) cloud cleared radiances for the entire AIRS spectrum; (ii) retrieved temperature and moisture profiles; (iii) retrieved surface temperature; and, (iv) retrieved IR and MW surface emissivity and reflectivity. Both the first guess and physical retrievals are produced for (ii) & (iii), while currently only a first guess retrieval is produced for (iv). These products provide a first solution to which additional adjustments are made by a final product system (described in Section 4.3).

The "first product" system is composed of three major components:

1. Cloud clearing procedure that produces clear column AIRS radiances in cloud contaminated fields of view
2. A regression procedure that produces first guess retrievals from AIRS/AMSU/HSB observations
3. A rapid physical retrieval procedure to produce retrievals from AIRS/AMSU/HSB observations using the output from (2) as an initial guess.

Each of these components will be discussed in detail below.

Level 1 Cloud Clearing Algorithm

The function of cloud clearing is to obtain clear column (cloud cleared) AIRS radiances from partially cloudy ones so that the retrieval process can be applied to the cloud cleared radiances. The basic approach of infrared radiance cloud clearing, as introduced by Smith (1968) as the N^* technique, and by Chahine (1970, 1974) as the Eta technique, is an approach in which cloudy information in "adjacent pairs" are used to extract clear radiances. NOAA has been developing and using cloud clearing procedures based on the N^* technique (McMillin and Dean, 1982) in its TOVS retrieval operations. The cloud clearing technique used for AIRS/AMSU/HSB has several important modifications from the current approach used in TOVS operations. The modified cloud clearing procedure is capable of utilizing the AIRS high spectral resolution data and operating in the presence of two layer gray clouds.

NOAA's cloud clearing technique is composed of (1) an eigenvector noise reduction of observed AIRS radiances, (2) an AMSU regression estimation of AIRS driver channels, and then (3) a two-layer cloud clearing based on quantities calculated from the two previous steps. To introduce the entire notion in a more logical way, fundamental concepts are discussed first and each of the steps is laid out as the discussion progresses.

Fundamental Concepts of NOAA Cloud Clearing

In the simulation study, two layer, non-overlapping clouds are present in the observational FOV. The clouds are assumed to be gray having infrared emissivities independent of frequency. Under these assumptions, the observed infrared radiance of any cloudy channel at frequency ν is expressed as:

$$\mathbf{R}^{\nu} = (1 - \alpha_1\varepsilon_1 - \alpha_2\varepsilon_2)\,\mathbf{R}^{\nu}_{c} + \alpha_1\varepsilon_1\,\mathbf{R}^{\nu}_{o1} + \alpha_2\varepsilon_2\,\mathbf{R}^{\nu}_{o2} \tag{4.2.1}$$

where $\mathbf{R}^{\nu}_{c}$ denotes the clear column radiance at wavenumber ν, $\mathbf{R}^{\nu}_{o1}$ denotes the overcast radiance if the first (lower) cloud covers the entire field of view, and $\mathbf{R}^{\nu}_{o2}$ denotes the overcast radiance if the second (higher) cloud covers the entire field of view. In Equation (4.2.1) α_1, ε_1 and α_2, ε_2 are the cloud fractions and cloud emissivities of the first and second clouds, respectively. Note that Equation (4.2.1) satisfies not only cloudy channels affected by both clouds but also the channels affected by one cloud or even clear channels. For example, if the weighting function peak of one channel is between the lower and higher clouds, and therefore only contaminated by the higher cloud, then overcast radiance of the channel for the low cloud is just the clear radiance ($\mathbf{R}^{\nu}_{o1} = \mathbf{R}^{\nu}_{c}$) and the equation degrades to a single cloud formation equation.

By rewriting Equation (4.2.1) and defining variables

$$\mathbf{R'}^{\nu} = \mathbf{R}^{\nu} - \mathbf{R}^{\nu}_{c},$$

$$\mathbf{R'}^{\nu}_{o1} = \mathbf{R}^{\nu}_{o1} - \mathbf{R}^{\nu}_{c}, \tag{4.2.2}$$

$$\mathbf{R'}^{\nu}_{o2} = \mathbf{R}^{\nu}_{o2} - \mathbf{R}^{\nu}_{c},$$

we have following equation:

$$\mathbf{R'}^{\nu} = \alpha_1\varepsilon_1\,\mathbf{R'}^{\nu}_{o1} + \alpha_2\varepsilon_2\,\mathbf{R'}^{\nu}_{o2} \tag{4.2.3}$$

Now if we have three channels with frequencies ν_1, ν_2 and ν_3 , Equation (4.2.3) may be written for each of the channels as follows:

$$\mathbf{R'}^{1} = \alpha_1\varepsilon_1\,\mathbf{R'}^{1}_{o1} + \alpha_2\varepsilon_2\,\mathbf{R'}^{1}_{o2} \tag{4.2.4}$$

$$\mathbf{R'}^{2} = \alpha_1\varepsilon_1\,\mathbf{R'}^{2}_{o1} + \alpha_2\varepsilon_2\,\mathbf{R'}^{2}_{o2} \tag{4.2.5}$$

$$\mathbf{R'}^{3} = \alpha_1\varepsilon_1\,\mathbf{R'}^{3}_{o1} + \alpha_2\varepsilon_2\,\mathbf{R'}^{3}_{o2} \tag{4.2.6}$$

where the superscripts 1, 2 and 3 represent the corresponding channels with frequencies ν_1, ν_2 and ν_3, respectively. Equations (4.2.4), (4.2.5) and (4.2.6) indicate that the observed radiances of the three channels lie on a plane that is defined by the three points ($\varepsilon_1\mathbf{R'}^{1}_{o1}$, $\varepsilon_2\mathbf{R'}^{1}_{o2}$), ($\varepsilon_1\mathbf{R'}^{2}_{o1}$, $\varepsilon_2\mathbf{R'}^{2}_{o2}$), and ($\varepsilon_1\mathbf{R'}^{3}_{o1}$, $\varepsilon_2\mathbf{R'}^{3}_{o1}$). The radiance for one channel can be expressed as a linear combination of the radiances at the other two channels as:

$$\mathbf{R'}^{1} = \mathbf{a}\,\mathbf{R'}^{2} + \mathbf{b}\,\mathbf{R'}^{3} \tag{4.2.7}$$

where **a** and **b** are constants. Combining Equations (4.2.2) and (4.2.7) gives the following equation:

$$\mathbf{R}^{1} = \mathbf{a}\,\mathbf{R}^{2} + \mathbf{b}\,\mathbf{R}^{3} + \mathbf{c} \tag{4.2.8}$$

where **c** is determined by an arbitrary point in the plane defined by Equation (4.2.7). $\mathbf{R'}^{i}_{o1}$ and $\mathbf{R'}^{i}_{o2}$ in Equation (4.2.7) as well as **a**, **b** and **c** in Equation (4.2.8) are fixed once the two cloud heights are defined. Equation (4.2.8) shows the equation for the plane defined in three dimensional space for several fields of view with the same low cloud height and

same high cloud height but varying cloud fractions for the two non-overlapping cloud formations. Therefore if we can (1) determine the relationship among the three channels (i.e. find constants **a**, **b** and **c**), and (2) determine clear column radiance for two of the three channels (e.g. $\mathbf{R}^2_c$ and $\mathbf{R}^3_c$),we can determine the clear column radiance of the third channel from Equation (4.2.9).

$$\mathbf{R}^1_c = \mathbf{a}\,\mathbf{R}^2_c + \mathbf{b}\,\mathbf{R}^3_c + \mathbf{c} \qquad (4.2.9)$$

Values of **a**, **b**, and **c** are found by taking the 9 values for a 3 by 3 array. These 9 measurements give 9 values of $\mathbf{R}^1$, $\mathbf{R}^2$, and $\mathbf{R}^3$, resulting in system of 9 equations for the 3 unknowns (**a, b, and c**). The solution is obtained by subtracting the mean values and doing a least squares solution for **a** and **b**. In this case, the expansion is about the mean of the values of the 9 samples since the clear values are not known. The value of **c,** is given by

$$\mathbf{c} = \overline{\mathbf{R}^1} - \mathbf{a}\,\overline{\mathbf{R}^2} - \mathbf{b}\,\overline{\mathbf{R}^3} \qquad (4.2.10)$$

where the bars represent average values.

In NOAA's two layer cloud clearing technique, two AIRS channels ν_2 and ν_3 are selected as driver channels to derive clear column radiance for any other channel $\mathbf{R}^1_c$. As expressed in Equation (4.2.9), $\mathbf{R}^2_c$ and $\mathbf{R}^3_c$ are necessary for calculating $\mathbf{R}^1_c$, therefore one of the criteria for selecting ν_2 and ν_3 is that there should be an easy and accurate way to determine $\mathbf{R}^2_c$ and $\mathbf{R}^3_c$. Once the driver channels are selected, the relationship between these drivers and any other channel ν_1, as expressed in Equation (4.2.8), needs to be determined so that Equation (4.2.9) can be used with knowledge of $\mathbf{R}^2_c$ and $\mathbf{R}^3_c$. In the following sections, procedures for calculating cleared radiances for driver channels, selecting drivers, and determining the relationship between the driver channels and the other channels will be presented. Finally, other important issues related to improving cloud clearing accuracy will be discussed.

Obtaining Clear Radiances for Driver Channels

In the preliminary version of NOAA's cloud clearing algorithm, there are two methods to determine driver channel clear radiance $\mathbf{R}^2_c$ and $\mathbf{R}^3_c$: (1) Use regression to estimate AIRS drivers from AMSU measurements making use of AMSU's ability to penetrate clouds; (2) Integrate retrieved geophysical data to obtain AIRS drivers. Both methods are used in the system depending on the resources available and the steps in the process.

AMSU regression is used to perform the initial cloud clearing since clouds are fairly transparent to microwave radiation and there is no other source of information about $\mathbf{R}^2_c$ and $\mathbf{R}^3_c$. Sources of error in the cloud clearing include AMSU instrumental noise, cloud liquid water contamination of the microwave measurement, microwave emissivity and regression uncertainty. The different surface response of the two instruments is a major source of error. Infrared and microwave emissivities and reflectivities respond differently to different surfaces (vegetation, sand, water etc.). These differences will be reflected in the regression uncertainty and eventually contribute to the cloud clearing error.

A simulated training data set of 12000 AIRS/AMSU collocated measurements covering all seasons is used to calculate regression coefficients to estimate AIRS clear radiances from AMSU brightness temperatures. In principle, AMSU temperature channels that are minimally affected by water vapor and surface contributions are the best candidates

in predicting AIRS drivers, which are preferably also temperature channels. When clouds are present AMSU temperature channels are also contaminated by cloud liquid water (Staelin *et al.*, 1975 and Grody *et al.*, 1980). To minimize these impacts, AMSU water burden channels 1, 2 and 15 (which are sensitive to liquid water) are included in the regression to correct the liquid water contamination in AIRS clear driver estimations.

Regression coefficients for predicting the brightness temperatures of the AIRS driver channels from the AMSU measurements are calculated using the 'Noise Guided Stepwise Regression' as described by McMillin (1991).

The AIRS forward calculation from the retrieval is used when a previous round of cloud clearing/retrieval procedure is finished and there is need to iterate the procedure for more accurate results. A forward model first calculates atmospheric transmittances for the designated AIRS channels from geophysical profile data, then integrates the transmittances with the Planck function to simulate clear column radiances (Susskind, *et al.*, 1983). The advantage of this method is that one can simulate and use the clear driver radiances without instrumental noise in deriving other AIRS clear radiances. Of course, the condition of using this method is that one has to have relatively accurate retrieval to start with. The preliminary version of NOAA's cloud clearing/retrieval algorithm has the option of one iteration which yields a significant improvement in some of the test cases.

Selecting Cloud Clearing Driver Channels

The selection of driver channels depends on several factors. Because clear radiances of the selected driver channels will later be used to derive clear radiances of all other AIRS channels, a great deal of effort should be made to satisfy following conditions in the selection process:

- There should be an easy and accurate way to calculate the clear radiances of the driver channels.
- Ideally one of the drivers should have it's weighting function peak at or lower than the lowest cloud top so that it is sensitive to the low cloud as well as the high cloud. The other driver should have it's weighting function peak close to the level of the second cloud to maximize the independent response to the second cloud.
- Instrumental noise in the driver channel radiances should be minimized before deriving the relationship expressed by Equation (4.2.8)

For an AMSU regression estimation of AIRS clear drivers, the regression coefficients are calculated from the training AIRS/AMSU simulated observations. The coefficients are then applied back to the training data set itself for dependent testing. Those AIRS temperature channels that yield the smallest RMS differences in the dependent test are selected as clearing driver channels.

Multiple clouds in the FOV may have single or multiple cloud formations as defined by Chahine (1977). Re-examining Equation (4.2.5) and (4.2.8) reveals that if α_1/α_2 is constant among nine AIRS spots (i.e. the AMSU footprint has only one cloud formation) then only one cloud clearing driver is needed. However, if there are two cloud formations, the second driver channel is necessary to provide adequate information for cloud clearing.

Currently, the simulated clouds are at or above 850 mb, AIRS channels with weighting function peaks around 875-825 mb will be contaminated by both clouds regardless of the cloud formation. Therefore an AIRS temperature channel in this region

that yields a minimum RMS residual in the AMSU regression dependent test can always be used as driver $\mathbf{R}^2$ to establish the relationship in Equation (4.2.8). The first clearing driver is illustrated in Figure 4.2.1 with it's weighting function plotted as a blackened solid line.

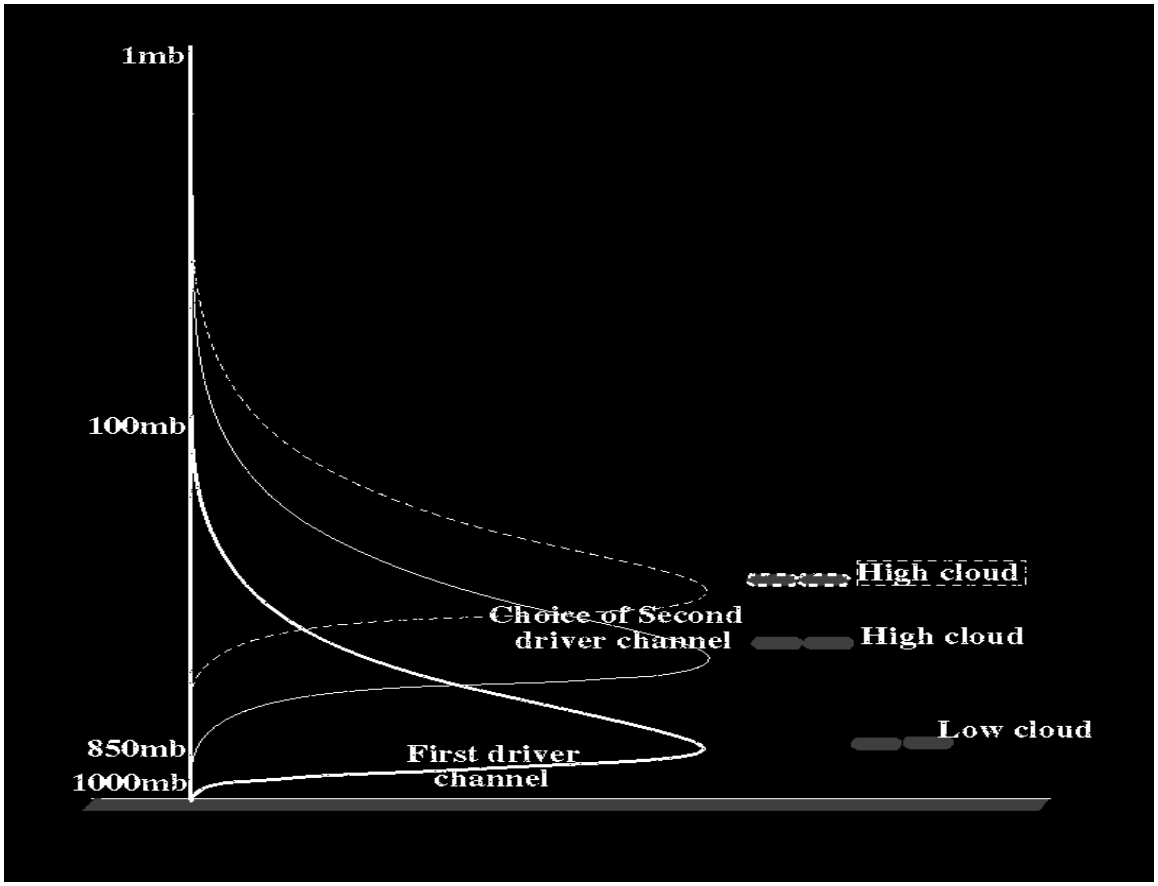

FIGURE 4.2.1 CLOUD CLEAR DRIVER CHANNEL SELECTIONS

In two cloud formation cases, we need to find a second driver channel that is only contaminated by the higher cloud. As shown in Figure 4.2.1, if the high cloud top is around 600 mb the second driver should to have it's weighting function peak around 600 mb as illustrated by the thin solid line. If the high cloud top is higher than 600 mb (as illustrated by the broken box plot), the second cloud clearing driver should be the one shown by the broken line. One consideration in selecting a second driver when two cloud formations are present is that the second driver should maximize its response to the high cloud only and consequently have a different behavior from the first driver. The best driver channel to detect the high cloud would be one that differs from the first driver (in terms of weighting function peaks) but is still at or under the high cloud so that it responds only to the high cloud. This makes it independent from the first driver. Of course, the cloud heights are not known.

To find the appropriate second driver, three candidates, having weighting function peaks around 600 mb, 400 mb and 200 mb respectively, are examined. The dependency of each of the candidate drivers upon the first driver is calculated in terms of the correlation coefficient. An inter-comparison of these calculated correlations is conducted. The candidate that is most independent of the first driver (i.e. gives the smallest correlation with the first driver) is selected as second driver and its radiance is used as $\mathbf{R}^3$.

In practice, the clearing drivers are not actually two channels but two groups of channels having the same weighting function peak heights within the group, but distinct weighting function peak heights between the groups. Radiances of channels in a group are averaged and used in the cloud clearing as one driver channel in Equation (4.2.8). This minimizes the instrumental noise. Table 4.2.1 lists selected groups of channels and their weighting function peak pressures.

Weighting Function Peak Pressure	875-825 (mb)	625-600 (mb)	425-400 (mb)	200-180 (mb)
	725.693	725.391	704.539	688.003
Driver Channel	726.601	729.939	706.009	691.164
Frequency ($1/cm^{-1}$)	728.116	739.428	706.303	691.452
	749.978	742.207	721.472	693.183

TABLE 4.2.1 SELECTED AIRS CLOUD CLEARING DRIVER CHANNELS

Each group has four channels (with weighting function peaks around the same pressure) to be averaged. However, radiance values for different channels can have a wide range even when they all correspond to the same atmospheric region due to the wavelength dependence. A direct average of radiances would over emphasize channels with large radiance values and neglect those with small radiance values. An effective average radiance is introduced as a weighted average of radiances of different channels. The weight of each channel is proportional to the inverse of the Planck function $\mathbf{B(\nu, T_0)}$ at a fixed temperature $\mathbf{T_0}$ = 270K, and frequency of this channel.

$$\mathbf{R_{ave}^{eff} = \Sigma\ w(\nu)\ R^{\nu}} \qquad (4.2.11)$$

$$\mathbf{w(\nu) \propto 1 / B\ (\nu, T_0\ )} \text{ and } \quad \mathbf{\Sigma\ w(\nu) = 1} \qquad (4.2.12)$$

where $w(\nu)$ is the weight of the channel with frequency ν in the driver group.

Determining Cloud Clearing Relationship

Having selected the cloud clearing driver channels and obtained the driver clear radiance, we will determine the relationship expressed in Equation (4.2.8). The determination of values of a, b and c in Equation (4.2.8) from AIRS observations is discussed next.

In the AIRS/AMSU simulation study, one AMSU footprint covers nine AIRS spots each of which has the same cloud type and height but different cloud fractions. For any given AIRS channel, the only difference among the nine radiances is due to the difference of cloud fractions and AIRS instrumental noise. The AIRS radiance is linearly related with cloud fractions among the nine AIRS footprints. This linear relationship also holds true for the cloud clearing driver effective average radiance which is a linear combination of AIRS radiances. These assumptions in the simulation indicate that AIRS radiances satisfy Equation (4.2.8) to within the AIRS noise level in an AMSU footprint. Using the nine AIRS observations as samples, the relationship between any channel and the two drivers (defined by **a**, **b** and **c**) can be found with a multiple regression.

Having determined the relationship between any AIRS channel radiance $\mathbf{R^1}$ and the two clearing drivers $\mathbf{R^2}$ and $\mathbf{R^3}$, we can calculate the clear radiance $\mathbf{R^1_c}$ of any channel from Equation (4.2.9) with the knowledge of the driver clear radiances $\mathbf{R^2_c}$ and $\mathbf{R^3_c}$.

AIRS Cloudy Radiance Noise Reduction

As in the N^* technique, NOAA's AIRS cloud clearing procedure is also sensitive to AIRS random instrumental noise. In the relationship between the driver channels and a given AIRS channel, coefficients **a, b** and **c** are affected when noise is present. Any error in the relationship will be carried to clear radiances when applying Equation (4.2.9). Before cloud clearing, any procedure that can reduce the observational noise level will be helpful in calculating accurate values of **a, b** and **c**, and consequently will improve the cloud clearing. An eigenvector analysis is introduced to reduce or remove the random factor (noise) in the observation data.

In order to reduce the noise, the AIRS brightness temperature observations are converted to an eigenvector expansion. The 30 coefficients associated with the 30 largest eigenvalues are kept and used to regenerate the radiances. Since errors tend to be associated with the smaller eigenvectors which are the ones that are ignored, this procedure reduces the random errors in the reconstructed radiances.

Cloudy and Clearing Channels under Cloudy Conditions

An important fact about cloud contamination of infrared observations is that, even in cloudy conditions, not all the infrared channels are affected by clouds. For example, if one AIRS channel is sensitive to the upper portion of the atmosphere, and therefore not contaminated by any low clouds, it should not be cleared if only low clouds are present. In this case averaging the nine AIRS spot radiances for this channel is the best solution for clear radiance. Clearing such a channel would only greatly amplify the noise. We therefore need to determine if a channel is cloudy or clear before proceeding to cloud clearing.

As shown in Equation (4.2.1), if a channel is cloud contaminated its radiance must be linearly related to the cloud fraction. In the simulation, and most likely in reality, the cloud fractions in the nine AIRS spots are variable, hence, for any cloudy channel with frequency ν the radiance standard deviation $\sigma(\nu)$ $(= 1/3 \sqrt{\Sigma [R_i(\nu)-R_{ave}(\nu)]^2}$, $i = 1,...,9)$ over the nine spots must be greater than a threshold (currently half of the channel's instrumental noise level) to reflect the existence of variable cloudiness. Homogeneous AIRS radiances over an AMSU footprint indicate the footprint is either clear or overcast for this AIRS channel. The quantity $\sigma(\nu)$ can then be used to indicate cloud contamination of any channel.

Weighting function peaks of all AIRS channels are pre-calculated and stored to help decide if a channel should be cleared. All AIRS channels are ordered in terms of weighting function peak pressures in an ascending sense. Cloud clearing proceeds from the bottom channel to the top. Each channel is checked to see if :

$$\sigma(\nu) > 0.5\ NE\Delta R(\nu) \qquad (4.2.13)$$

where $NE\Delta R(\nu)$ is the noise equivalent radiance for that channel. If Inequality (4.2.13) is true, this channel is cleared using Equation (4.2.9) and the next channel is considered. If Inequality (4.2.13) is false, all nine AIRS radiances are averaged to get the clear radiance. When the number of times Inequality (4.2.13) is false reaches 10, the cloud top is considered to be reached and all the remaining channels are assumed clear and clear radiances are calculated from averaging the nine radiances.

First Guess Regression Procedure

NOAA/NESDIS uses an eigenvector global regression procedure to provide fast and accurate initial guesses for temperature and moisture profiles as well as surface emissivity and reflectivity using simulated AIRS/AMSU/HSB data. It is assumed that all independent AIRS radiances have been preprocessed by the cloud clearing module described in the last section. Following the approach of Smith & Woolf (1976), eigenvectors from a brightness temperature covariance matrix, calculated over some dependent training ensemble, are used as basis functions to represent the AIRS/AMSU/HSB radiometric information. Eigenvectors of covariance matrices are commonly referred to as Empirical Orthogonal Functions (EOF's) in the literature, a convention that will be adopted throughout the remainder of this section. Because of the large number of channels measured by AIRS/AMSU/HSB, the eigenvector form of regression is crucial for exploiting the information content of all channels in a computationally efficient form. By representing radiometric information in terms of a reduced set of EOF's (much fewer in number than the total number of instrument channels) the dimension of the regression problem is reduced by approximately two orders of magnitude. Another advantage of using a reduced set of EOF's is that the influence of random noise is reduced by elimination of higher order EOF's which are dominated by noise structure. It should be noted that if all EOF's are retained as basis functions the eigenvector regression reduces to the ordinary least squares regression solution in which satellite measurements are used directly as predictors. The mathematical derivation of the EOF regression coefficients is detailed in the following sub-sections.

Generating the Covariance Matrix and Regression Predictors

A training ensemble of temperature, humidity, and ozone profile data are used to generate brightness temperatures for all AIRS/AMSU/HSB channels. The deviations of the brightness temperatures from their sample mean are stored in the matrix $\Delta\Theta_{Train}$, a matrix of dimensions [**nchan** x **nsamp**], where **nsamp** is the sample size of the training data set and **nchan** is the total number of instrument channels. The brightness temperature covariance matrix from which the EOF's are derived is then generated as follows:

$$\Theta_{cov} = \frac{1}{\mathbf{nsamp}} \Delta\Theta_{Train}(\Delta\Theta_{Train})^T \qquad (4.2.14)$$

where superscript T denotes matrix transpose and the matrix Θ_{cov} is a square matrix of order **nchan**. The diagonal elements of Θ_{cov} represent the variance of the respective channel brightness temperatures while the off diagonal elements represent the covariance between pairs of channels. An eigenvector decomposition is performed on the matrix Θ_{cov} giving:

$$\Theta_{cov} = \Gamma\Lambda\Gamma^T \qquad (4.2.15)$$

where Γ is the [**nchan** x **nchan**] matrix containing the eigenvectors, or EOF's, of Θ_{cov} in it's columns. Λ is the diagonal matrix of eigenvalues, the first eigenvalue being the first diagonal element, the second eigenvalue the second diagonal element etc. The EOF's are ordered in terms of the amount of the total data variance each explains; the first explains the most variance and each successive EOF explains progressively less of the total data variance. As discussed in the beginning of this section, some subset of the total number of EOF's is best for capturing the information content of the radiometric data while

minimizing the effects of random measurement noise. For the purposes of notation let **m** be the optimal number of EOF's for describing the information content of the covariance matrix from Equation (4.2.14). Considering the large number and interdependent nature of the AIRS/AMSU/HSB weighting functions it is reasonable to assume that **m** << **nchan**, where **m** represents in some sense the number of independent pieces of information available from the measurements. Experiments with AIRS/AMSU/HSB simulated data have shown **m** = 40 to be optimal for capturing the information content of the measurements from these three instruments. Only insignificant improvements in retrieval accuracy have been observed when using greater numbers of eigenvectors. Once **m** is determined from experimentation those EOF's are used as basis functions to represent the original brightness temperature information in terms of expansion coefficients commonly referred to as *principal components*. First we express $\Delta\Theta_{\text{Train}}$ as an expansion of the EOF's as follows:

$$\Delta T^{j}_{\text{Train}} = a^{j}_{1}\tilde{\Gamma}_{1} + a^{j}_{2}\tilde{\Gamma}_{2} + \cdots + a^{j}_{m}\tilde{\Gamma}_{m} \tag{4.2.16}$$

where $\Delta T^{j}_{\text{Train}}$ is the jth column of matrix $\Delta\Theta_{\text{train}}$ and $a^{j}_{1}, a^{j}_{2}, \cdots, a^{j}_{m}$ are the corresponding **m** principal components for the jth sample. In order to solve Equation (4.2.16) for the individual principal components recall that the EOF's $\tilde{\Gamma}_{1}, \tilde{\Gamma}_{2}, \cdots, \tilde{\Gamma}_{m}$ are mutually orthonormal. That is:

$$\tilde{\Gamma}_{i} \bullet \tilde{\Gamma}_{j} = \begin{cases} 1 & \text{for } i = j \\ 0 & \text{for } i \neq j \end{cases} \tag{4.2.17}$$

where (•) denotes the *inner product* of two vectors. Using the condition of orthonormality and the distributive property of the (•) operator, each individual principal component is expressed as:

$$a^{j}_{i} = \Delta T^{j}_{\text{Train}} \bullet \tilde{\Gamma}_{i} \qquad \begin{array}{l} i = 1, 2, \cdots, m \text{ and} \\ j = 1, 2, \cdots, \text{nsamp} \end{array} \tag{4.2.18}$$

Generating the Regression Coefficients

A standard least squares regression technique is used to generate regression coefficients using an *a priori* training data base such as an operational radiosonde match file. The following regression model is used to generate the coefficients:

$$\Delta V = C A_{\text{Train}} \tag{4.2.19}$$

where, ΔV is the matrix of deviations of the predictants (temperature, moisture etc.) from the training sample mean, A_{Train} is the [**m** x **nsamp**] matrix of principal components calculated using Equation (4.2.18), and C is the [**n** x **m**] matrix of regression coefficients to be solved for where **n** is the total number of predictants. More specifically:

$$\Delta V = \begin{bmatrix} V_1^1 - \overline{V}_1 & V_1^2 - \overline{V}_1 & \cdots & V_1^{nsamp} - \overline{V}_1 \\ \vdots & \vdots & \vdots & \vdots \\ V_n^1 - \overline{V}_n & V_n^2 - \overline{V}_n & \cdots & V_n^{nsamp} - \overline{V}_n \end{bmatrix} \tag{4.2.20}$$

and,

$$A_{Train} = \begin{bmatrix} a_1^1 & a_1^2 & \cdots & a_1^{nsamp} \\ \vdots & \vdots & \vdots & \vdots \\ a_m^1 & a_m^2 & \cdots & a_m^{nsamp} \end{bmatrix} \tag{4.2.21}$$

where, **n** = number of predictants (i.e. the number of temperature, moisture, and/or emissivity/reflectivity points), **nsamp** = number of samples in the training set, **m** = number of principal components used and bars indicate averages over the training sample set.

The least squares regression solution of Equation (4.2.19) is:

$$C = \Delta V A_{Trai}^T (A_{Train} A_{Train}^T)^{-1} \tag{4.2.22}$$

where the T superscript denotes matrix transpose, and the -1 superscript denotes matrix inversion.

Applying the Coefficients to Independent Data

Once the coefficient matrix, C, is calculated from equation (4.2.22) the coefficients may be applied to independent data using equation (4.2.19). The matrix defined in equation (4.2.20) would now contain deviations of the independent data from the training sample mean. Mathematically, the application process is:

$$\hat{V} = \overline{V} + CA_{obs} \tag{4.2.23}$$

where $\hat{V}$ is the [**n** x **nobs**] matrix of retrievals, $\overline{V}$ the training level 2 vector from equation (4.2.20), C is the [**n** x **m**] matrix of regression coefficients from equation (4.2.22), and A_{obs} is the [**m** x **nobs**] matrix of principal components calculated from the level 1B observations. A_{obs} is generated using equation (4.2.18) where $\Delta\Theta_{Train}$ is replaced with $\Delta\Theta_{obs}$, the matrix of deviations of observed brightness temperatures from the training mean.

Minimum Variance Physical Retrieval

The starting point of all physical retrieval algorithms is the definition of the radiative transfer equation to establish the relationship of atmospheric and surface geophysical parameters to the outgoing radiance that the instrument measures. Given a set of radiances, the objective of a physical retrieval algorithm is to find a realistic solution of geophysical parameters that will be consistent with those radiances.

In the InfraRed(IR) region of the spectrum the radiative transfer equation (RTE) for a clear sky, plane parallel, homogenous atmosphere in Local Thermodynamic Equilibrium (LTE) may be represented as:

$$R_\upsilon^c = \underbrace{\varepsilon_\upsilon B_\upsilon(T_s)\tau_{\upsilon s}}_{\substack{\text{surface}\\ \text{emission}\\ \text{term}}} + \underbrace{\int_{p=p_s}^{0} B_\upsilon(T(P))\frac{d\tau_\upsilon(p)}{dp}dp}_{\substack{\text{Atmospheric}\\ \text{Emission}\\ \text{Term}}} + \underbrace{\rho_\upsilon B_\upsilon(Tsun)\tau_{\upsilon s}^2\cos\theta}_{\substack{\text{Reflected}\\ \text{Solar}\\ \text{Term}}} \qquad \text{(InfraRed)} \quad (4.2.24)$$

where R_υ^c is the clear channel IR radiance at frequency υ measured by the satellite, T_s is the surface skin temperature, T(p) is the ambient atmospheric temperature at pressure p, Tsun is the blackbody temperature of the sun (assumed to be 5600K), $B_\upsilon(T)$ is the Planck radiance evaluated at frequency υ and temperature T, ε_ν is the surface spectral emissivity, ρ_ν is the surface spectral reflectivity, $\tau_{\nu s}$ is the spectral transmittance from the earth's surface to space, and $\tau_\nu(p)$ is the spectral transmittance from pressure p to space. A reflected downward IR component has been omitted in equation (4.2.24) because of it's small magnitude when compared with other terms in the equation.

In the microwave(MW) region equation (4.2.24) must be modified for several reasons. First, at microwave frequencies the Raleigh-Jeans approximation holds and the Planck function becomes approximately proportional to temperature. Secondly, the reflected atmospheric term (ignored in the IR) becomes large and significant whereas the reflected solar term becomes negligible. Lastly, the surface reflectivity in the microwave is assumed to be specular and is therefore expressed as one minus the surface emissivity. Incorporating these modifications, equation (4.2.24) is recast for microwave channels,

$$R_\upsilon^c = \underbrace{\varepsilon_\upsilon T_s \tau_{\upsilon s}}_{\substack{\text{surface}\\ \text{emission}\\ \text{term}}} + \underbrace{\int_{p=p_s}^{0} T(P)\frac{d\tau_\upsilon(p)}{dp}dp}_{\substack{\text{Atmospheric}\\ \text{Emission}\\ \text{Term}}} + \underbrace{(1-\varepsilon_\upsilon)\int_{p=0}^{p_s} T(P)\frac{d\tau_\upsilon^*(p)}{dp}dp}_{\substack{\text{Reflected Downward}\\ \text{MW component}}} \qquad \text{(Microwave)} \quad (4.2.25)$$

where all terms which appeared previously in equation (4.2.24) have the same definition except for R_υ^c which is now in units of brightness temperature, and the new variable, $\tau_\upsilon^*(p)$, is the two path transmittance from pressure p to the surface and back to space. Notice that all references to the Planck function have been replaced by T (atmospheric temperature) and the reflected solar term is replaced by the reflected downward atmospheric emission term.

The retrieval methodology requires that equations (4.2.24) and (4.2.25) are linearized about some *a priori* estimate. This is accomplished by expressing R_υ^c in equations (4.2.24) and (4.2.25) as a function of the regression guess using a first order Taylor expansion such that:

$$R_\upsilon^c = R_\upsilon^0 + \sum_{k=1}^{N} \frac{\partial R}{\partial V_k}(V_k - {}_kV_0)$$

where R_υ^0 is the total integrated radiance for frequency υ computed from the regression solution using either equation (4.2.24) or (4.2.25), V_k and ${}_kV_0$ are the nth elements of the solution and regression first guess geophysical parameter vectors, $\frac{\partial R}{\partial V_k}$ is the incremental change of the radiance with respect to a incremental change in a particular geophysical parameter (e.g. V_k= temperature at 50 mb), and N is the number of geophysical parameters. The value of $\frac{\partial R}{\partial V_k}$ is computed in a manner similar to Eyre (1989a) by differentiating the numerical quadrature form of equations (4.2.24) & (4.2.25) with respect to the geophysical parameters (see section "Computation of the Kernel Matrix"). Currently the geophysical parameters solved in the physical retrieval include surface and atmospheric temperature and moisture. The above equation is re-expressed in matrix notation as,

$$R = R_0 + A(V - V_0) \tag{4.2.26}$$

where R represents the vector of clear satellite observations for all retrieval channels, R_0 represents the vector of radiances computed from the regression first guess for all retrieval channels, V and V_0 represent the solution and regression first guess geophysical parameter vectors, and A, commonly referred to as the *kernel matrix*, contains the partial derivatives of radiance with respect to each of the individual geophysical parameters and for each of the retrieval channels. A minimum variance solution for V is employed in the retrieval process of the NOAA Core Algorithm. Minimum Variance has been used in the NOAA TOVS operational retrieval system since 1988 (Fleming et. al., 1986; Goldberg et. al., 1986). There are an infinite number of ambient atmospheric states that will satisfy the RTE to within the system noise (i.e. instrumental + cloud clearing + transmittance); the minimum variance solution uses *a priori* constraints, in the form of a regression estimate and covariance matrix of regression errors, to produce realistic atmospheric profile solutions which minimize average squared error over an ensemble. The iterative matrix form of the solution used is (Rodgers, 1976):

$$\hat{V}_{n+1} = V_0 + (A_n^T N^{-1} A_n + S^{-1})^{-1} A_n^T N^{-1} \left\{ (R - R_n) - A_n (V_0 - \hat{V}_n) \right\} \tag{4.2.27}$$

where $\hat{V}_{n+1}$ is the iterative estimate of the true profile of temperature or moisture (to be retrieved), $\hat{V}_n$ is the retrieved estimate of the true profile of temperature or moisture from the previous iteration, V_0 is the initial guess profile of temperature or water vapor mixing ratio, R is the vector of satellite observed radiances, R_n is the corresponding vector of radiances computed from the most recent iterative solution, A_n is the kernel computed from the most recent iterative solution, N is the instrument noise covariance matrix, and S is the estimate of the background error covariance matrix between the truth and the retrieval estimate. Superscripts T and -1 denote matrix transpose and matrix inversion, respectively.

Temperature/surface temperature and water vapor are retrieved separately rather than simultaneously with the temperature retrieval preceding the water vapor retrieval. The temperature profile is retrieved first using channels selected from the 15µm and 4.3µm bands that are relatively unaffected by water vapor. By first improving the temperature the subsequent H2O retrieval, based on the updated temperature information, will be more accurate because the temperature component of the signal in the water vapor channels will be better accounted for . Both retrieval steps can be iterated, however experiments with simulated data have shown that quite often the initial guess departure from the truth is in the linear regime such that only one iteration is required.

Expressing the Retrieval Solution in more Computationally Efficient Form

The retrieval solution in equation (4.2.27) can be re-expressed in a more computationally efficient form using eigenvector methods. Because S in equation (4.2.27) is a real symmetric matrix it may be written:

$$S = \Gamma \Lambda \Gamma^T \tag{4.2.28}$$

where Γ is an [n x n] orthonormal matrix, Λ is an [n x n] diagonal matrix, and superscript T denotes matrix transpose. Substituting equation (4.2.28) into equation (4.2.27) and making use of the properties of eigenvectors it is easy to show that equation (4.2.27) can be written in the following equivalent form,

$$\Delta \mathbf{V} = \Gamma\left(\Gamma^{\mathbf{T}}\mathbf{A}_{\mathbf{n}}^{\mathbf{T}}\mathbf{N}^{-1}\mathbf{A}_{\mathbf{n}}\Gamma + \Lambda^{-1}\right)^{-1}\Gamma^{\mathbf{T}}\mathbf{A}_{\mathbf{n}}^{\mathbf{T}}\mathbf{N}^{-1}\left\{\Delta\mathbf{R} - \mathbf{A}_{\mathbf{n}}\left(\mathbf{V}_{\mathbf{0}} - \hat{\mathbf{V}}_{\mathbf{n}}\right)\right\} \tag{4.2.29}$$

The [**n** x **n**] matrix Γ contains the **n** orthonormal 'eigenvectors' of S in it's columns and the diagonal matrix Λ contains the **n** ordered 'eigenvalues' of S. More specifically,

$$\Lambda = \begin{bmatrix} \lambda_1 & 0 & \cdots & 0 \\ 0 & \lambda_2 & \ddots & \vdots \\ \vdots & \ddots & \ddots & 0 \\ 0 & \cdots & 0 & \lambda_n \end{bmatrix} \quad \text{and} \quad \Gamma = \begin{bmatrix} \gamma_1^1 & \gamma_1^2 & & \gamma_1^n \\ \gamma_2^1 & \gamma_2^2 & \cdots & \gamma_2^n \\ \vdots & \vdots & & \vdots \\ \underbrace{\gamma_n^1}_{\Gamma_1} & \underbrace{\gamma_n^2}_{\Gamma_2} & & \underbrace{\gamma_n^n}_{\Gamma_n} \end{bmatrix} \tag{4.2.30}$$

where $[\Gamma_1, \Gamma_2, ..., \Gamma_n]$ are the **n** eigenvectors of S and $[\lambda_1, \lambda_2, ... , \lambda_n]$ are the corresponding eigenvalues.

The dimensions of the matrix to be inverted in equation (4.2.29) can be reduced by truncating the matrices of eigenvectors and eigenvalues. Suppose that we choose to retain **m** of the **n** eigenvectors (**m** < **n**) then equation (4.2.29) is rewritten:

$$\Delta V = \tilde{\Gamma}\left(\tilde{\Gamma}^T A_n^T N^{-1} A_n \tilde{\Gamma} + \gamma\tilde{\Lambda}^{-1}\right)^{-1} \tilde{\Gamma}^T A_n^T N^{-1} \left\{\Delta R - A_n\left(V_0 - \hat{V}_n\right)\right\} \tag{4.2.31}$$

where γ is a tuning parameter, and the definition of $\gamma\tilde{\Gamma}$ and $\tilde{\Lambda}^{-1}$ are as follows:

$$\gamma\tilde{\Lambda}^{-1} = \begin{bmatrix} \gamma/\lambda_1 & 0 & \cdots & 0 \\ 0 & \gamma/\lambda_2 & \ddots & \vdots \\ \vdots & \ddots & \ddots & 0 \\ 0 & \cdots & 0 & \gamma/\lambda_m \end{bmatrix} \quad \text{and} \quad \tilde{\Gamma} = \begin{bmatrix} \gamma_1^1 & \gamma_1^2 & & \gamma_1^m \\ \gamma_2^1 & \gamma_2^2 & \cdots & \gamma_2^m \\ \vdots & \vdots & & \vdots \\ \underbrace{\gamma_n^1}_{\Gamma_1} & \underbrace{\gamma_n^2}_{\Gamma_2} & & \underbrace{\gamma_n^m}_{\Gamma_m} \end{bmatrix} \tag{4.2.32}$$

Notice that the dimension of the matrix to be inverted in equation (4.2.31) is [**m** x **m**] compared to the larger [**n** x **n**] matrix in equation (4.2.29). In addition to reducing the number of floating point operations, truncating the eigenvectors may also filter out unwanted noise in the retrieval process by excluding higher order terms which contain spurious information.

Settings for the tuning parameter, γ, and the number of eigenvectors retained, **m**, are different for water vapor and temperature retrievals. Experimentally determined values for (γ, **m)** are currently set to (1.5, 30) for temperature, and (20, 20) for water vapor.

Computation of the Kernel matrix

The elements of the A_n matrix in Equation (4.2.31) are derived for IR and MW channels using a quadrature form of equations (4.2.24) and (4.2.25). As discussed, the elements of A_n are derivatives of radiance (brightness temperature for MW) with respect to individual geophysical parameters (e.g. 50 mb temperature, 500 mb water vapor mixing ratio, surface temperature) from the most recent iterative solution. We begin by writing equations (4.2.24) and (4.2.25) in quadrature form using the trapezoidal rule of integration. For the IR region the quadrature form of equation (4.2.24) is,

$$R_\upsilon^c = \varepsilon_\upsilon B_\upsilon\left[T_s\right]\tau_{\upsilon s} + \sum_{j=1}^{J}\frac{1}{2}\left(B_\upsilon\left(T(p_j)\right) + B_\upsilon\left(T(p_{j-1})\right)\right)\left\{\tau_\upsilon(p_{j-1}) - \tau_\upsilon(p_j)\right\}$$
$$+\rho_\upsilon B_\upsilon(Tsun)\tau_{\upsilon s}^2\cos\theta \tag{4.2.33}$$

where J represents the number of discrete pressure levels of the fast transmittance model, p_j is the pressure at the jth pressure level and all other quantities are as defined in equation (4.2.24). Similarly for the MW region of the spectrum equation (4.2.25) is expressed in equivalent quadrature form,

$$R_\upsilon^c = \varepsilon_\upsilon T_s\tau_{\upsilon s} + \sum_{j=1}^{J}\frac{1}{2}\left(T(p_j) + T(p_{j-1})\right)\left\{\tau_\upsilon(p_{j-1}) - \tau_\upsilon(p_j) + (1-\varepsilon_\upsilon)(\tau_\upsilon^*(p_j) - \tau_\upsilon^*(p_{j-1}))\right\} \tag{4.2.34}$$

where $\tau_\upsilon^*(p_j) = \tau_\upsilon^2(p_s) / \tau_\upsilon(p_j)$. Equation (4.2.34) can be simplified by using notation for *effective transmittances* which combine the upwelling and downwelling MW components of radiance into a single term. The form of the simplified equation is as follows,

$$R_\upsilon^c = T_s\hat{\tau}_{\upsilon s} + \sum_{j=1}^{J}\frac{1}{2}\left(T(p_j) + T(p_{j-1})\right)\left\{\hat{\tau}_\upsilon(p_{j-1}) - \hat{\tau}_\upsilon(p_j)\right\} \tag{4.2.35}$$

where $\hat{\tau}$ indicates the effective transmittance and is defined,

$$\hat{\tau}_\upsilon(p_k) = \left[1 - (1-\varepsilon_\upsilon)\left(\tau_\upsilon(p_s) / \tau_\upsilon(p_k)\right)^2\right]\cdot\tau_\upsilon(p_k) \tag{4.2.36}$$

Taking the derivative of equations (4.2.33) and (4.2.36), both with respect to temperature and water vapor mixing ratio, gives the elements of A_n.

Making the assumption that transmittance is independent of temperature the temperature elements of A_n for IR channels are defined as,

$$A_n^{ij} = \frac{dR_i^c}{dT_j} = \begin{cases} \frac{1}{2}\frac{dB_j}{dT_j}\left\{2 - \tau_j - \tau_{j+1}\right\} & \text{for } j = 1 \\ \frac{1}{2}\frac{dB_j}{dT_j}\left\{\tau_{j-1} - \tau_{j+1}\right\} & \text{for } 1 < j < J \\ \frac{1}{2}\frac{dB_j}{dT_j}\left\{\tau_{j-1} - \tau_j\right\} & \text{for } j = J \\ \varepsilon_s \frac{dB_s}{dT_s}\tau_s & \text{for surface skin term} \end{cases} \tag{4.2.37}$$

where J is the number of atmospheric levels and j = J corresponds to the lowest atmospheric level, τ_s is the atmospheric transmittance from the surface to space, τ_k is the atmospheric transmittance from the kth atmospheric pressure level to space, ε_s is the surface spectral emissivity, and $\frac{dB}{dT_k}$ is the derivative of the Planck function evaluated at channel i and atmospheric temperature T_k. Similarly for the MW region the definition of the temperature elements of A_n are as follows,

$$A_n^{ij} = \frac{dR_i^c}{dT_j} = \begin{cases} \frac{1}{2}\left\{2\hat{\tau}_0 - \hat{\tau}_j - \hat{\tau}_{j+1}\right\} & \text{for } j = 1 \\ \frac{1}{2}\left\{\hat{\tau}_{j-1} - \hat{\tau}_{j+1}\right\} & \text{for } 1 < j < J \\ \frac{1}{2}\left\{\hat{\tau}_{j-1} - \hat{\tau}_j\right\} & \text{for } j = J \\ \hat{\tau}_s & \text{for surface skin term} \end{cases} \tag{4.2.38}$$

where the effective transmittance, $\hat{\tau}$, is as defined above.

The water vapor elements of the A_n matrix for IR channels are defined as follows,

$$A_n^{ij} = \frac{dR_i^c}{dq_j} = \left[\varepsilon_s B_s + 2\rho_\upsilon B_{Tsun}\tau_s \cos\theta - \frac{(B_{J-1} + B_J)}{2}\right]\frac{d\tau_s}{dq_j} + \sum_{k=1}^{J-1}\frac{(B_{k+1} - B_{k-1})}{2}\frac{d\tau_k}{dq_j} \tag{4.2.39}$$

where B_{tsun} is the Planck function evaluated for channel i at the temperature of the sun, B_k is the Planck function evaluated for channel i at the first guess level temperature T_k, θ is the solar zenith angle, ρ_υ is the surface spectral reflectivity for channel i, q_k is the initial guess mixing ratio at level k, and all other terms are as defined in equations (4.2.36) and (4.2.37). Assuming an isothermal atmosphere above the uppermost pressure level the definition of the water elements of A_n in the MW is as follows,

$$A_n^{ij} = \frac{dR_\upsilon^c}{dq_j} = \left[T_s - \frac{1}{2}\left(T_J + T_{J-1}\right)\right]\frac{d\hat{\tau}_s}{dq_j} + T_1 \cdot \frac{d\hat{\tau}_0}{dq_j} + \sum_{k=1}^{J}\frac{1}{2}\cdot\left(T_{k+1} - T_{k-1}\right)\cdot\frac{d\hat{\tau}_k}{dq_j} \tag{4.2.40}$$

The derivative terms in equation (4.2.40) are evaluated using the definition of effective transmittance from equation (4.2.36),

$$\frac{d\hat{\tau}_k}{dq_j} = \frac{d}{dq_j}\left[\tau_k - (1-\varepsilon)\frac{\tau_s^2}{\tau_k}\right] \tag{4.2.41}$$

which after some manipulation reduces to the following form,

$$\frac{d\hat{\tau}_k}{dq_j} = \frac{d\tau_k}{dq_j} + (1-\varepsilon)\left[\frac{d\tau_k}{dq_j}\cdot\frac{\tau_s}{\tau_k} - 2\cdot\frac{d\tau_s}{dq_j}\right]\frac{\tau_s}{\tau_k} \tag{4.2.42}$$

The derivative of transmittance with respect to water vapor is given by:

$$\frac{d\tau_k}{dq_j} = \tau_k\,\frac{d\ln\tau_k}{dq_j} = \tau_k\,\frac{d\ln\tau_k}{du_k}\frac{du_k}{dq_j} \tag{4.2.43}$$

where u_k, the precipitable water from the space to pressure level k, is calculated by the following formula

$$u_k = \tfrac{1}{2g}\sum_{n=1}^{k}\left(q_n + q_{n-1}\right)\left(p_n - p_{n-1}\right) \tag{4.2.44}$$

the derivative of precipitable water is given by,

$$\frac{du_k}{dq_j} = \begin{cases} (1/2g)\left(p_{j+1} - p_{j-1}\right) & \text{for } j < k \\ (1/2g)\left(p_j - p_{j-1}\right) & \text{for } j = k \\ 0 & \text{for } j > k \end{cases} \tag{4.2.45}$$

and the derivative of the natural log of transmittance with respect to precipitable water is,

$$\tau_k\,\frac{d\ln\tau_k}{du_k} = \tau_k\,\frac{\ln(\tau_{k-1}) - \ln(\tau_k)}{u_{k-1} - u_k} \tag{4.2.46}$$

[Note: $\tau_0 \equiv 1$ in the calculation of the above derivatives.]

The Instrument Noise Covariance Matrix N

The instrument noise covariance matrix, N, is a diagonal matrix whose non-zero elements (the diagonal elements) represent the variance of the instrument noise for each of the retrieval channels. Thus N is defined as:

$$N = \begin{bmatrix} \sigma_1^2 & 0 & \cdots & 0 \\ 0 & \sigma_2^2 & \cdots & 0 \\ \vdots & \vdots & \ddots & 0 \\ 0 & 0 & 0 & \sigma_n^2 \end{bmatrix} \tag{4.2.47}$$

The diagonal values, $[\sigma_1^2, \sigma_2^2, \cdots, \sigma_n^2]$, represent the noise of the **n** retrieval channels, and all off diagonal elements (i.e. all interchannel covariances) are assumed to be zero. Operationally N will include the total system noise and may include off diagonal elements. The total system noise for each channel is due to the combined effects of measurement noise, forward model inaccuracies, and calibration error.

The Thermal and Moisture Covariance Matrix S

The retrieval parameter covariance matrix, denoted by S in the previous mathematical description of the physical retrieval, should represent the expected error of the background field. As discussed in the First Guess Section, NOAA/NESDIS generates a background field from a regression scheme which uses a large training data base to estimate geophysical quantities from principal components derived from AIRS/AMSU brightness temperature observations. This same training data is used to estimate the magnitude of expected background errors when the regression coefficients are applied to independent data. The coefficients, matrix C from equation (4.2.22), are applied back onto the dependent training data as follows:

$$\Delta\hat{V} = C\Delta T \tag{4.2.48}$$

where $\Delta\hat{V}$ is the regression retrieval of the dependent geophysical training data ΔV in equation (4.2.20). The covariance matrix, S, is then calculated as follows:

$$S = \frac{1}{m} EE^T, \text{ where } E = \Delta V - \Delta\hat{V} \tag{4.2.49}$$

where S is an [**n** x **n]** matrix whose diagonal elements represent the expected background variance of each of the predictants, and whose off diagonal elements represent expected interlevel covariances amongst the various predictants.

4.3 Final Product - (Susskind lead, Chahine)

Introduction

To satisfy the science requirements of EOS, a final adjustment is made to the NOAA first product based on the difference between calculated radiances and cloud-cleared radiances. It is also in this part of the code that the cloud parameters, and the research products (not described in this document) will be calculated.

When solving for a set of geophysical parameters, it is desirable to be able to choose an appropriate set of parameters to solve for and select channels that are both sensitive to those parameters and relatively insensitive to other parameters. In general, channels will be affected by more than one type of parameter. For example, channels with radiances sensitive to the water vapor or ozone distribution are also sensitive to the temperature profile and often to the surface skin temperature. Our approach is to solve sequentially for the surface parameters, temperature profile, water vapor profile, and ozone profile in that order. In this approach, variables already solved for, used in conjunction with first guess variables, are kept fixed when solving for the next set of variables. Table 4.3.1 lists the variables solved for and the number of channels used in each step. The above order is chosen because channels can be selected for a given step that are relatively insensitive to variables to be solved for subsequently.

A total of 222 AIRS channels, 12 AMSU A channels, and 4 HSB channels were selected for use in the AIRS/AMSU retrieval algorithm. Some of the surface parameter sounding channels are also used in the water vapor or temperature profile retrievals. Therefore, the total number of channels is less than the sum of the channels in column 2. Likewise, the water vapor solved for in the ground temperature retrieval is subsequently

updated in the water vapor profile retrieval step. Therefore, the 238 channels are used to solve for 39 different variables.

The general AIRS/AMSU retrieval algorithm does not require any field-of-view to be cloud free (Susskind *et al.*, 1996). The algorithm used in AIRS retrieval consists of the following main steps: (0) Obtain an initial guess for the temperature, moisture, and ozone profiles. (1) Derive a first estimate of the cloud cleared radiances and channel noise covariance matrix. (2) Retrieve surface parameters. If necessary, the first guess and cloud cleared radiances may be improved at this point and the surface retrieval may be repeated. This loop ends the basic startup procedure. (3) Retrieve temperature profile. (4) Retrieve water vapor profile. (5) Retrieve ozone profile. (6) Produce final cloud cleared radiance estimates. Repeat (2) - (5) starting with the new parameter estimates in place of the first guess. The general approach to solve for the parameters in steps (2) - (5) is in the form of iterative constrained least squares solutions, one for each set of variables to be solved for. The form of the equations to be solved is identical for each of the four steps.

Treatment of radiances in cloudy atmospheres

Three basic approaches used for accounting for effects of clouds in satellite remote sensing are: 1) identify clear areas and only perform retrievals in those areas, with no cloud correction needed; 2) use channel observations in adjacent potentially partially cloudy scenes to reconstruct what the channel radiances would have been if the scenes were clear, and use these reconstructed observations to determine geophysical parameters; and 3) determine both surface and atmospheric geophysical parameters, as well as cloud properties, from the radiance observations themselves. An example of the first approach is given by Cuomo *et al.*(1993). Eyre (1989a, 1990) has used the third approach in simulation by assuming an unknown homogeneous amount of black clouds at an unknown

Variables	Channels	Frequencies
		Ground Temperature Retrieval
T_s , $\Delta\ell nW$, 8 spectral emissivity function, 3 spectral bi-directional reflectance functions	21 27	758 $\rightarrow$ 1235 cm^{-1} 2170 $\rightarrow$ 2669 cm^{-1}
		Temperature Profile Retrieval
13 layer temperature-functions (trapezoids)	96 29 12	651 $\rightarrow$ 742 cm^{-1} 2228 $\rightarrow$ 2501 cm^{-1} 50.3 $\rightarrow$ 57.29 GHz
		Water Vapor Profile Retrieval
8 layer column density functions	30 4	790 $\rightarrow$ 2650 cm^{-1} 150-183.31 GHz
		Ozone Profile Retrieval
5 layer column density functions	23	1001 $\rightarrow$ 1069 cm^{-1}
		AMSU Temperature Profile Retrieval
T_s , ε_m, 13 layer temperature profile functions	17 12	666 cm^{-1}- 676 cm^{-1} 50.3 - 57.29 GHz

Total: 39 variables 238 channels (AIRS + AMSU)

TABLE 4.3.1. VARIABLES AND CHANNELS

pressure, and attempted it with real TOVS data as well (Eyre, 1989b). Our approach, like that used in Susskind (1993), is of the second type and is an extension of that used by Smith (1968), Chahine (1974), and Chahine (1977). This approach utilizes satellite observed radiances, $\overline{R}_{i,k}$, corresponding to channel i and field-of-view k, made over adjacent fields-of-view. In this approach, there is no need to model the radiative and reflective properties of the clouds. The only assumption made is that the fields-of-view are homogeneous except for the amount of cloud cover in K different cloud formations in each field-of-view. $R_{i,clr}$ the radiance which would be observed if the entire field of view were clear and $R_{i,cld,\ell}$, the radiance which would be observed if the entire field of view were covered by cloud formation ℓ, are therefore assumed to have the same respective values in each field-of-view. If the observed radiances in each field-of-view are different, the differences in the observed radiances are then attributed to the differences in $\alpha_{\ell k}$, the fractional cloudiness for cloud formation ℓ in field-of-view k.

Using the above assumptions, Chahine (1977) showed that the reconstructed clear-column radiance for channel i, $\hat{R}_{i,CLR}$, can be written as a linear combination of the measured radiances in the K+1 fields-of-view, $\overline{R}_{i,1} \ldots \overline{R}_{i,K+1}$, according to

$$\hat{R}_{i,CLR} = \overline{R}_{i,1} + \eta_1 \left[\overline{R}_{i,1} - \overline{R}_{i,K+1}\right] + \ldots + \eta_k \left[\overline{R}_{i,1} - \overline{R}_{i,(K+2)-k}\right] + \ldots + \eta_K \left[\overline{R}_{i,1} - \overline{R}_{i,2}\right], \tag{4.3.1}$$

where $\eta_{1\ldots}\eta_K$ are unknown channel independent constants, and K+1 fields-of-view (FOV's) are needed to solve for K cloud formations. The fields-of-view are ordered such that FOV 1 is the clearest field-of-view based on observations in the 11 μm window (the field-of-view with the highest 11 μm radiances is assumed to be FOV 1) and FOV K+1 is the cloudiest. Thus η_1 multiplies the largest radiance differences and η_K the smallest. Once $\eta_{1\ldots}\eta_K$ are determined, Eq. 4.3. is used to produce the reconstructed clear column radiances for all channels used in the retrieval process. The reconstructed clear column radiances are then used when solving for the geophysical parameters. Susskind *et al.* (1984), Susskind and Reuter (1985a) and Chahine and Susskind (1989) have successfully used this approach with two fields-of-view, assuming one cloud formation, in the analysis of HIRS2/MSU operational sounding data. Chahine and Susskind (1989) show that retrieval accuracy, verified by co-located radiosondes, does not degrade appreciably with increasing cloud cover, for retrieved cloud fractions of up to 80%. An analogous assumption is made by NOAA/NESDIS in production of their clear column radiances used in generation of operational HIRS2/MSU retrievals (McMillin and Dean, 1982). Susskind and Reuter (1985b) have performed simulations with two cloud formations and three fields-of-view for the AMTS instrument -- an earlier version of AIRS (Chahine, *et al.*., 1984), used in conjunction with MSU. We have developed a new methodology to account for multiple cloud formations using the AIRS and AMSU instruments. The methodology to determine η_k is first presented for a single cloud formation and then generalized for use with multiple cloud formations.

Single cloud formation with two fields-of-view

For one cloud formation and two fields-of-view, the reconstructed clear-column radiance for channel i from Eq. 4.3.1 is given by

$$\hat{R}_{i,CLR} = \overline{R}_{i,1} + \eta_1\left[\overline{R}_{i,1} - \overline{R}_{i,2}\right]. \qquad (4.3.2)$$

Given the above mentioned assumptions, the value of η_1 is independent of cloud spectral properties and has the same value for all channels. η_1 can be written in terms of α_1 and α_2 and has a unique value given by

$$\eta_1 = \frac{\alpha_1}{\alpha_2 - \alpha_1}, \qquad (4.3.3)$$

where α_1 and α_2 are the cloud fractions in each field-of-view (Chahine, 1974). It is not necessary to know α_1 or α_2 to determine η_1.

The determination of η is sequential and is done in a number of passes based on the latest estimate of the surface and atmospheric parameters. An expected value of $R_{i,CLR}$ for any channel can be used to estimate η according to

$$\eta^n_{i,1} = \frac{R^n_{i,CLR} - \overline{R}_{i,1}}{\overline{R}_{i,1} - \overline{R}_{i,2}}, \qquad (4.3.4)$$

where $\eta^n_{i,1}$ is the nth pass estimate of η, obtained from channel i, based on the nth pass estimate of the clear column radiance $R^n_{i,CLR}$. $R^n_{i,CLR}$ is obtained by using the radiative transfer equation to compute the channel i radiance with the nth pass estimates of

atmospheric and surface parameters. The general multi-pass procedure referred to by n will be discussed later.

If the estimate of temperature profile is too warm (cold) over coarse layers of the atmosphere, the estimated clear column radiances $R^n_{i,CLR}$ will be too high (low), and $\eta^n_{i,1}$ will be too large (small). In performing HIRS2/MSU retrievals, Susskind *et al.* (1984) correct potential biases in n^{th} iterative coarse layer temperatures by adjusting computed brightness temperatures for the IR channels used to estimate η according to the difference between the observed brightness temperature for an MSU channel sensitive to mid-lower tropospheric temperatures and that computed from the nth iterative temperature profile. This in effect adjusts the nth iterative temperature profile to be consistent with the observations in a single MSU channel.

We can utilize the superior sounding capability of AMSU, compared with MSU, to first produce an AMSU only retrieval of atmospheric temperature-moisture profile for use as the initial guess to start the retrieval process, and use in the first pass estimation of η_1. The AMSU retrieval can be done before the cloud correction because AMSU radiances are not significantly affected by non-precipitating clouds. The temperature retrieval obtained from AMSU will have the property that radiances computed from it agree well with all AMSU channels and should not be very biased over coarse layers of the atmosphere, though local errors will still exist. Alternatively, we can use the regression guess of NOAA's physical retrieval or the NOAA first product retrieval itself for this purpose. These profiles will also be unbiased, as long as the NOAA cloud clearing step, described in section 4.2, is sufficiently accurate.

Using different IR channels in Eq. 4.3.4 will result in different estimated values of $\eta_{i,1}$ as a result of a combination of local errors in the temperature profile, and channel noise effects. Many channels can be used to estimate η_1 in order to reduce potential errors. For the case of a single cloud formation, this can be accomplished by simply taking a weighted average of $\eta_{i,1}$ over a set of cloud filtering channels to get a single value of η_1 as done in Susskind and Reuter (1985a) and Susskind *et al.*. (1993). Once a value of η_1 is computed, the clear-column radiances for all channels can be reconstructed using Eq. 4.3.2.

If the denominator in Eq. 4.3.4 is small, errors in estimating the numerator will be amplified in the determination of η. Therefore, it is important that cloud filtering channels have a large contrast in radiance between the two fields-of-view. This implies the channels should be sensitive to the presence of clouds. The contrast can be further enhanced by averaging together observations in the warmest spots and averaging observations in the coldest spots within a scene to produce two high contrast fields-of-view as done by Reuter *et al.* (1988). Averaging spots also reduces the effects of instrumental noise. The methodology for selecting and weighting channels used to determine η is described in the next section.

Channel selection for cloud filtering

Chahine (1974) showed that 15 μm channels are preferable for use in the determination of η compared to 4.3 μm channels, because the error in $\hat{R}_{i,CLR}$, caused by an error in the estimated temperature profile, will result in a smaller error in η as determined from Eq. 4.3.4. This analysis is a result of the properties of the blackbody function in the two spectral regions. Moreover, Chahine (1974) and Halem *et al.* (1978) show that if one has infra-red observations in both the 15 μm and 4.3 μm temperature

sounding bands, but no microwave observations, soundings can be done in cloudy conditions if η is determined using observations in 15 μm channels and the temperature sounding channels for the mid-lower troposphere come from the 4.3 μm region. Along the lines of Chahine (1974), we initially selected channels in the 15 μm band that sound the mid-lower troposphere for cloud filtering. These channels were selected to be between absorption lines so as to produce sharp weighting functions that would have less of an upper tropospheric and stratospheric contribution in order to maximize sensitivity to the clouds. We also avoided channels contaminated by water vapor and ozone absorption, that could cause errors in $R_{i,CLR}$. This same channel selection methodology was used in Susskind *et al.* (1993).

The rationale for use of only 15 μm channels for cloud filtering neglected the effects of solar radiation reflected off clouds. When sunlight is reflected off the surface and clouds, the scene can exhibit more contrast in the 4.3 μm region, especially for low clouds. In addition, cloud effects on radiances can be of opposite sign at short wavelengths than at long wavelengths. This change in sign makes it easier to distinguish cloud effects on the radiances from thermal effects of the clear atmosphere. Therefore, it is desirable to include 4.3 μm channels in the cloud filtering set during the day. We feel that it is desirable to use the same methodology for both cloud filtering and retrieval of geophysical parameters during the day and night. We therefore use both 15 μm and 4.3 μm channels in the channel set used to estimate η. The 15 μm and 4.3 μm cloud filtering channels are a subset of the channels used to determine the atmospheric temperature profile. Window channels are more sensitive to clouds than atmospheric sounding channels, but are also more sensitive to uncertainties in surface parameters. We have developed improved methodology to include window channels in the determination of η, with a weight that properly reflects the uncertainty in their clear column radiances. An analogous weighting procedure is done for all channels. The relative weighting of the 15 μm and 4.3 μm channels in the determination of η is done objectively and will differ under daytime and nighttime conditions as described later.

Determination of η for a single cloud formation

The method we use to determine η is analogous to that used by Susskind *et al.* (1993), who set

$$\eta = \frac{\sum_i^I W_i^2 \, \eta_i}{\sum_i W_i^2} \quad , \tag{4.3.5}$$

where W_i is a weight for channel i. An appropriate value of W_i should take into account propagated errors in η_i resulting from instrumental and computational noise. For example, channels more sensitive to clouds, with large values of $\left| \overline{R}_{i,1} - \overline{R}_{i,2} \right|$, should receive larger weight.

One can write Eq. 4.3.4 in the form of I equations, one for each channel i, in matrix form

$$W \left(R^{\eta}_{CLR} - \overline{R}_1 \right) = W \left(\overline{R}_1 - \overline{R}_2 \right) \; \eta^{\eta} \, , \tag{4.3.6}$$

where W is an I x I diagonal weight matrix with weight W_{ii} for channel i, $\left(R^n_{CLR} - \overline{R}_1\right)$ and $\left(\overline{R}_1 - \overline{R}_2\right)$ are I x 1 vectors, and η^n is the unknown. The standard weighted least squares solution to this matrix problem is given by

$$\eta^n = \left[\left(\overline{R}_1 - \overline{R}_2\right)' W' W \left(\overline{R}_1 - \overline{R}_2\right)\right]^{-1} \left(\overline{R}_1 - \overline{R}_2\right)' W' W \left(R^n_{CLR} - \overline{R}_1\right) \tag{4.3.7}$$

and reduces to

$$\eta^n = \frac{\sum_i W_i^2 \left(\overline{R}_{i,1} - \overline{R}_{i,2}\right)\left(R^n_{CLR,i} - R_{i,1}\right)}{\sum W_i^2 \left(\overline{R}_{i,1} - \overline{R}_{i,2}\right)^2} = \frac{\sum_i W_i^2 \left(\overline{R}_{i,1} - \overline{R}_{i,2}\right)^2 \eta_i^n}{\sum_i W_i^2 \left(\overline{R}_{i,1} - \overline{R}_{i,2}\right)^2} \tag{4.3.8}$$

where η_i^n is given by Eq. 4.3.4. Eq. 4.3.8 is analogous to Eq. 4.3.5, but in Eq. 4.3.8, the contribution of the difference of radiances in the two fields-of-view to the channel weight is explicitly taken into account. Therefore W_i in this context represents any residual weight factors we may want to add, such as effects of channel noise. Susskind *et al.* (1993) used Eq. 4.3.6, including in W_i the term $\left|\overline{\Theta}_{i,1} - \overline{\Theta}_{i,2}\right|^2$, that is roughly proportional to $\left|R_{i,1} - R_{i,2}\right|^2$ for the 15 μm channels they used.

The above discussion is accurate as long as sources of channel noise are uncorrelated from channel to channel. Under these conditions, an appropriate value of W_i should be inversely proportional to sources of noise. There are two sources of noise in Eq. 4.3.6, instrumental noise and computational noise. Instrumental noise is random and affects $\overline{R}_{i,1}$ and $\overline{R}_{i,2}$. Computational noise affects $R^n_{i,CLR}$ and will be correlated from channel to channel. In the case of channel correlated noise, the appropriate equation is given by

$$\eta^n = \left[\left(\overline{R}_1 - \overline{R}_2\right)' N^{-1} \left(\overline{R}_1 - \overline{R}_2\right)\right]^{-1} \left(\overline{R}_1 - \overline{R}_2\right)' N^{-1} \left(R^n_{CLR} - \overline{R}_1\right), \tag{4.3.9}$$

where N is the channel noise covariance matrix, indicating errors in $\left(R^n_{CLR} - \overline{R}_1\right)$.

The iterative methodology to determine clear column radiances consists of three passes to determine η^n (n=1,2,3), using three sets of conditions, to give $R^n_{i,CLR}$, in which $R^n_{i,CLR}$ and hence η^n become increasingly more accurate in each iteration. Each pass has its own N^n, reflecting expected errors in $R^n_{i,CLR}$ - $R_{i,1}$. We currently model the noise covariance matrices as diagonal according to

$$N^n_{ii} = NE\Delta N_i^2 + \left[\frac{\partial R_i}{\partial T}\Delta T^n_s\right]^2 + \left[\frac{\partial R_i}{\partial \varepsilon_i}\Delta\varepsilon^n_i\right]^2 + \left[\frac{\partial R_i}{\partial p_i}\Delta p^n_i\right]^2 + \left[\frac{\partial R_i}{\partial T(p)}\Delta T(p)^n\right]^2 + \left[\frac{\partial R_i}{\partial q(p)/q}\Delta q(p)^n / q\right]^2 \tag{4.3.10}$$

where $NE\Delta N_i$ is the channel i instrumental noise and the remaining terms are contributions to errors in the computed value of $R^n_{i,CLR}$ resulting from errors in estimated parameters. The partial derivatives are computed empirically. The profile terms are obtained by either shifting the entire temperature profile by a constant amount or multiplying the moisture profile by a constant percent change. The uncertainties, such as ΔT_s^n, are specified so as to be indicative of the expected errors for that parameter in each pass.

Cloud filtering channels which do not see the clouds appreciably for a given scene are not included in the determination of η. Channel i is excluded from the set used to determine η if $\left|\overline{R}_{i,1} - \overline{R}_{i,2}\right| \le 3\sqrt{2}\ NE\Delta N_i$. If we have situations where there are not at least 2 useful cloud filtering channels, the scenes have little or no contrast. Under these conditions, we assume both fields-of-view to be clear and set $\eta = -1/2$. This has the effect of setting the clear column channel radiances to the average of the observed radiances in both fields-of-view. The other possibility for very little contrast is that both scenes have essentially identical, but non-zero, cloud cover, such as full overcast. In such a case, if we treat the scene as clear, we will find a mismatch between the AMSU observations, unaffected by clouds, and the AIRS observations, that are cloud contaminated. The final result will be rejection of the profile in the retrieval step as non-convergent in a manner to be described later. The constant cloud cover case can also be detected and rejected by comparison R^n_{CLR} with $\overline{R}_1$. Simulations show that cloudy low contrast scenes can be identified and rejected if

$$\sqrt{\sum_{i=1}^{I} \frac{\left(R^n_{i,CLR} - \overline{R}_{i,1}\right)^2}{N_{ii}}} > 15 \quad . \tag{4.3.11}$$

Rejection criteria are described in more detail in section 7.2.

Multiple Cloud Formations with Multiple Fields-of-view

In order to solve for K cloud formations with unknowns $\eta_1 \ldots \eta_K$, K+1 fields-of-view are needed. A simple relationship between α_k and η_k does not exist for the case of multiple cloud formations, nor is the solution $\eta_1 \ldots \eta_K$ necessarily unique. For example, consider a case of only one cloud formation with cloud fractions of 20%, 40%, and 60% in fields-of-view 1 - 3 respectively. $\eta_1^{(1)} = 1$, $\eta_2^{(1)} = 0$ and $\eta_1^{(2)} = 0$, $\eta_2^{(2)} = .5$ are two examples of solutions to the problem, as are appropriate linear combinations of these solutions, given by

$$\begin{pmatrix} \eta_1 \\ \eta_2 \end{pmatrix} = (1-f)\begin{pmatrix} \eta_1^{(1)} \\ \eta_2^{(1)} \end{pmatrix} + f\begin{pmatrix} \eta_1^{(2)} \\ \eta_2^{(2)} \end{pmatrix} . \tag{4.3.12}$$

The optimal solution should provide the correct clear column radiances and do so with the smallest values of η in order to minimize amplification of instrumental noise when used in Eq. 4.3.1.

The methodology to determine an optimal set of η_k is analogous to that for a single cloud formation. If one uses a set of I channels to estimate K values of η, Eq. 4.3.1 may be expressed as a set of linear equations in matrix form according to

$$\begin{pmatrix} R^n_{1,CLR} - \overline{R}_{1,1} \\ R^n_{2,CLR} - \overline{R}_{2,1} \\ \vdots \\ R^n_{l,CLR} - \overline{R}_{l,1} \end{pmatrix} = \begin{pmatrix} \overline{R}_{1,1} - \overline{R}_{1,K+1} & \overline{R}_{1,1} - \overline{R}_{1,K} & \cdots & \overline{R}_{1,1} - \overline{R}_{1,2} \\ \overline{R}_{2,1} - \overline{R}_{2,K+1} & \overline{R}_{2,1} - \overline{R}_{2,K} & \cdots & \overline{R}_{2,1} - \overline{R}_{2,2} \\ \vdots & \vdots & \ddots & \vdots \\ \overline{R}_{l,1} - \overline{R}_{l,K+1} & \overline{R}_{l,1} - \overline{R}_{l,K} & \cdots & \overline{R}_{l,1} - \overline{R}_{l,2} \end{pmatrix} \begin{pmatrix} \eta^n_1 \\ \eta^n_2 \\ \vdots \\ \eta^n_K \end{pmatrix} \quad (4.3.13)$$

or

$$C^n = D\eta^n \ , \quad (4.3.14)$$

The solution to Eq. 4.3.14 is given by

$$\eta^n = \left(D' N^{-1} D\right)^{-1} D' N^{-1} C^n \ , \quad (4.3.15)$$

where N is the channel noise covariance matrix as given in Eq 4.3.10. Given η^n , $\hat{R}^n_{i,clr}$ is constructed for all channels according to Eq 4.3.1. $\hat{R}^n_{i,clr}$ are used as the observations in the general retrieval process. If the observation in a channel is not sensitive to the presence of clouds in the field of view, it is better to average the observations in all fields of view

$$\hat{R}_{i,clr} = \frac{1}{K+1} \sum_{k=1}^{K+1} \overline{R}_{i,k} \ . \quad (4.3.16)$$

This is equivalent to defining separate values of η for channels that do not see clouds, $\eta^n_{i,clr} = -\frac{1}{K+1}$, and using them to produce $\hat{R}^n_{i,clr}$ for the appropriate channels. Currently, channel i is considered not to be sensitive to clouds if $\left|R_{i,1} - R_{i,k+1}\right| \le 3\sqrt{2}\ NE\Delta N_i$ and it is included in a set of channels expected not to see clouds given the retrieved cloud height.

Steps in the AIRS Final Product Processing System

The AIRS final product processing system is comprised of a number of sequential steps listed below.

1. Obtain an initial guess which agrees with AMSU A and HSB radiances.
2. Determine an initial η^1_1, η^1_2 from equation 4.3.15 using the initial guess parameters. Also produce the retrieval noise covariance $\overline{N}^1$ as described later.
3. Do a start up surface parameter retrieval using $\hat{R}^1_i$ obtained from equation 4.3.1. All channels used in this step are sensitive to clouds, so there is no need for a cloud height retrieval.
4. Produce an improved AMSU A temperature profile retrieval, using the retrieved value T^1_s, and radiances in AMSU A channels and a set of AIRS stratospheric sounding channels which never see clouds.

5. Determine updated η_1^2, η_2^2 taking advantage of the refined parameters. Also determine cloud parameters to decide which channels do not see clouds. This information is used to produce $\hat{R}_i^2$ as well as the retrieval channel noise covariance matrix $\overline{N}^2$. This is the end of start up system.

6-9 Use $\hat{R}_i^2$ and $\overline{N}^2$ to refine the surface parameters, temperature profile, humidity profile, and ozone profile. These steps give the first pass retrieved parameters.

10. Using the first pass retrieved parameters, determine refined η_1^3, η_2^3 and final cloud parameters.

11. Produce the final clear column radiances $\hat{R}_i^3$, which is a product of the system, and $\overline{N}^3$.

12. Repeat steps 6-9 using $\hat{R}_i^3$ and $\overline{N}^3$ to obtain the final products, using the first pass parameters as the initial guess.

General Iterative Least Squares Solution

Because the radiative transfer equation is nonlinear, an iterative approach is used to linearize it about the nth iterative parameters X_ℓ^{n+1}. The iterative retrieval process described here is different from the use of different passes in the determination of η. The values of $\hat{R}_{i,clr}$ used in the iterative retrieval loop are held fixed in a given pass. The $n+1^{th}$ iterative estimate of X_ℓ is expanded according to

$$X_\ell^{n+1} = X_\ell^n + \sum_{j=1}^{J} F_{\ell j}\, \Delta A_j^n = X_\ell^o + \sum_{j=1}^{J} F_{\ell j}\, A_j^n \quad , \tag{4.3.17}$$

where the columns of F represent a set of functions, X_ℓ^o is the initial guess, and A_j^n are corresponding coefficients given by

$$A_j^n = A_j^{n-1} + \Delta A_j^n \tag{4.3.18}$$

which together with X_ℓ^o determine the solution. A solution is found that attempts to minimize the residuals $\Delta\Theta_i^n$, weighted inversely with respect to expected noise levels, for the channels used to determine A_j. The residual for channel i is given by

$$\Delta\Theta_i^n = \hat{\Theta}_i - \Theta_i^n \quad , \tag{4.3.19}$$

where $\hat{\Theta}_i$ is the observed (clear column) brightness temperature and Θ_i^n is the brightness temperature computed from the nth iterative parameters. The nth iteration residual for channel i is attributed to errors in the coefficients, δA_j^n, and to noise effects, i.e.,

$$\Delta\Theta_i^n = \sum_j S_{ij}^n \, \delta A_j^n + \tilde{\Theta}_i \ , \tag{4.3.20}$$

where S_{ij} is an element of the sensitivity matrix or Jacobian given by

$$S_{ij}^n = \frac{\partial \Theta_i^n}{\partial A_j^n} \ , \tag{4.3.21}$$

and the noise factor $\tilde{\Theta}_i$ for a given case has two parts: errors in observed clear column radiances $\delta\hat{\Theta}_i$, which are affected by instrumental noise and cloud clearing errors, and computational noise $\delta\Theta_i^c$.

In our simulations, we assume perfect knowledge of physics, i.e., if we know all of the variables exactly, we can compute exact noise free radiances. Nevertheless, the transmittances depend on the variables to be solved for. Therefore, computational noise exists. Computational noise, arising from errors such as too low (high) an estimate of atmospheric water vapor, will produce noise that is correlated between channels. Instrumental noise is uncorrelated from channel to channel but cloud cleared errors are correlated from channel to channel. Each retrieval step uses an appropriate noise covariance matrix

$$\overline{N}_{ii'} = \hat{N}_{ii'} + N_{ii'}^c \tag{4.3.22}$$

with values which depend on the pass. We further define W as $\overline{N}^{-1}$.

A general form of the solution to this problem is given by

$$\Delta A^n = \left[S'^n \, W \, S^n + H^n \right]^{-1} S'^n \, W \Delta\Theta^n = M^n \Delta\Theta^n, \tag{4.3.23}$$

where ΔA^n and $\Delta\Theta^n$ are column vectors of the updates to the coefficients and of the residuals, respectively, and H^n is a stabilizing or damping matrix.

If the noise covariance matrix $\overline{N}$ were diagonal, with values $\overline{N}_{ii} = \tilde{\Theta}_i^2$, W^n would be diagonal with values $W_{ii} = \tilde{\Theta}_i^{-2}$. Under these conditions, one can define a channel weight W_i as $W_{ii}^{1/2} = \tilde{\Theta}_i^{-1}$. With correlated noise, W^n contains off diagonal matrix elements. One can still think of an effective channel weight that decreases with increasing channel noise

$$W_i = [W'W]_{ii}^{1/4} = \left[\sum_{i'} W_{ii'}^2 \right]^{1/4} . \tag{4.3.24}$$

For optimal determination of the solution vector ΔA^n, an accurate treatment of $\overline{N}$, and hence W, is needed. The treatment of $\overline{N}$ will be discussed later. The matrix $S'W\,S$ in Eq. 4.3.23 can be thought of as an information content matrix, proportional to the square of the sensitivity of brightness temperatures to changes in parameters and inversely proportional to the square of the noise estimates of the channels.

Hanel *et al.* (1992) and Rodgers (1976) have reviewed several methods of constraining the ill-conditioned inverse problem. In the minimum variance approach (Rodgers, 1976), H is taken to be the inverse of the *a priori* error covariance. If the statistics of both the measurement and *a priori* are Gaussian, the maximum likelihood solution is obtained. If the *a priori* covariance is taken to be $H = \gamma I$, the maximum

entropy solution is obtained. Other forms of H include the first or second derivative formulations (Twomey, 1963) that force a smoothness constraint on the solution. The solution can also be constrained by the relaxation method (Chahine, 1968) and by the Backus and Gilbert (1970) method.

The minimum variance and maximum likelihood solutions are often considered to be "optimal." However, if the *a priori* error covariance is not known or estimated incorrectly, the solution will be sub-optimal. If the *a priori* errors are underestimated, the solution could be overconstrained. This could potentially create biases in the retrievals. The biases may mask small trends in the retrieved data that one may be trying to extract. The approach described here attempts to keep the effects of instrument noise at a tolerable level without assumptions regarding the *a priori* data error covariance.

Transformation of Variables

As a consequence of stabilizing the potentially ill-conditioned solution, the addition of H may also have the effect of damping the information content (reducing ΔA for all modes). We transform variables to apply a constraint such that the well-determined components of the variables are solved for without appreciable damping. If we had originally chosen a different set of functions which were linear combinations of original functions, i.e.,

$$G = FU \quad , \tag{4.3.25}$$

where U is a unitary transformation ($UU' = 1$), and expanded the solution in the same way as in Eq. 4.3.17 with unknowns ΔB^n, we would have obtained in matrix form

$$X^{n+1} = X^n + G\Delta B^n = X^n + FU\Delta B^n = X^n + F\Delta A^n \ . \tag{4.3.26}$$

The objective is to find a transformation matrix U with desirable properties. In the new basis set, the transformed Jacobian is given by

$$T^n = \frac{\partial \Theta}{\partial B^n} = S^n U \ . \tag{4.3.27}$$

The constrained solution, as given by Eq. 4.3.23, in terms of this new set of functions is given by

$$\Delta B^n = \left(T'^n \, W \, T^n + H\right)^{-1} T'^n \, W \left(\Delta\Theta^n - \delta\Theta^{n-1}\right) = U'\Delta A^n \quad . \tag{4.3.28}$$

The term $\delta\Theta^{n-1}$, that has been included in Eq. 4.3.28, is an iterative background correction term that is zero in the first iteration and will be discussed later. U^n can be selected such that $T'^n \, \overline{W}^n \, T^n = U' \, S' \, \overline{W} \, SU$ is diagonal with real non-negative eigenvalues λ_j^n. The inverse of each eigenvalue is the variance in that eigenmode. The total variance is the trace of the $(S'WS)^{-1}$ or, equivalently, the trace of $(U'S'WSU)^{-1}$. The unconstrained solution (H=0), with no background correction $\left(\delta\Theta^{n-1} = 0\right)$, is then given by

$$\Delta B_j^n(0) = \left(\lambda_j^n\right)^{-1} \sum_{k,i} T_{kj}^n \, W_{k,i} \, \Delta\Theta_i^n = \left(\lambda^n\right)_j^{-1} m_j^n \, \Delta\Theta^n \ , \tag{4.3.29}$$

where m_j^n is the vector corresponding to the jth row of $T'W$. In general, the ill-conditionedness arises from those components of G having low information content and small eigenvalues (high variance), indicating that those components cannot be well determined from the observations alone and need damping. Components with large eigenvalues may be quite well determined and require little or no damping to achieve a stable solution. If we choose H to be diagonal with values $\Delta\lambda$, the constrained solution with no background correction term is given by

$$\Delta B_j^n\left(\Delta\lambda^n\right) = \left(\lambda_j^n + \Delta\lambda_j^n\right)^{-1} m_j^n\ \Delta\Theta^n\ . \tag{4.3.30}$$

The coefficients $\Delta B_j^n\left(\Delta\lambda_j^n\right)$ are damped from the unconstrained coefficients $\Delta B_j^n\ (0)$ by

$$\Delta B_j^n\left(\Delta\lambda_j^n\right) = \frac{\lambda_j^n}{\lambda_j^n + \Delta\lambda_j^n}\ \Delta B_j^n\ (0) = \Phi_j^n\ \Delta B_j^n\ (0)\ , \tag{4.3.31}$$

where Φ_j can be thought of as a filter or damping function. This formulation is the same as the maximum entropy solution, applied in transformed space, if $\Delta\lambda$ is set equal to a constant. However, instead of using a single constant for every $\Delta\lambda_j^n$, we compute a different value for each eigenfunction. For well determined eigenmodes, $\Delta\lambda$ is set equal to 0, giving no weight to the *a priori*. For modes that are not well determined by the measurements, $\Delta\lambda$ is determined in such a way as to limit the propagation of instrument noise to a pre-specified amount. The determination of $\Delta\lambda_j^n$ is discussed in detail in the next section.

Application of a Constraint

The residual $\Delta\Theta_i^n$ can be thought of as having both a signal and a noise component, i.e.,

$$\Delta\Theta_i^n = \Delta\Theta_i^{signal} + \tilde{\Theta}_i\ . \tag{4.3.32}$$

The component of ΔB_j that arises from the propagation of channel noise, $\tilde{\Theta}_i$, is given by

$$\Delta\tilde{B}_j^n\left(\lambda_j^n\right) = \left(\lambda_j^n + \Delta\lambda_j^n\right)^{-1}\left[T'^n\ W\right]\tilde{\Theta}\ . \tag{4.3.33}$$

A statistical estimate of $\Delta\tilde{B}_j^n$ over an ensemble of profiles can be obtained by

$$\Delta\tilde{B}_j^n = \left[\Delta\tilde{B}^n\ \Delta\tilde{B}^{n\prime}\right]_{jj}^{1/2} = \left(\lambda_j^n + \Delta\lambda_j^n\right)^{-1}\left[T'\ W\ \tilde{\Theta}\ \tilde{\Theta}'\ W'\ T\right]_{jj}^{1/2} = \frac{\left(\lambda_j^n\right)^{1/2}}{\lambda_j^n + \Delta\lambda_j^n} \tag{4.3.34}$$

because $\tilde{\Theta}\tilde{\Theta}' = \overline{N} = W^{-1}$. This formulation of $\Delta\tilde{B}$ is similar to that given by Rodgers (1990). If $\Delta\lambda_j^n$ were zero, $\Delta\tilde{B}_j^n$ can become large if λ_j^n is small. $\Delta\lambda_j^n$ can be selected such that $\Delta\tilde{B}_j^n$ will be less than or equal to a threshold value. If we allow $\Delta\tilde{B}_j^n$ to be no more than ΔB_{MAX}, we can set $\Delta\lambda_j = 0$ if $\lambda_j \geq \Delta B_{MAX}^{-2}$ and set $\Delta\lambda_j = \dfrac{\lambda_j^{1/2} - \Delta B_{MAX}\,\lambda_j}{\Delta B_{MAX}}$ otherwise. For example, if $\Delta B_{MAX} = 0.5$, $\Delta\lambda_j = 0$ for $\lambda_j \geq 4$, and if $\Delta B_{MAX} = 1$, $\Delta\lambda_j = 0$ for $\lambda_j \geq 1$, corresponding to less damping. Constraints are only applied to those eigenfunctions with lower information content than the critical value corresponding to ΔB_{MAX}. The value of ΔB_{MAX} was determined empirically for each type of retrieval being done. The AMSU temperature retrieval step behaved best with $\Delta B_{MAX} = 1.0$, the AIRS surface temperature retrieval step with a value of $\Delta B_{MAX} = 0.35$, the AIRS temperature and moisture profile retrieval steps with $\Delta B_{MAX} = 1.75$ and 1.30, respectively, and the ozone profile retrieval with $\Delta B_{MAX} = 15$. The computation of all matrix elements shown above, including λ and $\Delta\lambda$, is done in each iteration.

Formulation of the background term

The need for an iterative process arises because the radiative transfer equation is not linear. In every iteration, we recompute Θ_i^n, as well as S^n, U^n and λ^n. If the solutions were completely linear, and we applied no damping, then

$$\Delta\Theta^{n+1}(0) = \hat{\Theta} - \Theta^{n+1}(0) \cong \Delta\Theta^n - S^n\,U^n\,\Delta B^n(0)\ , \tag{4.3.35}$$

and $\Delta B^{n+1}(0)$ would be determined to be zero because $\Delta B^n(0)$ would have already minimized the residuals.

Eq. 4.3.35 is not exact, both because $\Theta^{n+1}(0)$ is not given exactly by $\Theta^n + S^n U^n \Delta B^n$, and because $\Delta B_j^n \neq \Delta B_j^n(0)$. As a result of applying ΔB_j^n rather than $\Delta B_j^n(0)$, which would have minimized the radiance residuals, we obtain

$$\Delta\Theta^{n+1} \approx \Delta\Theta^{n+1}(0) + S^n U^n \left[\Delta B^n(0) - \Delta B^n\right] = \Delta\Theta^{n+1}(0) + \delta\Theta^n\ . \tag{4.3.36}$$

In Eq. 4.3.36, $\Delta\Theta^{n+1}(0)$ represents the portion of $\Delta\Theta^{n+1}$ that is due to effects of non-linearity on the solution, while $\delta\Theta^n$ represents the residual portion of $\Delta\Theta^{n+1}$ due to the effects of damping in iteration n. The second term is zero for undamped modes and increases in significance with increased damping. This term is also zero for all modes in the first iteration. We only want to include the effects of non-linearity in the iterative procedure used in the determination of ΔB^n. Therefore, the background term to be used in Eq. 4.3.28 is given by

$$\delta\Theta^n = S^n\ U^n \left[\Delta B^n\ (0) - \Delta B^n\right]$$

and we solve for ΔB_j^{n+1} according to

$$\Delta B_j^{n+1} = \left(\lambda_j^{n+1} + \Delta\lambda_j^{n+1}\right)^{-1} U'^{n+1} S'^{n+1} W^{n+1}\left[\Delta\theta^{n+1} - \delta\theta^n\right]$$
$$= \Phi^{n+1} \Delta B_j^{n+1}(0) - \left(\lambda_j^{n+1} + \Delta\lambda_j^{n+1}\right)^{-1}\left[U'^{n+1} S'^{n+1} W^{n+1} S^n U^n \left(\Delta B_j^n(0) - \Delta B_j^n\right)\right] \tag{4.3.37}$$

where ΔB_j^n is the value of ΔB_j which was applied in iteration n. Inclusion of the background term in Eq. 4.3.37 insures second order convergence along the lines discussed by Rodgers (1976) with regard to treatment of the <u>*a priori*</u> term. The next section defines the criteria used to terminate the iterative process.

Convergence Criteria

In solving Eq. 4.3.37, we are attempting to find solutions to the radiative transfer equations which minimize weighted residuals of observed and computed brightness temperatures, corrected for the background term. To test convergence of the solution, we monitor the weighted residual

$$R = \left[\left(\Delta\Theta - \delta\Theta\right)' V' V \left(\Delta\Theta - \delta\Theta\right)\right]^{1/2} , \tag{4.3.38}$$

where the weight matrix V accounts for noise effects on the channel residuals, as well as the relative information content of the channels with regard to the variables being solved for. For example, if a channel (or linear combination of channels) carries little information content in terms of signal to noise, it should be given little weight in the estimation of the residual in Eq. 4.3.38. An appropriate choice of V, expressing the information content of the channels, would therefore be

$$V = \left(\lambda_j + \Delta\lambda_j\right)^{-1} \left(T' W\right) , \tag{4.3.39}$$

in which case we obtain

$$R = \left[\Delta B' \Delta B\right]^{1/2} . \tag{4.3.40}$$

As shown in Eq 4.3.40, a reasonable way to determine if the solution has converged, in terms of weighted residuals of observed minus computed brightness temperatures, is to see if the solution has converged in terms of the iterative changes in the solution itself. Initially, we set $\Delta B_j = 0$ if $\Phi_j^1 < 0.05$, that is, coefficients of very heavily damped components with little information content are not believed at all. The solution is said to have converged when the RMS value of ΔB_j^n is less than 10% of the RMS value of $\Delta\tilde{B}^n$ for all components not set equal to zero. The iterative procedure is also terminated if the RMS value of ΔB_j^n is not less than 75% of ΔB_j^{n-1} for the non-zero components. This indicates the solution is not converging rapidly enough and may be responding primarily to unmodeled noise. The iterative procedure, which usually converges by 3 iterations, is carried out analogously for all retrieval steps. The detailed application of the constrained least squares formalism will be described in the next section for each retrieval step.

The retrieval noise covariance matrix

The retrieval noise covariance matrix $\overline{N}$ to be used in Eq. 4.3.23 (as $W = \overline{N}^{-1}$) is given by a sum of two terms

$$\overline{N} = \hat{N} + N^c \tag{4.3.41}$$

where $\hat{N}$ represents the error covariance in the reconstructed clear column brightness temperatures and N^c represents the error covariance in the brightness temperatures computed from the estimated profile, as a results of errors in parameters assumed known (being held fixed) in a retrieval step.

<u>Clear column brightness temperature error covariance matrix</u> $\hat{N}$

Errors represented in $\hat{N}$ arise from both instrumental noise and errors in η_k. Under cloudy conditions, the computation of the reconstructed clear-column radiances using Eq. 4.3.1 has the effect of amplifying observational (but not computational) noise. If the channel instrument noise has a normal distribution with a standard deviation $NE\Delta N_i$, and the channel random noise in the K+1 fields-of-view is uncorrelated, the random noise in the reconstructed clear column radiances has a standard deviation $NE\Delta N_i^{ran}$ in radiance units given by

$$NE\Delta N_i^{ran} = NE\Delta N_i \sqrt{\left(1 + \sum_{k=1}^{K} \eta_k\right)^2 + \sum_{k=1}^{K} \eta_k^2} = NE\Delta N_i \; A(\eta_k) \tag{4.3.42}$$

where $A(\eta_k)$ is the noise amplification factor. The noise amplification factor can be considerable. Even for a single cloud formation, $A(\eta_k)$ is $\sqrt{5}$ for $\eta_1 = 1$ and $\sqrt{13}$ for $\eta_1 = 2$. If it is determined that a channel does not see the clouds, we set $\eta_k = -\frac{1}{K+1}$ for all k and $A(\eta_k) = \frac{1}{(K+1)^{1/2}}$ for that channel.

Errors in the values of η_k add an additional source of noise to the reconstructed clear-column radiances. However, unlike the amplification of instrumental noise that is uncorrelated from channel to channel, errors in η_k also result in channel correlated errors in reconstructed clear-column channel radiances. For example, if η_k is estimated too high (low), it will have the effect of making a correlated radiance error for all channels, with a relative magnitude proportional to $\overline{R}_{i,1} - \overline{R}_{i,K+2-k}$. This source of error will contribute to both diagonal and off-diagonal terms in the noise covariance matrix.

If we assume all sources of observational errors to be uncorrelated, we can estimate the diagonal contribution of observational noise to the noise covariance matrix according to

$$\overline{NE\Delta N_i} = \sqrt{\left(NE\Delta N_i^{ran}\right)^2 + \sum_{k=1}^{K}\left(\Delta\eta_k\left[\overline{R}_{i,1} - \overline{R}_{i,K+2-k}\right]\right)^2} \quad , \tag{4.3.43}$$

where $\Delta\eta_k$ is the estimated error in η_k. The diagonal contribution of estimated measurement error to the clear column brightness temperature noise covariance matrix $\hat{N}_{ii}$, is given by

$$\hat{N}_{ii} = \left[\left(\frac{\partial B_i}{\partial T}\right)_{\hat{\Theta}_i}^{-1} \overline{NE\Delta N_i}\right]^2 \quad , \tag{4.3.44}$$

where $\partial B_i / \partial T$ is evaluated at the reconstructed clear-column brightness temperature $\hat{\Theta}_i$. Multiplication by this factor is necessary to change form radiance units to brightness temperature units.

Allowing for correlated errors in η_k and $\eta_{k'}$, it is more appropriate to write

$$\overline{NE\Delta N_i} = \sqrt{(NE\Delta N_i^{ran})^2 + \left[\Delta R \Delta\eta \Delta\eta' \Delta R'\right]_{ii}} \tag{4.3.45}$$

where $\Delta R_{i,k} = \overline{R}_{i,1} - \overline{R}_{i,K+2-k}$ and $(\Delta\eta\Delta\eta')_{kk'}$ is the error covariance matrix of $\Delta\eta$. The error covariance matrix $\Delta\eta\Delta\eta'$ can be approximated in a straightforward manner from Eq. 4.3.15. If we assume that the major source of error in the determination of η via Eq. 4.3.15 is due to errors in the vector C^n (given by $R^n_{i,CLR} - R_{i,1}$), then

$$\Delta\eta = (D'N^{-1}D)^{-1}D'N^{-1}\Delta C \tag{4.3.46}$$

and

$$\Delta\eta\Delta\eta' = (D'N^{-1}D)^{-1}D'\left(N^{-1}\Delta C\Delta C'\right)\left(N^{-1}\right)' D\left(D'N^{-1}D\right)^{-1'} = \left(D'N^{-1}D\right)^{-1} \tag{4.3.47}$$

if we can replace $\Delta C\Delta C'$ by N, the error covariance matrix of C. We use the form of Eq. 4.3.47 to represent $\Delta\eta\Delta\eta'$ in Eq. 4.3.45, but set $\Delta\eta\Delta\eta' = \gamma\left(D'N^{-1}D\right)^{-1}$, where the empirical coefficient γ allows for errors in $\Delta\eta$ that differ from those predicted theoretically. This term is independent of channel for all channels that see the clouds. Currently, we find $\gamma = 1$ works satisfactorily.

The diagonal term of the clear column brightness temperature error covariance matrix is then given by

$$\hat{N}_{ii} = \left[\left(NE\Delta N_i \, A(\eta_k) \right)^2 + \left(\Delta R \Delta\eta \Delta\eta' \Delta R' \right)_{ii} \right] \left[\left(\frac{\partial B}{\partial T} \right)^{-1}_{\hat{\Theta}_i} \right]^2 . \tag{4.3.48}$$

The off-diagonal contribution to the clear column brightness temperature noise covariance matrix $\hat{N}_{ii'}$ arises only from the correlated errors made in the reconstructed clear column radiances of channels i and i' due to $\Delta\eta\Delta\eta'$

$$\hat{N}_{ii'} = \left(\Delta R \Delta\eta \Delta\eta' \Delta R' \right)_{ii'} \left(\frac{\partial B}{\partial T} \right)^{-1}_{\hat{\Theta}_i} \left(\frac{\partial B}{\partial T} \right)^{-1}_{\hat{\Theta}_{i'}} . \tag{4.3.49}$$

The contributions to the noise in channels i and i' are positively (negatively) correlated when the difference in channel radiances in the two fields-of-view have the same (opposite) sign. This term is combined with the channel correlated computational noise due to estimated errors in variables.

If channel i does not see clouds, then we set $A(\eta_k) = \left(\frac{1}{K+1} \right)^{1/2}$ in Eq. 4.3.48 and all terms involving $\Delta\eta\Delta\eta'$ in Eq. 4.3.48 and 4.3.49 are set equal to zero.

Computational noise covariance matrix N^c

The computational noise covariance matrix is designed to account for errors in the computed clear column brightness temperature Θ_i^n, resulting from errors in the geophysical parameters used in the retrieval step. It is assumed that these errors arise primarily from errors in variables X_j assumed known and held fixed in the retrieval step. We model N^c according to

$$N^c_{ii} = \sum_j \left[\frac{\partial \Theta_i}{\partial X_j} \Delta X_j^{(m)} \right]^2 + 0.1^2 \tag{4.3.50}$$

and

$$N^c_{ii'} = \sum_j \frac{\partial \Theta_i}{\partial X_j} \frac{\partial \Theta_{i'}}{\partial X_j} \Delta X_j^{(m)2} \tag{4.3.51}$$

where $\frac{\partial \Theta_i}{\partial X_j}$ represents the derivative of $\Theta_{i,CLR}$ with respect to parameter X_j and $\Delta X_j^{(m)}$ is the estimated uncertainty in parameter X_j in pass m through the system. The parameters used for X_j in modeling N^c represent uncertainties in surface skin temperature, surface emissivity and surface reflectance, as well as constant (in height) shifts in the temperature profile, and multiplication of the water vapor and ozone profiles by a constant as a function of height. The derivatives $\frac{\partial \Theta_i}{\partial X_j}$ are computed empirically. The term 0.1 in Eq. 4.3.50 is taken to represent additional unmodeled errors.

Variable and Channel Selection in the Application of Constrained Least Square Solution

Surface Parameter Retrieval

Channel radiances depend on several unknown surface parameters: the surface skin temperature (T_s); the spectral emissivity, $\varepsilon(\nu)$, and bi-directional reflectance $\rho(\nu)$; and the microwave emissivity (ε_m). Radiances in microwave window channels are more sensitive to errors in emissivity than to surface temperature and also have a significant atmospheric contribution. For this reason, only infrared channels are included in the surface parameter retrieval step and ε_m is not solved for.

In the surface parameter retrieval, we selected window channels from both long- and short-wave IR window regions generally avoiding even weak absorption lines. For window channels, the transmittance at the surface, $\tau(p_s)$, is generally close to 1. Although the opacity of infrared window channels is small, there is absorption and emission due to the water vapor continuum and the nitrogen continuum, both absorbing primarily in the lowest portions of the atmosphere. Therefore, the radiance in window regions depends not only on T_s, ε_ν, and ρ'_ν, but also on the temperature and moisture in the boundary layer. The radiances of window channels do not depend appreciably on temperature and moisture above the boundary layer. To account for the additional dependencies in the surface parameter retrieval, we also can solve for two additional variables by scaling the total precipitable water ($\Delta\ell n\, W$) and shifting the air temperature (ΔT_{AIR}). A few channels centered on weak water vapor absorption lines were included to help account for these additional variables that will be subsequently modified in the temperature and moisture retrievals. These weak water vapor lines are in the 3.7 μm window and are sensitive to water vapor absorption as well as reflected solar radiation. The reflected solar radiation causes the surface to appear hotter than in other window regions not affected by reflected solar radiation. Therefore, in the short wavelength window, the contrast between the radiance leaving the surface and that emitted by the boundary layer is enhanced. This effect, coupled with the increased path length of the solar radiation, makes channels on weak water vapor lines in this window very sensitive to water vapor in the boundary layer. Several of the channels in the surface parameter retrieval are also used later in the moisture profile retrieval. Currently, we do not attempt to shift the temperature profile in any pass because the input temperature profile agrees with AMSU A radiance and is assumed to be accurate enough. We do not scale the water vapor profile in the second pass surface parameter retrieval because we have already retrieved a water vapor profile using AIRS channels in the first pass.

When we do scale the water vapor, a total of thirteen variables are solved for in the surface parameter retrieval for a daytime case (ten for a nighttime case). The perturbation functions include a perturbation to T_s, a perturbation to each of 8 infrared spectral emissivity functions, 3 spectral bi-directional reflectance functions, and a scaling of the water vapor profile. The values of the perturbations were selected to give comparable values of the S matrix for a typical case. If all perturbation functions F_j were half as large, S_{ij} would be half as large for each mode, and the solution vector ΔA_j would be twice as large. The perturbations should be large enough to produce significant S matrix elements, but not so large as to produce an appreciable non-linear response.

The Jacobian or sensitivity matrix S^n is computed every iteration. The partial derivative of channel brightness temperature with respect to the coefficients of each of the

above functions is computed empirically as follows: (1) Compute the channel i radiance and corresponding brightness temperature using the nth iteration parameters (i.e., T_s^n, ε_ν^n, $q^n(P)$, etc.) (2) Compute the channel i transmittance (if necessary), radiance, and corresponding brightness temperature, using the nth iteration parameters but setting the coefficient (ΔA_j) of perturbation function F_j to unity. (3) The sensitivity S_{ij}, or change in channel i brightness temperature per unit change in coefficient ΔA_j, is given by the difference in brightness temperatures computed in steps (1) and (2). The sensitivity or partial derivative of brightness temperature with respect to ground temperature, spectral emissivity, and surface bi-directional reflectance can be computed theoretically by differentiating the clear column radiative transfer equation (and converting to brightness temperature) because the transmittance functions do not depend on these parameters.

After the sensitivity matrix is computed, the inversion procedure described earlier proceeds. In the ground temperature retrieval, we did not include modeled channel computational noise in the noise covariance matrix, but including only the estimate 0.1°C for unmodeled computational noise from other sources in Eq. 4.3.50. The retrieved values of T_s, ε_ν, and ρ_ν will be held constant and used in the subsequent iterative steps for temperature, moisture, and ozone profile retrievals. The shifted water vapor profile will be held fixed in the transmittance and radiative transfer calculations for the temperature profile retrieval and used as the first guess in the water vapor retrieval.

Temperature Profile Retrieval

The temperature profile retrieval problem is set up and solved in a manner completely analogous to the surface parameter retrieval. The solution for the retrieved temperature profile is written in the form

$$T^n(P_\ell) = T^o(P_\ell) + \sum_{j=1}^{J} F_j(P_\ell)\, A_j^n = T^o(P_\ell) + FA \quad , \tag{4.3.52}$$

where ℓ ranges over the number of levels used to compute channel transmittances and radiances, and j ranges over the number of functions that we solve for, currently set equal to 13. The functions in the surface parameter retrieval were taken as discrete changes in different surface or atmospheric parameters. Following the approach of the surface parameter retrieval, the functions F_j are selected as localized functions of pressure, corresponding to changes in temperature primarily in a layer from P_j to P_{j-1}. Use of localized functions is convenient for computing the S matrix and makes the problem more nearly linear. The methodology discussed previously does not require the functions to be orthogonal. In order for the solution to be continuous, the functions chosen are trapezoids, with a value of 0.5° between P_j and P_{j-1} and falling linearly in log P to 0° at P_{j+1} and P_{j-2}. The highest and lowest functions in the atmosphere are special cases, with values of 1° at the upper or lower limit of the atmosphere (1 mb or the surface), 0.5° at the adjacent pressure, and followed by 0° at the next pressure level.

The Jacobian matrix is computed exactly as in the surface parameter retrieval. In any iteration, transmittances and brightness temperatures Θ_i are computed for the temperature sounding channels using $T^n(P)$ and $T^n(P) + F_j(P)$, where $F_j(P)$ is one of the trapezoids, and the Jacobian is obtained empirically according to

$$S_{ij}^{n} = \Theta_i \left[T^n(P) + F_j(P)\right] - \Theta_i \left[T^n(P)\right]. \tag{4.3.53}$$

It can be shown that for an opaque temperature sounding channel, a shift of the entire atmospheric temperature profile by 1° will cause roughly a 1° change in brightness temperature (Susskind *et al.*, 1984). Moreover, a localized change of 1° in an atmospheric layer containing the non-zero part of the channel's weighting function will likewise result in a 1° change in brightness temperature. This brightness temperature change will drop off as the layer becomes thinner than the weighting function. To insure sensitivity of at least one sounding channel to changes in the layer (trapezoid) temperatures, layers were selected to be coarse enough to have an element of the S matrix of at least 0.2 for the layer. While the Jacobian is profile dependent, the layer structure used to define the trapezoid functions was held fixed for all soundings. They were selected so as to be neither too thin, resulting in lack of sensitivity, nor too coarse, resulting in lack of resolution. The pressure boundaries for the 13 functions used in this study are shown in Table 4.3.2. According to Eq. 4.3.52, the only structure in the solution finer than the spacing of these boundary levels must come from the initial guess. In fact, transforming and damping functions as discussed earlier will further decrease the ability of the solution to discern fine structure not contained in the information content matrix $S'WS$. This damping is profile dependent.

In the temperature profile retrieval, it is desirable to select channels which are relatively insensitive to the ozone and water vapor distributions because these variables have not been solved for except for an estimate of the vertically integrated water vapor content obtained in the surface temperature retrieval step. In addition, it is desirable to select temperature sounding channels between absorption lines to obtain the best channel weighting functions (Kaplan *et al.* 1977). Along the lines of Kaplan *et al.* (1977) and outlined in Table 4.3.1, we selected 96 channels in the 15 μm CO_2 band, using Q-branch channels near 666 cm^{-1} to sound the mid to upper stratosphere; channels in between CO_2 absorption lines and near the 720 cm^{-1} and 740 cm^{-1} Q branches to sound through the upper troposphere; and twenty nine channels in the CO_2 4.3 μm band P and R branches, primarily in the vicinity near 2380 cm^{-1}, to sound the mid to lower troposphere. The noisiest spectral region is near 15 μm. For this reason, many of the 15 μm channels used represent spectral intervals sampled twice per channel width. This adds little information about the vertical structure but increases signal to noise. We also included 12 AMSU-A channels, (2-14 from Table 2.3), in the temperature profile retrieval.

Unlike Kaplan *et al.* (1977), we have also included 17 temperature sounding channels between absorption lines in the 15 μm CO_2 band that are sensitive to the mid-lower tropospheric temperature profile. The inclusion of these channels does not appreciably affect sounding accuracy under clear conditions but are very significant under cloudy daytime conditions, for which effective noise levels of the 4.3 μm tropospheric sounding channels can become large. In selection of these channels, we avoided spectral regions near water vapor lines of appreciable strength. The channel radiances of the mid-lower tropospheric temperature sounding 15 μm channels are still affected by water vapor because of absorption due to the wings of nearby water vapor lines as well as the water vapor continuum.

Errors in the estimate of the water vapor profile used to compute the radiances will produce errors in the computed brightness temperature for a given channel, as well as correlated errors in other temperature sounding channels sensitive to water vapor absorption. These errors must be accounted for in the channel computational noise covariance matrix N^c if channels sensitive to water vapor are to be used optimally. While

it is difficult to estimate the radiance error due to errors in the water vapor profile, the error in a channel radiance due to a multiplicative error in the entire water vapor profile is easily

Temperature retrieval	Moisture retrieval	Ozone retrieval
1	20	1
2	100	20
5	200	60
10	300	140
20	400	300
60	500	surface
100	600	
140	700	
190	850	
300	surface	
475		
650		
825		
surface		

TABLE 4.3.2. TRAPEZOID OR LAYER ENDPOINTS

computed. If the fractional error in total water vapor is x, then the error in computed brightness temperature is given by

$$\frac{\partial \Theta_i}{\partial \ell_n W} = \frac{\Theta_i^n(x) - \Theta_i^n(0)}{x}, \tag{4.3.54}$$

where $\Theta_i^n(x)$ is the brightness temperature computed for channel i using all n^{th} iterative parameters, but with the water vapor profile scaled by 1 + x. In computing the noise covariance matrix for the temperature profile retrieval, we set $\Delta \ell n W = 30\%$ at night and 20% during the day, during which the surface parameter retrieval provides an improved estimate of total precipitable water. Both values are set to be larger than the error in total precipitable water obtained after the ground temperature retrieval, because we did not take detailed profile errors into account.

The effects of errors in the estimated water vapor profile on computed channel radiances, as well as radiance errors due to errors in ozone profile and surface parameters, are taken into account in the computational noise covariance matrix (Eqs. 4.3.50, 4.3.51). The noise due to errors in the ozone profile is computed analogously to that for the water vapor profile with the value $\Delta \ell n O_3$ set equal to 20%. Errors in retrieved ground temperature, surface emissivity, and bi-directional reflectance are correlated with each other. For example, high values of surface skin temperature will be compensated for by low values of emissivity. To account for this, we set the effective error of T_s to a value which is less than the actual error in estimated surface skin temperature in computing the noise covariance matrix. We then define $\frac{\partial \Theta_i^n}{\partial T_s}$ as the error in brightness temperature for

channel i given the effective error in T_s. We also include an analogous term for $\frac{\partial \Theta_i^n}{\partial \rho_i}$. We set $\Delta T_s = 1°$ and $\Delta\rho$=0.005.

Incorporation of these terms into the noise covariance matrix has the effect of making channels sensitive to water vapor absorption, ozone absorption and/or the surface temperature appear noisier. It should be noted that in general, the mid-lower tropospheric sounding 15 μm channels will be "noisier" for moist cases than for very dry ones, where uncertainty in water vapor profile will have a smaller effect on the 15 μm radiances. Conversely, 4.3 μm channels are “noisier” during the day than at night.

The contributions to the noise covariance matrix due to errors in estimated total precipitable water and surface skin temperature are included for all temperature sounding channels. Neither is included in the ground temperature retrieval because both variables are being solved for. The estimated error in surface temperature is included in the noise covariance matrix in the subsequent steps of water vapor profile retrieval and ozone profile retrieval, and the estimated error in water vapor profile is also included in the ozone profile retrieval, but not in the water vapor retrieval.

The retrieval step described above is done after the AMSU retrieval step has been done in the start up system. That AMSU retrieval step is analogous, but uses only AMSU A channels and stratospheric AIRS temperature sounding channels, and solves for the microwave emissivity as well as coefficients of the 13 temperature perturbation functions.

Water Vapor Profile Retrieval

Unlike the surface parameter and temperature profile retrievals, the water vapor profile retrieval problem is highly non-linear. A change in water vapor abundance in a given level affects the transmittances and atmospheric emission and absorption at all higher pressure levels in a complex manner. Nevertheless, the problem can be set up and solved in a completely analogous manner. In the surface parameter retrieval, the entire water vapor profile (up to 50 mb) was multiplied by a constant unknown factor. Following this form, the solution for the retrieved moisture profile is expressed as

$$q^n(P_\ell) = q^0(P_\ell)\left[1+\sum_{j=1}^{J} F_j(P_\ell)\, A_j^n\right], \qquad (4.3.55)$$

where ℓ ranges over the 64 levels used to compute transmittances and radiances, and j ranges over J solution functions. The functions $F_j(P_\ell)$ are expressed as trapezoids with a value of 0.05 in coarse atmospheric layers, in a manner analogous to that described above in the temperature profile retrieval. The endpoints of the 8 trapezoids used in the moisture profile retrieval in this work are included in Table 4.3.2. The highest trapezoid has a value of 0.05 at 100 mb and 200 mb and 0 at 20 mb. The water vapor profile is not adjusted above 20 mb due to the lack of sensitivity of the radiances to the small abundance of water vapor in the stratosphere, assumed to be relatively constant. The lowest function is comprised of two straight lines, with a value at the surface and 850 mb of 0.05, and a value of 0. at 700 mb.

In the moisture retrieval, we included channels between absorption lines in the 6.3 μm water vapor band that are sensitive to humidity throughout the troposphere. These channels provide sharper weighting functions (more localized absorption) than centers of strong lines and make the problem more linear. We also included channels on and off

weak water vapor absorption lines in both the 11 μm and 8 μm windows, that are sensitive to the water vapor continuum and improve sounding capability of the lower tropospheric humidity, and in the 3.7 μm window, that provide improved sensitivity to low level moisture during the day. The S matrix is computed empirically exactly as in the temperature profile retrieval. The parameters determined from the surface and temperature profile retrievals are assumed true and kept fixed in the calculations.

In constructing the noise covariance matrix, we included terms for uncertainties in ground temperature, as in the temperature profile retrieval, as well as a term shifting the entire temperature profile by a constant, as done in the noise covariance matrix used in the determination of η (Eq. 4.3.10).

Ozone Profile Retrieval

The solution for the ozone profile retrieval has the same form as that for the moisture retrieval. For the ozone retrieval, we used 5 trapezoid functions with values of 0.05, as in the water vapor retrieval. The end points of the trapezoids are included in Table 4.3.2. The same steps outlined in the previous section are used to compute the Jacobian. It is critical to solve for water vapor before ozone because ozone channels are sensitive to absorption by boundary layer water vapor. We selected 23 channels in the 9.6 μm ozone band for the ozone retrieval. Uncertainties in surface parameters, temperature profile, and water vapor profile are included in the ozone noise covariance matrix.

Subsequent to the ozone profile retrieval, the 4 retrieval steps are repeated, using all retrieved quantities as the first guess. This produces a small improvement in results because the surface parameter retrieval, while not highly sensitive to temperature and moisture profiles above the boundary layer, has some residual sensitivity to these parameters. Likewise, the temperature profile retrieval and all other steps benefit from improvements in all other variables. The results do not change appreciably if we repeat the retrieval steps a third time.

Retrieval of Cloud Properties

The observed radiance for channel i, $\overline{R_i}$, in a scene with j different cloud types is given by

$$\overline{R_i} = \left(1 - \sum_j \alpha_j\right) R_{i,CLR} + \sum_j \alpha_j R_{i,CLD,j} \quad , \tag{4.3.56}$$

where α_j is the fraction of the scene (as seen from above) covered by cloud type j, $R_{i,CLR}$ is the clear-column channel i radiance (i.e., the radiance emerging from the clear portion of the scene), and $R_{i,CLD,j}$ is the channel i radiance emerging from the cloudy portion of the scene covered by cloud type j, (Chahine, 1982).

The computation of $R_{i,CLD,j}$ for a given scene is complex due to the detailed spectral absorption and reflection properties of clouds, cloud morphology within the field-of-view, and geometric shadowing factors. If we assume plane parallel cloud formations and assume nadir viewing, $R_{i,CLD,j}$ can be expressed as

$$R_{i,CLD,j} = \tau_{ic_j} R_i(p_{c_j})\tau_i(p_{c_j}) + \varepsilon_{ic_j} B_i(T_{c_j})\tau_i(p_{c_j}) + \int_{p_{c_j}}^{o} B_i[T(p)]\left(\frac{d\tau_i}{d\ell np}\right) d\ell np$$
$$+\rho'_{ic_j} H_i \tau'_i\left(p_{c_j}\right)\cos\theta_o, \tag{4.3.57}$$

where $R_i(p_{c_j})$ is the upwelling radiance at cloud top pressure p_{c_j}, and τ_{ic_j} and ε_{ic_j} are respectively the transmissivity and emissivity of cloud type j at channel frequency ν_i, $B_i\left(T_{c_j}\right)$ is the Planck function evaluated at channel frequency ν_i and cloud top temperature T_{c_j}, ρ'_{ic_j} is the cloud bi-directional reflectance of solar radiation incoming at solar zenith angle θ_o and outgoing in the direction of the satellite, $\tau'_i(p_{c_j})$ is the two path atmospheric transmittance from the top of the atmosphere to the cloud top pressure p_{c_j}, and H_i is the solar irradiance. In Eq. 4.3.57, the first term represents upwelling radiation from below the cloud that passes through the cloud; the second term represents radiation emitted by the cloud that is transmitted by the atmosphere to the satellite; the third term represents that portion of the radiation absorbed and emitted by the atmosphere above the cloud, and the fourth term represents solar radiation reflected by the cloud in the direction of the satellite. We have neglected a small term due to downwelling thermal radiation reflected off the cloud in the direction of the satellite.

If there is only one cloud type in the scene, $R_{i,CLD,1}$ can be expressed as

$$R_{i,CLD,1} = \tau_{ic_1} R_{i,CLR} + \varepsilon_{ic_1} B_i(T_{c_1})\tau_i(p_{c_1}) + (1-\tau_{ic_1})\int_{p_{c_1}}^{o} B_i[T(p)]\left(\frac{d\tau_i}{d\ell np}\right) d\ell np$$
$$+\rho'_{ic_1} H_i \tau'_i(p_{c_1})\cos\theta_o \quad . \tag{4.3.58}$$

When doing cloud property retrievals, we limit the channels to frequencies less than 1250 cm^{-1}, for which the last term in equation 4.3.58 is not significant. If we make the approximation that $\tau_{ic_1} = (1 - \varepsilon_{ic_1})$, then equations 4.3.56 and 4.3.58 can be combined to give

$$\overline{R_i} = \left(1-\alpha_1\varepsilon_{ic_1}\right)R_{i,CLR} + \left(\alpha_1\varepsilon_{ic_1}\right) R^B_{i,CLD}\left(p_{c_1}\right) \tag{4.3.59}$$

where $R^B_{i,CLD}(p_{c_1})$ is the radiance one would get from a black cloud $\left(\tau_{ic} = 0, \varepsilon_{ic} = 1\right)$ at cloud top pressure p_{c_1}. It is apparent that the term $\alpha_1 \varepsilon_{ic_1}$ appears only as a product in equation 4.3.59. Therefore α and ε_{ic} cannot be determined independently from each other, but only as their product, which can be thought of as a radiatively effective cloud fraction that may be a function of frequency. To the extent that ε_{ic} is a function of frequency, one can express the frequency dependent term $\alpha_1\varepsilon_{ic_1}$ as $\left(\alpha\varepsilon_{c\bar{\nu}}\right)_1 F_1(\nu)$ where

$(\alpha\varepsilon_{c\bar{\nu}})_1$ is a representative value of the effective cloud fraction $\alpha_1\varepsilon_{c_1}$ at a given frequency $\bar{\nu}$, and $F_1(\nu)$ expresses the frequency dependence of $\frac{\varepsilon_{c\nu}}{\varepsilon_{c\bar{\nu}}}$.

If we consider the case of two cloud types, where we again assume $\tau_{ic_2} = (1 - \varepsilon_{ic_2})$, then the radiances can be written as

$$R_i = (1 - \overline{\alpha\varepsilon}_{i,1} - \overline{\alpha\varepsilon}_{i,2})R_{i,CLR} + \overline{\alpha\varepsilon}_{i,1} R_i^B(p_{c_1}) + \overline{\alpha\varepsilon}_{i,2} R_i^B(p_{c_2}) \qquad (4.3.60)$$

where $\overline{\alpha\varepsilon}_{i,1}$ and $\overline{\alpha\varepsilon}_{i,2}$ are radiatively effective cloud fractions for the clouds at p_{c_1} and p_{c_2}. For the higher cloud at p_{c_1}, $\overline{\alpha\varepsilon}_{i,1} = \alpha_1\ \varepsilon_{ic_1}$ as before. On the other hand, for the lower cloud

$$\overline{\alpha\varepsilon}_{i,2} = \varepsilon_{ic_2}\ [\alpha_2 + (1 - \varepsilon_{ic_1})\alpha_1\alpha_{12}] \qquad (4.3.61)$$

where α_{12} is the fraction of the area covered by cloud type 1 which is under- covered by cloud type 2. In equation 4.3.61, ε_{ic_2} multiplies the cloud fraction for layer 2 as seen from above, which is comprised of two parts: α_2 being the fraction of the scene covered only by clouds in layer 2, and $(1 - \varepsilon_{ic_1})\alpha_1\alpha_{12}$ being that part of the scene covered by clouds of both type 1 and type 2, which is seen through cloud type 1, with transmissivity $(1 - \varepsilon_{ic_1})$. If either ε_{ic_1} is independent of frequency or α_{12} is the same for all fields of view, this situation corresponds to two cloud formations. In the first case, the radiances are equivalent to a well defined, frequency independent amount of each type of black cloud. In the second case, cloud type 1 has a constant spectral dependence in each field of view which combines properties of cloud types 1 and 2. To the extent that $(1 - \varepsilon_{ic_1})$ is frequency dependent, and α_{12} depends on field of view, this situation actually contains three cloud formations, because the spectral dependence of radiances in areas covered by clouds at both levels is different from that of clouds at either of the two levels, in a manner that is field of view dependent. The significance of this with regard to determination of clear column radiances remains to be tested. With regard to determination of cloud parameters, the spectral dependence of $\overline{\alpha\varepsilon}_{i,2}$ contains the product of two spectrally dependent terms ε_{ic_2} and ε_{ic_1}. To first order, we can still write $\overline{\alpha\varepsilon}_{i,2} = \alpha\varepsilon_{c_2}\ F_2(\nu)$ but care must be taken in interpreting $F_2(\nu)$.

We have currently attempted cloud parameter retrievals using the AIRS team simulations, which had two layers of clouds with constant known spectral emissivity (=0.9) with α_{12} equal to zero for all fields of view. Observations in each of the three fields of view k=1,3 used to do cloud clearing were used to determine the cloud parameters. The channel radiances $\overline{R}_{i,k}$ can be expressed as

$$\overline{R}_{i,k} = \left(1 - \left(\overline{\alpha\varepsilon}\right)_{1k} - \left(\overline{\alpha\varepsilon}\right)_{2k}\right)R_{i,CLR} + \left(\overline{\alpha\varepsilon}\right)_{1k} R_i^B\left(p_{c_1}\right) + \left(\overline{\alpha\varepsilon}\right)_{2k} R_i^B\left(p_{c_2}\right) \qquad (4.3.62)$$

The cloud parameter retrieval is performed after all other parameters are solved for, in an exactly analogous manner to that of all other retrieval steps. Given a surface skin temperature, surface spectral emissivity, and atmospheric temperature-moisture-ozone profile, $R_{i,CLR}$ and $R_i^B(p_{c_j})$ can be readily computed. The only unknowns in equation 4.3.62 are $(\overline{\alpha\varepsilon})_{jk}$ $j = 1, 2;\ k = 1, 3$, and p_{c_1} and p_{c_2}. We use observations $\overline{R}_{i,k}$ in the 3 fields of view for the 15 μm and 8-12 μm channels used to determine η to solve for these 8 variables. The noise covariance matrix N used to retrieve cloud parameters, which represents both noise in the observations and uncertainties in the computed values of $R_{i,CLR}$, is taken to be identical to that used to determine η (Eq. 4.3.10).

Given the mth iterative cloud parameters $\overline{\alpha\varepsilon}^m_{1k}$, $\overline{\alpha\varepsilon}^m_{2k}$, p^m_{c1}, p^m_{c2} we define

$$Y^m_{ik} \equiv \overline{R}_{i,k} - R^m_{ik} = \left(\overline{R}_{i,k} - R_{i,CLR}\right) + \sum_{j=1,2} \overline{\alpha\varepsilon^m_{jk}} \left(R_{i,CLR} - R_i\left(p^m_{c_j}\right)\right) \tag{4.3.63}$$

where $\overline{R}_{i,k}$ is the observed channel i radiance in field of view k and R^m_{ik} is computed from the mth iterative parameters. This gives rise to the iterative equation

$$\begin{aligned} Y^{m+1}_{ik} - Y^m_{ik} &= \sum_{j=1,2}\left[\left(R_{i,CLR} - R_i(p^m_{c_j})\right)\right]\Delta\overline{\alpha\varepsilon}^m_{jk} + \sum_{j=1,2}\left[\overline{\alpha\varepsilon}^m_{jk}\left(\frac{-\partial R_i(\partial p_{c_j})}{\partial p_{c_j}}\right)\right]\Delta p^m_{c_j} \\ &= \sum_{j=1,2}\left[S^m_{ik,\Delta\alpha\varepsilon_{jk}}\right]\overline{\alpha\varepsilon}^m_{jk} + \sum_{j=1,2}\left[S^m_{ik,\Delta p_{c_j}}\right]\Delta p^m_{c_j} \end{aligned} \tag{4.3.64}$$

where the terms in brackets are the appropriate Jacobians, which are computed empirically as are all other Jacobians. It should be noted that if $\overline{\alpha\varepsilon}_{jk}$ (for all k) and/or $\frac{\partial R_i}{\partial p_{c_j}}$ (for all i) are small for a given p_{c_j}, the Jacobian for that cloud top pressure will be small and that cloud top pressure will be contained primarily in a heavily damped mode and not be changed significantly from the initial guess. In the AIRS team simulations conducted thus far, the second cloud formation usually contained small amounts of low clouds, and p_{c_2} was in general not well determined from the data.

For our retrievals, the first guess cloud top pressures were taken as 350 mb and 650 mb, and the first guess effective cloud fractions were taken as 0.25 for each cloud type. The solution was constrained such that $p_{c_1} \geq 100$ mb, $p_{c_2} \leq p_s - 50$ mb where p_s is the surface air pressure. In addition $\alpha\varepsilon_{1,k} + \alpha\varepsilon_{2,k}$ was constrained to be ≤ 10. If the second cloud fraction is either set very small in the first guess, or becomes very small in the retrieval, one can no longer determine useful information about the second cloud top pressure.

Product Error Estimates

Error estimates of AIRS team products, on a retrieval by retrieval basis, are an important part of the dataset. This involves estimating likely sources of error and propagating them through the retrieval process.

Clear column radiance error estimates

The most straightforward example of error estimation in our retrieval is the estimate of the channel error covariance matrix of the cloud cleared radiance. Obtaining cloud cleared radiances, including their error estimates, is a critical step in the retrieval of other geophysical parameters from AIRS because they are included in the noise covariance matrix of each retrieval step. The clear column radiances are also an important product for those desiring to do radiance assimilation using AIRS observations.

The clear column noise covariance matrix $\hat{N}$ is given in Eqn. 4.3.48. The predicted error in clear column radiances, $\hat{R}_{i,\ell}$, for channel I and case ℓ is given by the square root of the diagonal term of the clear column radiance noise covariance matrix, $\hat{N}$:

$$\delta\hat{R}_{i,\ell} = \left[NE\Delta N_i^2 \; A\left(\eta_{i,1},\eta_{i,2}\right)_\ell^2 + \gamma\left[\Delta R_{OBS,i,\ell}\left(\Delta\eta\Delta\eta'\right)_\ell \; \Delta R'_{OBS,i,\ell}\right]^2\right]^{1/2} \quad . \qquad (4.3.65)$$

This prediction has a strong case dependence resulting from the noise amplification factor, $A\left(\eta_{i,1},\eta_{i,2}\right)_\ell$; differences in the vector $\Delta R_{OBS,i,\ell}$, corresponding to differences in the fields of view $\left(\overline{R}_{i,1} - R_{i,k}\right)_\ell$; as well as differences in the predicted error covariance $\left(\Delta\eta\Delta\eta'\right)_\ell$. There is also a strong channel dependence resulting from $NE\Delta N_i$, $\Delta R_{OBS,i}$, and $A\left(\eta_{i,1}, \eta_{i,2}\right)$, which is much smaller for channels that do not see clouds.

Product error estimates

In each retrieval step we solve for the change in coefficients of functions which will minimize the radiance residuals. In Eqn. 4.3.34, an estimate of the uncertainty of these coefficients, $\Delta\tilde{B}_j^n$ is given. $\Delta\tilde{B}_j^n$ has a strong case dependence due to the propagation of the clear column radiance error in the noise covariance term (see Eqn. 4.3.41). The uncertainty coefficients are transformed in exactly the same manner as the solution coefficients, ΔB_n, to obtain the propagated error in the geophysical parameters:

$$\delta A^n = U \cdot \Delta\tilde{B}^n = U \cdot \frac{\sqrt{\lambda^n}}{\lambda^n + \Delta\lambda^n} \quad . \qquad (4.3.66)$$

The error estimates are calculated at each retrieval step and each iteration; however, they are updated estimates, not a change to an existing error estimate. Errors in A (δA) propagate into geophysical parameters according to

$$\delta X^{n+1} = \sqrt{\sum_j F_j \cdot \left(\delta A_j^n\right)^2} \qquad (4.3.67)$$

In addition, we need to add another component of the uncertainty due to the non-uniqueness of the solution. This null-space error, δX_N, is derived from a large ensemble of cases. In general, the propagated error estimate is given as

$$\delta X^{n+1} = \sqrt{\left(\delta X_N\right)^2 + \sum_j F_j \cdot \left(\delta A_j^n\right)^2} \quad . \tag{4.3.68}$$

This equation is analogous to the equation for the solution, Eqn. 4.3.17. For example, for the temperature profile, we use 13 trapezoidal functions to solve for the change to 13 coefficients, ΔA_j. We would compute the error estimate for the temperature column with our estimates of δA as follows:

$$\delta T^{n+1}(p) = \sqrt{\left(\delta T_N(p)\right)^2 + \sum_{j=1}^{13} F_j(p) \cdot \left(\delta A_j^n\right)^2} \tag{4.3.69}$$

For moisture estimates we solve for a % change in the column density that best matches the observed radiances. The moisture error estimates are calculated in an analogous manner to the solution coefficients (given in Eqn. 4.3.55) and given by

$$\delta q^{n+1}(p) = q^n(p) \cdot \sqrt{\left(\frac{\delta_{qN}(p)}{q(p)}\right)^2 + \sum_j F_j(p) \cdot \left(\delta A_j\right)^2} \tag{4.3.70}$$

<u>Closed-loop operation</u>

Our experience with simulated radiances has shown that improving the noise covariance matrix in the retrieval and cloud-clearing steps will improve the results. The case dependent error estimates, δX, can be used to compute the computation noise covariance matrix, N^c, instead of the ensemble estimates that are currently used. The error estimates will allow the case dependence of the cloud cleared radiance error estimate to propagate through the retrieval into error estimates for the geophysical retrieval. These estimates can then in turn, be used to re-estimate the cloud cleared radiance estimates through the updated and case dependent value of N^c. Difficult cases (i.e., low scene contrast) may benefit substantially from more realistic weighting of the channels in the later retrieval stages.

5. Tuning and uncertainty estimates

5.1 Tuning (McMillin)

To be useful for numerical forecasts, AIRS data must be consistent with data from other sources. Errors in both the AIRS data and the other data contribute to systematic differences between different data sets. These are removed by a statistical adjustment procedure. There are errors in the AIRS data that can be recognized in the data and removed. A linear shift in the detector array is one example. It is assumed that these corrections have been made. It is also assumed that a set of match data are available in which there are pairs of radiances, one calculated from some measure of truth and one observed by the AIRS. The problem is to make an adjustment to remove the systematic differences.

Before proceeding, it is useful to discuss the calculation procedures. Although the calculation of radiances is easy using the procedures of section 3 once the atmospheric state is completely specified, radiosondes and other sources of information often provide an incomplete description of the atmospheric state. For example, a radiosonde specifies the temperature and water vapor in the lower part of the atmosphere. The radiances depend on the these data as well as the upper atmosphere and the surface skin temperature. These can be obtained from the satellite retrieval. Values of other gases such as ozone can be obtained from the retrieval as well. When this is done, the adjustment will preserve the original, theoretical relationships between the atmospheric state and the calculated values for these variables, but will adjust the theoretical relationships for those variables for which an measure of truth is available.

Approach

An obvious way to do the adjustment is to use measured values to predict the calculated values. It is common to adjust the measured values because the data are frequently used in an iterative retrieval procedure in which the radiances are calculated at each iteration. This means the adjustment needs to be done only once. Using normal regression for the adjustment has some problems. One is that the regression is likely to be numerically unstable. A second is that the coefficients are physically unrealistic. It is reasonable to expect that the regression coefficients should be slight perturbations to the identity matrix. That is, the calculated radiance should depend on the measured radiance with a coefficient that is nearly unity, and the dependence on other channels should be small. This is the form one would expect for a slight error in the weighting function height. The desired solution is given by the shrinkage operator (Oman *et al.*. 1982). The particular derivation is found in the appendix of Crone *et al.*. (1996). The shrinkage estimator, C_s is obtained by finding the C that minimizes the trace of $[(C-C_0)^T (C-C_0)]$ subject to the constraint that the trace of $[(Y-CX)(Y-CX)^T]$ is held constant. This can be done by setting the derivative $\frac{\partial}{\partial C}\left[\mathrm{Tr}(C-C_0)^T(C-C_0)\right]$ equal to zero. Doing this gives

$$2(C-C_0)+\gamma(-2YX^T+2CXX^T)=0 \qquad (5.1.1)$$

which leads to

$$C_s = (YX^T + \gamma C_0)(XX^T + \gamma I)^{-1} \tag{5.1.2}$$

For many purposes, this form of the equation is fine and is the one used for current sounders which have tens of channels. However, for a high resolution instrument like AIRS, the number of channel increases by a factor of about 100. Not only does the large number of channels increase the computations, the larger number, coupled with the fact that more channels are similar, increases the numerical instability. The retrievals are being done with linear transformations such as eigenvectors or "super channels", which are averages of channels that are highly correlated with each other. Thus they contain no unique information, but are averaged to reduce the noise. If we consider a linear transformation of X, then we have the equations

$$Y = C\,X = C_{0t}\,E \tag{5.1.3}$$

which can be solved to give

$$C_{0t} = CE^T(EE^T)^{-1} \tag{5.1.4}$$

provided that the inverse exists. This transformation is needed because the initial coefficients are known in the form of C_0, but the values of C_{t0} are required to solve the equation. In some cases the inverse may have problems so it is best to avoid the problem by writing equation (5.1.2) as

$$C_s = (YX^T + \gamma C_0 + C_0XX^T - C_0XX^T)(XX^T + \gamma I)^{-1} \tag{5.1.5}$$

which can be rearranged to give

$$C_s = C_0 + (Y + -C_0X)X^T(XX^T + \gamma I)^{-1} \tag{5.1.6}$$

which is the same as ridge regression on the quantity (Y-C_0X) instead of Y. In this form, a linear transformation becomes

$$C_s = C_{t0} + (Y + -C_{t0}EX)X^TE^T(EXX^TE^T + \gamma I)^{-1} \tag{5.1.7}$$

which leads to

$$Y - C_{t0} = [(Y + -C_{t0}EX)X^TE^T](EXX^TE^T + \gamma I)^{-1}EX \tag{5.1.8}$$

In this form, it is possible to replace $C_{t0}E$ with C_0 to give

$$Y - C_0X = [(Y + -C_0EX)X^TE^T](EXX^TE^T + \gamma I)^{-1}EX \tag{5.1.9}$$

This is a particularly attractive form when C_0 consists of the identity matrix. We note that the problem is trivial when the linear combination consists of the eigenvectors, because EE^T is the identity matrix for that case. However, the form given above is completely general. It may turn out that the best transformation to a smaller subspace is to perform a stepwise regression. The exact subspace is a detail that will be resolved when data with the appropriate error structure (simulated or real) become available.

In use, the value of gamma is empirically adjusted to give small departures from the expected values. The result is a set of coefficients that give nearly the same reduction in variance on the dependent set as is given by normal regression, but that have the desirable physical property that the calculated value for each channel is given by the measured value plus small corrections. Procedures for doing constrained regressions have been

documented in a series of papers (McMillin *et al.*. 1989 , Crone *et al.*. 1996, Uddstrom and McMillin 1994a, Uddstrom and McMillin 1994b).

Use of coefficients

Once the coefficients are available, they can be used to make adjustments to the radiances. The adjustment takes the form

$$Y = [Y_0 - (C_0 + C)X_0] + (C_0 + C)X \tag{5.1.10}$$

where Y represents the adjusted radiances, Y_0 represents the sample mean, C_0 represents the initial coefficients, X represents the measured radiances and other predictors, X_0 represents their mean values, and C is given by

$$C = [(Y - C_0 X)X^T E^T](EXX^T E^T + \gamma I)^{-1} E. \tag{5.1.11}$$

In this form, values of C represent minor perturbations to the values of C_0 which perform most of the prediction. For example, C_0 would generally have a value of 1.0 for the channel being corrected, and a value of zero elsewhere. The values of C would represent the empirical adjustments.

5.2. Simulation System (Haskins, Aumann)

The current software has a full level 0 to level 2 data product simulation with three goals in mind: (1) core algorithm performance is based on the simulation, (2) robustness testing of the AIRS data product algorithms is based partly on simulation, (3) data product validation requires an extensive simulation effort. The simulations are to be as realistic and challenging as possible as well as extensive enough to provide a complete set of exception conditions. The components in the AIRS simulation are described in Figure 5.2.1.

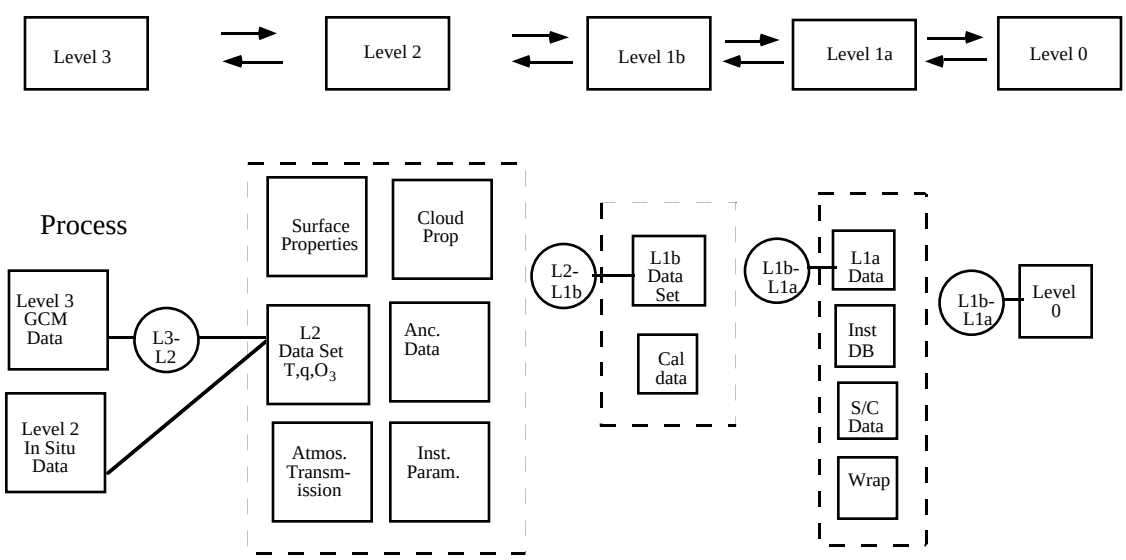

FIGURE 5.2.1: AIRS SIMULATION SYSTEM

This discussion will focus on the simulation of level 2 data. The AIRS simulation effort involves several independent groups within the AIRS Science Team:

1. The geophysical data are generated by team members at NOAA's National Center for Environmental Prediction (NOAA/NCEP) using experimental mesoscale models. The model used for the current simulation comes from the forecast for July 1, 1993. It covers about 3080 km in longitude, 4700 km in latitude with a 40 km spacing grid, and is centered on the western part of the United States. At every grid point the model lists the temperature, water vapor, and fractional cloud cover as functions of pressure between 30 mb and the surface. These data are called Level 2 geophysical data by EOS.
2. The simulation team selects satellite tracks from the mesoscale model and converts them to the radiances (level 1B) which the AIRS, AMSU and HSB instruments would observe. All important instrument-related effects, such as detector noise, gaps in the spectral coverage, wavelength, and the spectral response function of each channel, are included in the calculations of the Level 1 data.

Three types of data are distributed to facilitate the task of the algorithm developers:

1. Training data: This is a set of about 2000 temperature/moisture profiles which are statistically representative of the mesoscale model data.
2. Truth data: This is both Level 1 data and the exact retrieval solution (the Level 2 data which was used to create the Level 1 data). The developers use this data to test the accuracy of their algorithms.
3. Test data: This is Level 1 data, which is statistically similar to the Level 1 truth data, but for a different ensemble of cases which are known only to the simulation team.

The algorithm development teams return their results from the test data and the truth data, together with the software used to obtain the results, to the simulation team. The retrievals are evaluated for accuracy. The software is evaluated for computer resource requirements (CPU and I/O utilization) and compliance with reasonable software engineering standards. Periodic meetings of the AIRS Science Team are used for discussions of simulation procedures, retrieval accuracy, and retrieval resource requirements.

The algorithm development, as described above, was started in 1992. The initial tests were simple: Night time, cloud free, surface with no elevation (i.e., at 1000 mb pressure) and with known, wavelength-independent emissivity and reflectivity. Since then, the simulation has advanced to include daytime, wavelength-dependent and unknown surface emissivity and reflectivity, realistic topography, and cloud covered scenes.

TOVS data from HIRS 2/MSU indicate that 45 percent of the time, there are clear conditions, about 35 percent of the data are partly cloudy, but the retrievals are acceptable, while the remaining 20 percent of the data are too cloudy for the HIRS 2/MHS to produce usable retrievals. The first test data including clouds was released to the algorithm development teams in August 1994. This test was called the single layer gray cloud test. The statistical distribution and cloud granularity were patterned using the statistics obtained from the TOVS data. The level 2 truth was taken from a 6-hour forecast using the NCEP Eta model for July 19, 1993. For this test, the simulation program used Level 2 data from four satellite tracks crossing the model area from south to north (tracks A, B, C, D in Figure 5.2.2) and converted them to the spectral radiances as described above. (The curvature of the tracks is an artifact of the mercator map projection).

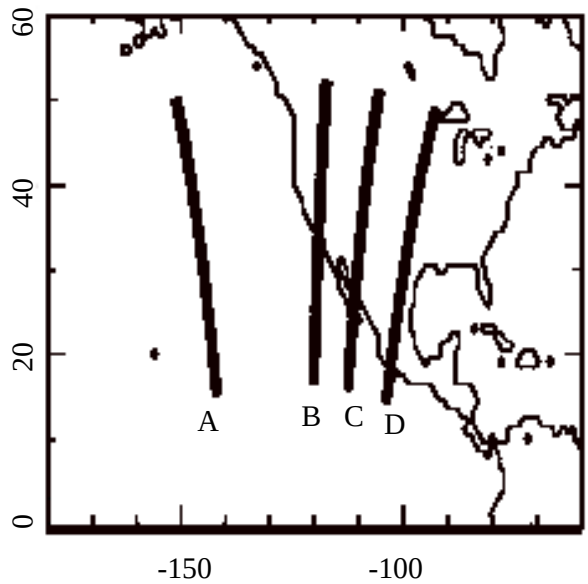

FIG 5.2.2: SIMULATION TRACKS

There are 45 cases taken across each track, each covering as area the size of a nadir AMSU A footprint. The model forecast for the center of the footprint was taken as truth across the entire footprint. AMSU-A radiances were simulated for this spot, as well as AIRS and HSB radiances. for a 3x3 array of spots within the AMSU-A spot. These smaller spots were assumed to differ only in the amount of clouds, which behaved identically in all 9 spots (i.e. different amounts of the same type of cloud).

As this was the first simulation of cloudy data, the data set was limited to two layers of clouds, but a single cloud formation and the clouds were simulated as spectrally gray, i.e., the emissivity and reflectivity were unknown, but wavelength independent. Figure 5.2.3 shows the fractional cloud cover averaged over the 9 spots for each of the 45 cases along track B. The fractional cloud cover in the AIRS FOV ranged from 20 to 90 percent. The cloud top pressure ranged from 850 mb to 100 mb. Figure 5.2.4 shows the cloud liquid water content along track B. It averages about 0.01g/cm^2, but exceeds 0.03 g/ cm^2 near latitudes 44 and 52°N. The onset of precipitation is between 0.02 and 0.04 g/ cm^2. This data set represented a severe test of the ability of the combined infrared and microwave sounding capability of AIRS/AMSU and HSB.

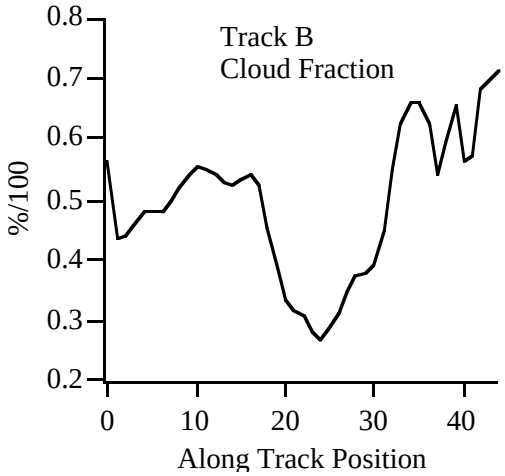

FIGURE 5.2.3: TRACK B CLOUD FRACTION

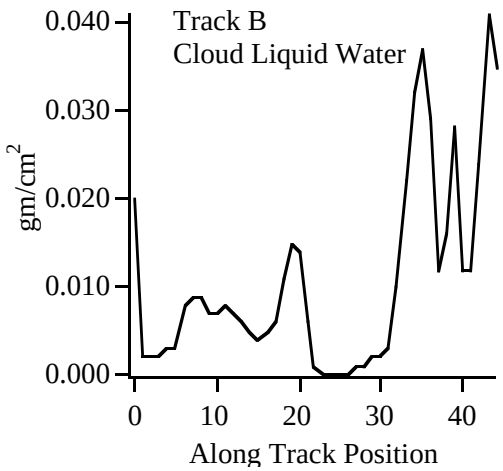

FIGURE 5.2.4: TRACK B CLOUD LIQUID WATER

Current Team Algorithm Simulation results (July 96)

Current simulation results of the AIRS Team Algorithm are summarized in Table Figure 5.2.1 and a sample vertical profile of RMS errors for Track NB is presented in figure 5.2.5. Results are shown for temperature are for RMS layer mean temperature errors in 1 km layers up to the tropopause, then 2 km layers. Results shown for water vapor are for RMS percent errors in layer precipitable water for 2 km layers up to 200 mb. The statistics are broken out for each track and each step of the algorithm. In the following the first letter refers to night (N) or day (D). The second letter refers to the track (A,B,C,D). The Track DP is the day 'D' track with two independent cloud formations.

Night Simulation Track	**NA**			**NB**			**NC**		
Retrieval Stage	**MW only**	**RET 1**	**RET 2**	**MW only**	**RET 1**	**RET 2**	**MW only**	**RET 1**	**RET 2**
Surface Temperature RMS Error (°K)	1.6	0.4	0.1	2.7	0.5	0.1	3.2	0.8	0.2
Tropospheric Temperature RMS Error (°K)	1.8	1.4	1.1	1.9	1.2	1.0	2.0	1.1	0.8
Total Water Vapor Column Density RMS Error (%)	20.8	6.9	6.4	13.9	16.8	15.2	15.1	10.6	7.6
Total Liquid Water Column Density RMS Error (%)	88.3	N/A	N/A	100.0	N/A	N/A	85.0	N/A	N/A
Total Ozone Column Density RMS Error (%)	N/A	N/A	1.8	N/A	N/A	2.5	N/A	N/A	3.7

Day Simulation Track	**DB**			**DC**			**DD**			**DP**		
Retrieval Stage	**MW only**	**RET 1**	**RET 2**	**MW only**	**RET 1**	**RET 2**	**MW only**	**RET 1**	**RET 2**	**MW only**	**RET 1**	**RET 2**
Surface Temperature RMS Error (°K)	6.1	1.2	1.2	7.5	1.2	0.7	9.0	0.8	0.6	9.0	2.1	1.2
Tropospheric Temperature RMS Error (°K)	1.7	1.3	1.1	1.5	1.1	0.9	1.7	1.2	1.0	1.7	1.3	1.2
Total Water Vapor Column Density RMS Error (%)	13.0	10.6	9.2	13.1	7.2	3.9	17.6	7.1	3.9	17.6	5.8	5.3
Total Liquid Water Column Density RMS Error (%)	86.0	N/A	N/A	69.5	N/A	N/A	98.8	N/A	N/A	98.8	N/A	N/A
Total Ozone Column Density RMS Error (%)	N/A	N/A	2.1	N/A	N/A	1.6	N/A	N/A	2.1	N/A	N/A	1.7

TABLE 5.2.1: SUMMARY STATISTICS FOR THE AIRS TEAM ALGORITHM

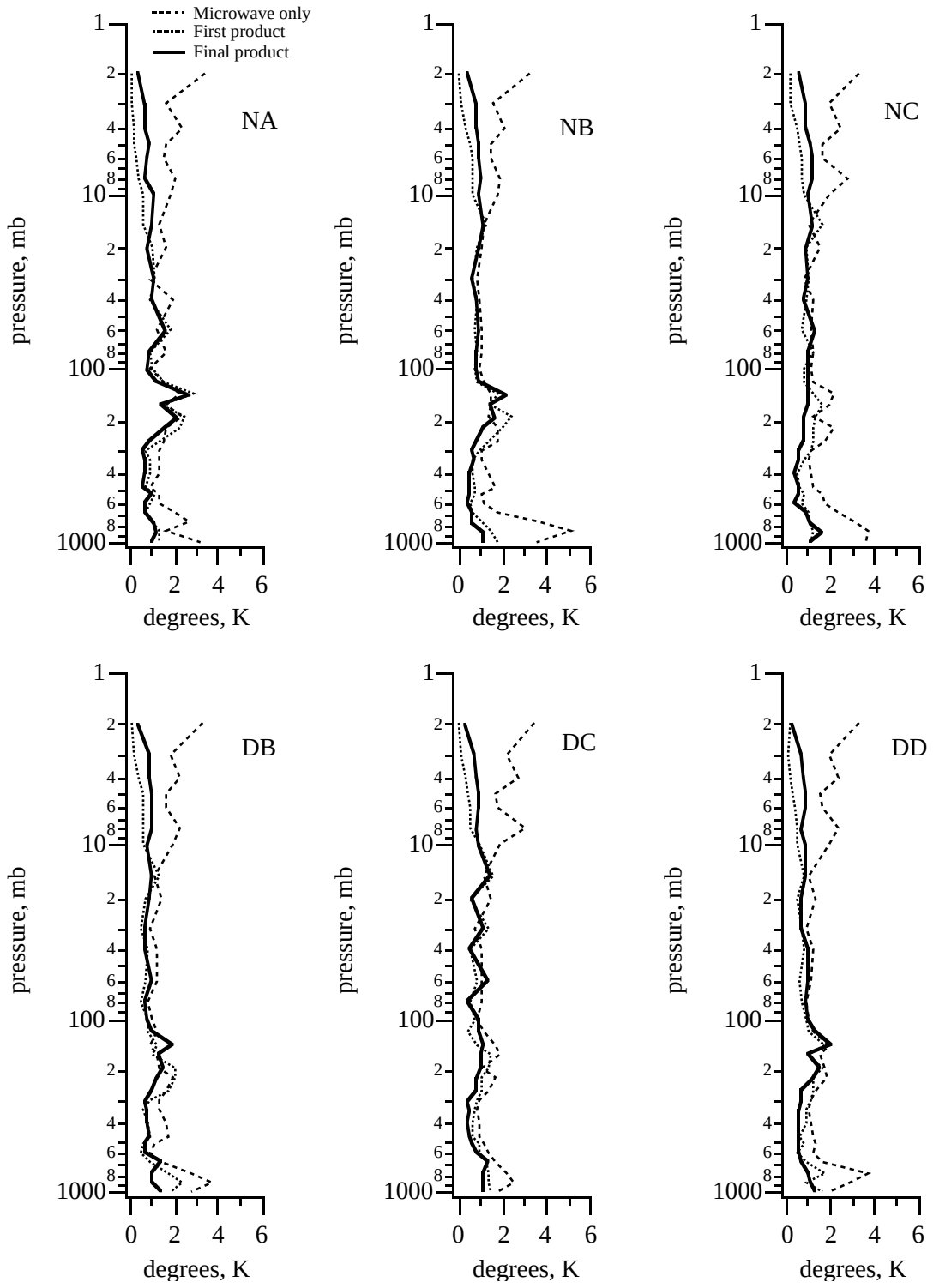

FIGURE 5.2.5A: TEAM ALGORITHM RETRIEVAL ERROR FOR ATMOSPHERIC TEMPERATURE)

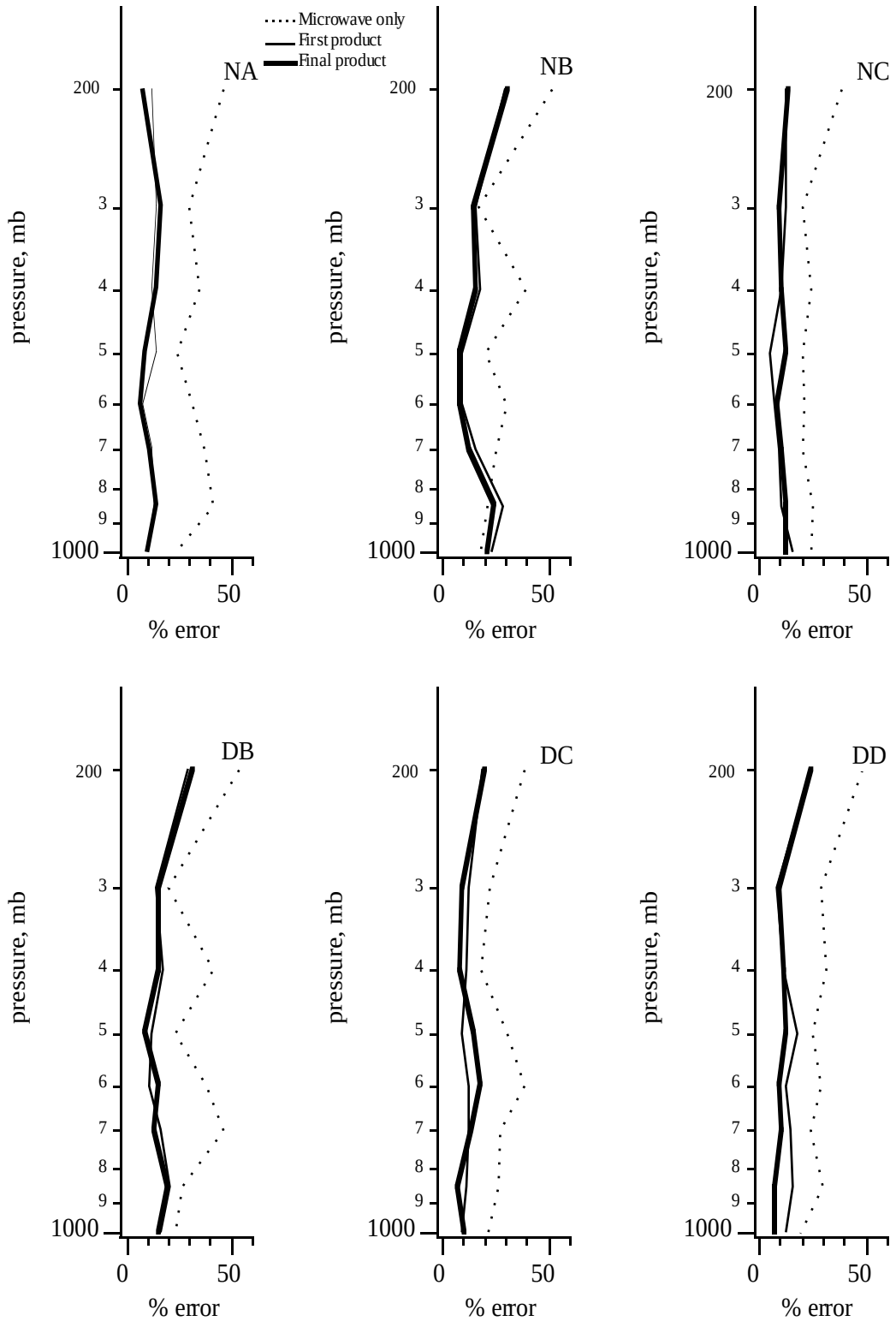

FIGURE 5.2.5B: TEAM ALGORITHM RETRIEVAL ERROR FOR ATMOSPHERIC WATER VAPOR)

Robustness Testing

The Simulation Team has the following additional simulations planned to test for Core Algorithm Level 2 robustness:

1. Gradient Effects -- effects of inhomogeneous temperature, water, and emissivities within the 9 AIRS FOVs
2. Cij effects -- errors associated with mis-alignment of the FOVs (current specification is 99% alignment).
3. First Guess -- sensitivities to first guess fields
4. Multi-spectral non-gray Clouds
5. Viewing angle simulation
6. Channel outages
7. Frequency Shift
8. Calibration Errors
9. Tuning (see 5.1) -- used to account for radiative transfer errors
10. Optical Effects -- shifts in the Slit Response Function (SRF - see section 3.2)
11. Others as needed

Data product Validation

The simulation is one methodology to provide theoretically-based estimates of parameter space errors. For example, given a one degree error in temperature, how does this effect the accuracy of, say, the ozone retrieval. Also, the simulation can be used to provide estimates based on formal error propagation analysis.

6. Numerical Computational Considerations (Lee)

6.1 Parameter Description

The table 6.1.1 lists the products from the AIRS level 2 data processing software and the major parameters (and parameter numbers) in the products. The third column in the table are the short description of the parameters and their units. All the products will have associated error estimates and/or quality flags.

Product Number	**Product name** Parameter name (parameter #)	Short description
AIR04	**Cloud product**	
	Cloud cover (2062)	Cloud fraction (unitless)
	Cloud emissivity (2128)	Cloud top spectral emissivities (unitless)
	Cloud top height (1423)	Cloud top pressure in mb
	Cloud top temperature (2463)	Atmospheric temperature at the cloud top in K
AIR05	**Humidity product**	
	Humidity profile (1828)	Water vapor profile (in gm-cm^{-2} unit, in 15 layers)
	Total Precipitable water (1869)	Total precipitable water in gm-cm^{-2} (this is the integral of water vapor profile and does not include cloud liquid water or ice.)
AIR07	**Temperature Product**	
	Temperature profile (1588)	Layer-mean temperature profile in K in 30 pressure layers
	Sea Surface Temperature (2523)	Sea surface skin temperature in K
	Land surface temperature (2481)	Land surface skin temperature in K
	Land surface emissivity (2113)	spectral IR emissivities (linearly interpolated between tie points)
	Day/Night Land surface temperature difference (2539)	Day/night (1:30 AM/PM) land surface skin temperature difference in K
AIR08	**Ozone product**	
	Ozone concentration profile (3690)	ozone column density profile in 3 layers in Dobson units.
	Total ozone burden (1332)	the integral of ozone profile in Dobson units.
AIR09	**Cloud cleared radiances**	
	Cloud cleared radiances(3683)	AIRS spectral radiances that would have been observed if there were no clouds. This product may be replaced by software to compute the product because of data volume.

TABLE 6.1.1 RETRIEVED PARAMETERS

6.2 Data Storage estimates.

The table 6.2.1 has preliminary storage estimate for the AIRS level 2 data processing. The levels 0, 1A and 1B storage estimates were included for comparison.

Data	KByte/Sec	GByte/Day
AIRS/VIS Level 0 *	170.00	14.70
AMSU-A Level 0 *	0.25	0.022
MHS Level 0 *	1.41	0.122
AIRS Level 1A *	200.00	17.29
VIS Level 1A *	27.20	2.35
AMSU-A Level 1A *	4.85	0.42
MHS Level 1A *	19.00	1.64
AIRS Level 1B *	318.30	27.50
VIS Level 1B *	40.86	3.53
AMSU-A Level 1B *	1.86	0.16
MHS Level 1B *	13.66	1.18
AIRS Level 2	19.10	1.65
AIRS Level 3 #	0.56	0.048
Total	**817.05**	**70.612**

TABLE 6.2.1 DATA STORAGE ESTIMATE

*radiances (16 bits) and 5/10% (level 0/1) extra for engineering and other data
1x1 degree, twice daily, 100 fields

6.3 Data Processing requirements.

The table 6.3.1 shows preliminary estimate of floating point operations for the level 2 data processing software. The data processing requirement for the levels 1, 3, 4 is included here for comparison and for completeness.

Processing Level	FLOPS MFlop/Sec	I/O rate KByte/Sec
AIRS Level 1 *	74.03	520.29
AMSU-A Level 1 *	0.05	1.20
MHS Level 1 *	0.16	1.54
Total Level 1	74.24	523.02
AIRS+ Level 2	1456.79	196.33
AIRS+ Level 3	100.00	24.41
Total	**1705.27**	**1266.79**

TABLE 6.3.1 DATA PROCESSING REQUIREMENT

*Assuming that Level 1 processing needs 1000 floating point operation per channel.

6.4 Required input data.

The AIRS/AMSU-A/MHS level 1b data sets are the main input to the level 2 data processing software. There are various tables and coefficients data sets for many parts of the software. The following two table are the lists of auxiliary input data sets used for the level 2 data processing. Some of the data sets will be used for the level 2 data processing and others will be used in the off-line validation software.

Input File Name	Short Description
AIRS_TC	AIRS Tuning Coefficients
AIRS_RTC	AIRS Rapid Transmittance Algorithm Coefficients
AIRS_URF	AIRS Upwelling Radiance Features
ANC_EDC_DEM	10 x 10 arc min Digital Elevation Map, employed as backup for determination of surface pressure
ANC_DCW_Land/Sea	Land/Sea Boundary data from ONC digitized maps
ANC_NAVY_DATABASE	Navy 10 x 10 arc min database of surface elevation, surface type and percent water
TOMS_GSFC_CLIM	TOMS ozone climatology based on monthly profiles (used operationally)

TABLE 6.4.1 STATIC INPUT DATA SETS (LEVEL 2 PROCESSING)

Input File Name	Short Description
MOD34_L3_30DY	Gridded vegetation index for estimation of land surface emissivity, 1x1 degree, monthly
MOD12_L3_96DY	Gridded land cover type for estimation of land surface emissivity, 1x1 degree, quarterly
ANC_NOAA/NCEP_SNOW/ICE	Gridded snow and sea ice extent from AVHRR for first guess surface emissivity over land and ocean, 1x1 degree, weekly
ANC_NOAA/NCEP_SST	Gridded NCEP Reynolds blended sea surface temperature climatology, 1x1 degree, weekly
ANC_NCEP_MRF	Gridded analysis data of Medium Range Forecast product, 1x1 degree every 6 hours (used in validation)
ANC_NCEP_PROF	Gridded NCEP global model temperature, moisture and ozone profiles 1x1 degree, every 6 hours (used operationally)
ANC_NOAA/NESDIS_O3BUV2	Gridded Ozone profiles from SBUV-2/NOAA, 1x1 degree, daily
ANC_NOAA/NCEP_SURF	Gridded NCEP Global Model Surface Parameters (winds, relative humidity, pressure, air-sea temperature differences, etc.), 1x1 degree, every 6 hours
ANC_NOAA/NESDIS_NDVI	Gridded Level 3 NDVI Product created from processing daily AVHRR GAC data, 1x1 degree, weekly
ANC_NOAA/NCEP_SFC_OBS	Surface Observations collected daily from NOAA's surface network of observation stations (including ships & buoys), every 6 hours
ANC_NOAA/NCEP_RDSONDS_OBS	In situ observations collected from radiosondes and Rawinsondes, every 6 hours
ANC_EDC_LANDCOVER	Surface land cover & vegetation type (to estimate surface emissivities over land), quarterly
ANC_GSFC_O3TOMS	Gridded Ozone profile from TOMS, 1x1 degree, daily (used in validation)

TABLE 6.4.2 DYNAMIC INPUT DATA SETS (LEVEL 2 PROCESSING)

7. Quality Control, Diagnostics, and Exception Handling (Kalnay / McMillin / Susskind / Haskins /Lee)

There are four phases of quality control to be implemented on the AIRS, AMSU, HSB data for Level 2 processing:

- pre-retrieval quality control
- profile rejection during the retrieval phase
- Assimilation-based quality control
- statistical error-bar assessment.

Pre-retrieval quality control consists of automated limit-checking on input radiances as well as the use of EOFs to characterize bad points. Profile rejection is based on the use of residuals, or difference between computed and measured radiances, to reject poorly-behaved retrievals. Assimilation-based quality control uses proven NCEP procedures applied directly to the radiances. Finally, an EOF technique will be used to statistically characterize the error for the Level 2 Core Products. All of these quality control indicators will be provided to the data users.

7.1 Pre-retrieval Quality Control (Lee)

The input data will be subjected to a series of automatic internal quality checks before being passed to the Level 2 retrieval stage. Failure to pass any of these quality checks will cause the corresponding AMSU footprint to be skipped and generate a message in the internal quality check log. A non-exhaustive list of internal input data quality checks follows:

Failure	Pre Level 2 Retrieval Action
Auxiliary data missing	Log what is missing, notify DAAC, time-out if no corrective action
Auxiliary data dropout	Log dropout. If a threshold for maximum duration of allowed dropout is exceeded, notify DAAC
AIRS/AMSU/HSB data missing	Log what is missing, notify DAAC, time-out if no corrective action
AIRS/AMSU/HSB full data dropout	Log dropout. If a threshold for maximum duration of allowed dropout is exceeded, notify DAAC
AIRS/AMSU/HSB partial data dropout	Log dropout. If a threshold for maximum duration of allowed dropout is exceeded, notify DAAC
AIRS/AMSU/HSB invalid data	1. Log particulars. 2. Negative Radiance Values All radiances must be non-negative. A negative value would arise from an instrument problem or calibration failure. 3. Too Large Radiance Values There is an absolute limit beyond which a radiance value is non-physical. There will be a threshold defined for each instrument (AIRS/AMSU/HSB) and possibly for ranges of channels within AIRS. Values which are too large indicate an instrument problem or mis-pointing (i.e., looking at the sun) or calibration failure. 4. Insufficient Range of Radiance Values Selected channel pairs should exhibit radiance values which differ by at least a minimum threshold (and in the proper sense). Insufficient range indicates an instrument problem or calibration failure.

TABLE 7.1.1 INTERNAL INPUT DATA QUALITY CHECK FAILURE ACTIONS

Upon detecting a Level 2 retrieval failure, the software will gracefully recover and move on to the next valid AMSU footprint. An abort should be necessary only in the case where the DAAC has not provided the required valid data sets.

Use of EOFs to Characterize Input Radiances (Haskins/McMillin)

We have also studied the use of a pre-computed set of Empirical Orthogonal Functions (EOFs) to use as radiance filters for corrupted radiances. The technique is similar in spirit to using Fourier analysis time-series techniques for data quality control. The EOFs provide a more economical framework.

For clear radiances and the microwave radiances, the technique is straightforward. Given a statistical ensemble of radiances, the EOFs are calculated off-line based on the covariance. Then the current radiance profile is projected against the EOFs and any three sigma radiance is rejected.

For cloudy radiances, we plan to explore a technique described in section 4.2 using a cloud-contaminated ensemble of radiances. Clouds introduce a greater individual uncertainty in the variance of each tropospheric channel. However, the channel-to-channel variances are quite similar. For example, the surface sounding channels will be all approximately affected equally by clouds. It is the channel-to-channel variance we will exploit through the use of EOFs as outlined above (see Haskins, *et al.*, 1996).

7.2 Rejection criterion (Susskind)

A major source of error for the Level 2 Core Products is an inaccurate cloud clearing. In the following discussion we will focus on that aspect. In the case of indeterminate values of η, spurious solutions can occur which match the infra-red radiances but are incorrect. Under these conditions, there will be a mismatch between the microwave radiances, unaffected by clouds, and the infra-red clear column radiances, incorrectly affected by clouds. This mismatch can show up in two ways. First, the temperature solution obtained from an AMSU only retrieval may produce significantly different results from that obtained with the combined AIRS/AMSU temperature profile retrieval. Second, the RMS differences of the observed minus computed brightness temperatures for the AMSU channels resulting from the coupled AIRS/AMSU temperature retrieval may be large. We reject the retrieval as having a spurious cloud solution if either

$$\left[\frac{1}{K}\sum_{k=1}^{K}\left(T(p_k)-T_A(p_k)\right)^2\right]^{1/2} > 1.5^\circ \qquad (7.2.1)$$

for pressures $p_k \geq 500$ mb, where T(p) is the final AIRS/AMSU temperature profile and $T_A(p)$ is an AMSU only temperature profile determined after the first pass through the retrieval scheme, or

$$\left[\frac{\sum_{\ell=1}^{L} W_\ell^2\left(\Theta_{A,\ell}-\hat{\Theta}_{A,\ell}\right)}{\sum_{\ell=1} W_\ell^2}\right]^{1/2} > 1.5^\circ \qquad (7.2.2)$$

where $\left(\Theta_{A,\ell} - \tilde{\Theta}_{A,\ell}\right)$ represents the differences of the observed AMSU brightness temperatures and those computed from the final solution $T(p)$, for the L AMSU-A tropospheric sounding channels 3-11, and W_ℓ are inversely proportional to the channel noise. This test did not reject any of the well conditioned cases we tried.

Another rejection criteria was discussed in section 4.3. If a low contrast overcast condition exists, then Eq. 4.3.11 will be used to reject those cases.

A similar condition exists if a cloud formation is constant within all fields of view. In a multiple cloud formation case, this can be detected by calculating a clear radiance estimate, $R_{i,CLR}$ with the reconstructed clear column radiance, $\hat{R}_i$, for the cloud clearing channels. The channels are weighted with the inverse of the diagonal of the noise covariance matrix, $W_{ii} = 1/N_{ii}$, where N_{ii} is given by Eq. 4.3.10. The profile should be rejected if the root-mean-square difference exceeds a threshold:

$$\frac{\sqrt{\sum_i W_{ii}\left(R_{i,CLR} - \hat{R}_i\right)^2}}{\sqrt{\sum_i W_{ii}\left(\left.\frac{\partial B_i}{\partial T}\right|_{\Theta_{i,CLR}}\right)^2}} > 0.5°K \qquad (7.2.3)$$

7.3 NCEP Quality Control (Kalnay)

The NCEP operational data assimilation and forecasting system will provide two unique contributions to AIRS: an advanced Quality Control (QC) performed within the operational data assimilation in near real time, and the monitoring of the results of this QC, which provides an early warning of any problem detected.

There are basically two major approaches to the sounder QC: a) comparing retrievals to collocated data (such as rawinsondes); b) direct QC of the radiances from the AIRS ‘superchannels’. The concept of ‘superchannels’ is still being defined by the AIRS Science Team but a superchannel will be either be a linear combination of selected AIRS channel or a selected subset of the entire channel set. The basic aim of the superchannel set is to fit into the computational envelope at NCEP.

The two QC approaches are complementary, but the second approach is much more powerful for several reasons discussed later, and in practice it is best carried out within the operational assimilation of the radiances. The 3-D variational direct assimilation of TOVS radiances, implemented at NCEP on October 1995, has provided both the infrastructure for this approach, and a clear proof of its power.

The results of the monitoring will be posted in real time on the NCEP file server, and will be available in several formats, including a rotating monthly/seasonal archive and graphic display of the fit to the first guess of each of the AIRS channels or superchannels that will be used in the data assimilation, and the rate of data rejection by the QC for each of the channels. This will provide the AIRS team the ability to easily assess the status of the instrument, an early warning of detected problems, and the ability to test the impact of corrective measures, or improvements in the algorithms or selections of the superchannels.

The 3-D variational assimilation of radiances and the present TOVS radiances QC

The 3-D variational (3DVAR) direct assimilation of cloud-cleared radiances implemented at NCEP in October 1995 (Derber and Wu, 1996) has resulted in the largest increase in forecast skill ever obtained in either the Northern Hemisphere (NH) or the Southern Hemisphere (SH) due to any other single change in more than a decade (Fig. 7.3.1). In fact, it has provided the first large, significant positive impact in the NH, and greatly improved the impact that TOVS data already had in the SH. The reasons for this large impact are better understood when looking at the cost function minimized every 6 hr in the operational data assimilation:

$$J = \int \left[\left\langle \left(x_a - x_{FG}\right)^T B^{-1} \left(x_a - x_{FG}\right) \right\rangle + \left\langle \left(F(x_a) - y_{obs}\right)^T (O+M)^{-1} \left(F(x_{a)} - y_{OBS}\right) \right\rangle + J_{BAL} \right] dxdyd\sigma \tag{7.3.1}$$

where x_a represents the full 3-dimensional analysis in the model variables (about one million degrees of freedom), x_{FG} is the first guess (a 6-hour forecast), $F(x_a)$ is the transformation of the analysis variables into observed variables via the forward model, yobs are the observations, and the last term is a constraint on the time changes of the divergence equation, which maintains a balanced state and eliminates the need in the NCEP system to perform nonlinear normal mode initialization. The matrices B, O and M are the error covariance matrices for the model error, the observational error, and the forward model F respectively.

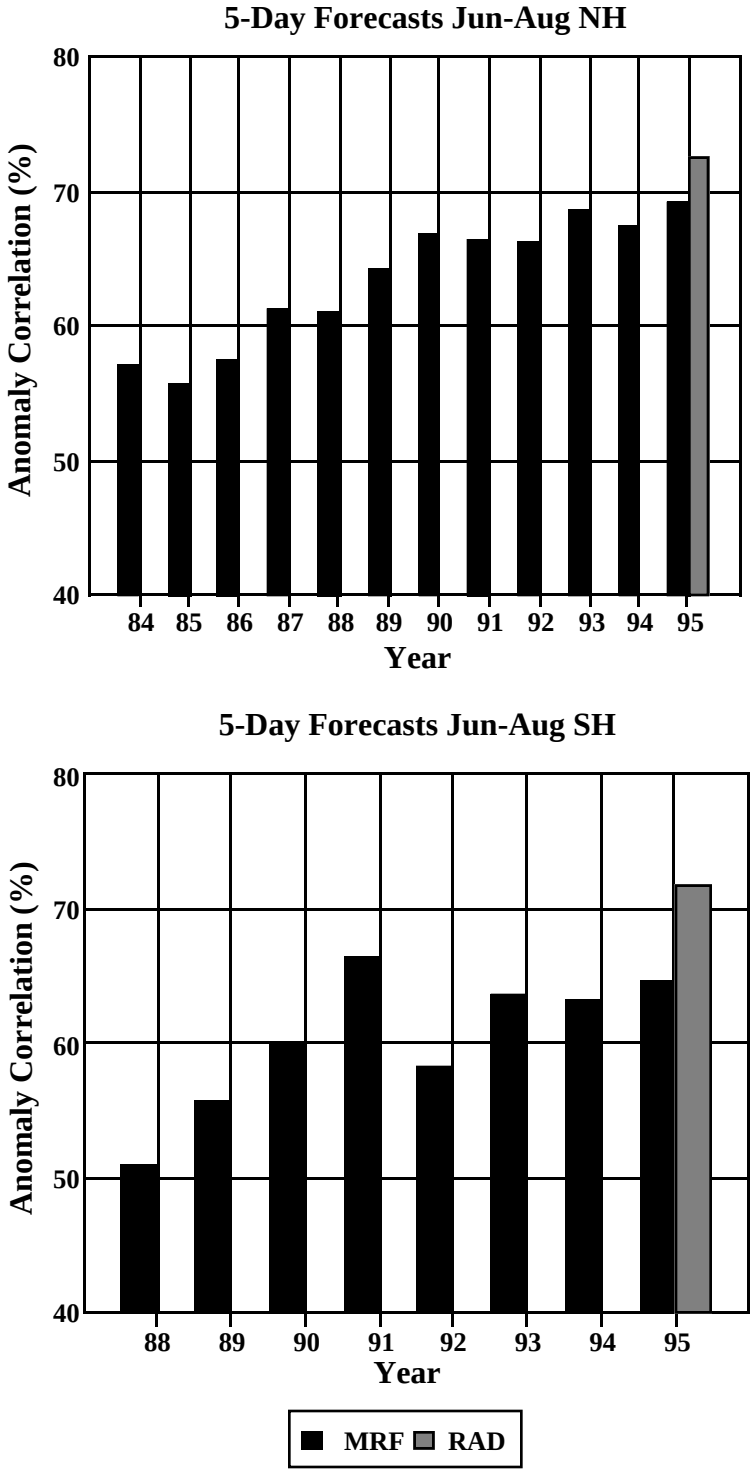

FIG 7.3.1: EVOLUTION OF THE 5-DAY FORECAST SKILL (ANOMALY CORRELATION) FOR THE NOAA/NCEP OPERATIONAL FORECASTS FOR THE JUNE-AUGUST SEASON FOR THE LAST DECADE USING TOVS RETRIEVALS (MRF). FOR THE YEAR 1995 AN EXPERIMENTAL SYSTEM IN WHICH THE RADIANCES WERE DIRECTLY ASSIMILATED IS ALSO SHOWN (RAD) TOP: NH; BOTTOM:SH.

The first term represents the fit of the analysis to the first guess, the second the fit of the analysis to the observations, and the third is measures its lack of balance. The minimization of this objective cost function ensures that the analysis is the 3-D model state which is closest to the first guess and to the observations (and also maintains a proper

balance). The transformation of the analysis variables to the observed variables is crucial: with this approach any type of observation can, in principle, be used in its original form (such as satellite radiances), rather than produce model variables from observed radiances through retrievals.

There are several advantages to the direct use of cloud-cleared radiances:

1. QC of the radiance data is much more efficient than the QC of the retrievals;
2. biases in the measurements can be detected and corrected, for the same reason;
3. unlike the retrieval problem, which is ill-posed because the radiances do not provide enough information for a vertical sounding, the assimilation of radiances is well posed;
4. all the 3-dimensional data (satellite and non-satellite) are used simultaneously, which produces a more accurate analysis, and can be considered, in turn, as the best possible retrieval. The assimilation of radiances uses only the information contained in the data and, unlike the retrieval process, it is not contaminated by inconsistent guesses and statistics.

The reason that QC of the radiances is more effective is that the forward model provides a very accurate first guess for each measurement, and the errors characteristics for the radiances are cleaner, allowing the detection of small errors. By contrast, in the retrievals the QC is difficult because the information and the errors originating from the different channels and the algorithms are all scrambled together.

In the present operational assimilation of TOVS radiances (Derber and Wu, 1996) there is a careful determination of the bias between the observed and simulated data (discussed in more detail in section 8.4 on the AIRS model validation). The operational QC of TOVS radiances is made by two tests: a gross test (checking whether the observations are within a reasonable range), and (most important) a check against the predicted values based on the first guess and nearby observations. The decision whether to accept or reject a measurement is based on the ratio between the observational residual (the difference between the predicted and observed radiance), and the expected error standard deviation for that channel. This quantity is modified by the position across the track of the scan, whether it is over land or sea, the elevation, the difference between the atmospheric model and the real orographic elevation, and the latitude (the criterion is made tighter in the tropics). Some of these modifications are to eliminate poor observations, and some to eliminate situations where the forward model may result in deficient simulated observations. The data rejections are performed independently for each channel.

These checks provide a rich and precise information source about the error characteristics of the TOVS channels: the difference of the observed and simulated radiance, its bias, the dependence on the orbital parameters, geography, etc. These data provide the most powerful basis for real time monitoring of the quality of the data, by for example monitoring the rate of data rejection for each channel, and also for the improvement of the algorithms

Planned AIRS QC and monitoring

Obviously the present TOVS operational data assimilation system discussed above provides only an example of how the QC of the AIRS data and the monitoring will be carried out. A lot will depend on the choice of AIRS data that will be actually used in the data assimilation (see the AIRS model validation section 8.4). Here we assume that an appropriate data compression will be chosen by the science team, and implemented by the

AIRS operational team. We denote the result of the data compression (if any is deemed necessary) as superchannels.

Assuming that the superchannels will provide the most significant information from AIRS, we plan to follow a similar path as TOVS, but with parameters appropriately adapted to AIRS:

a) The forward model (which the science team has to develop) will provide (from the first guess and nearby observations) a very accurate estimate of what the superchannels radiances should be.
b) These will be compared with the actual superchannels radiances and the ratio between the difference (observational residual) to the expected (instrumental, representativeness, etc.) standard deviation of the error for each superchannel will be used to guide the accept/reject decision.
c) As for TOVS the rejection criteria will have to be tuned to the characteristics of the system. For example, in TOVS the interchannel error covariances for the radiances are assumed to be zero, and this may not be the case for superchannels.
d) As is the case for TOVS, the bias between the simulated and observed superchannel observations will be measured and corrected.
e) The results of these checks (number of out-of-range observations, bias, rms difference between observational residuals, percentage of observations rejected, etc., will be saved for each superchannel and archived.
f) These archives will be posted on NCEP file servers and made available by ftp and internet. The results will be also graphically displayed on a monthly and/or seasonal rotating archive on the internet. NCEP has considerable experience posting such data in near real time (see for example meteograms displayed on the NCEP EMC home page, nic.fb4.noaa.gov:8000/), which are widely used by the academic community and the public.

The graphic displays will allow the AIRS operators and the science team to monitor and in real time and get an early warning of instrumental problems, and the immediate impact of remedial actions or of improvements in the algorithms, such as the selection of superchannels or the forward algorithms.

7.4. Statistical Error-Bar Assessment (Haskins)

The error budget for the geophysical retrieval of any space-based measurement consists of the following sources of uncertainty (see Rodgers, 1990):

1. Instrument noise, which is relatively small for the AIRS instrument but can be more significant for the microwave components.
2. ‘Null Space’ or unresolvable fine scale solution structure which is generally manifested through the initial guess to the retrieval process
3. The mathematical retrieval error itself which has two major parts for the infrared retrievals; errors due to cloud clearing and parameter retrieval errors. Both of these error sources will be closely examined and has been described in Section 4.3.3.
4. Errors in the radiative transfer calculation that generally result from incomplete knowledge of underlying physics (line shape, line strength, etc.). These types of errors are systematic in nature and for the AIRS retrieval system the errors are

greatly reduced by 'tuning' against Radiosondes or possibly forecast models (see section 5).

The solution error is characterized by the difference between measurement and the retrieved geophysical parameters mapped back into brightness temperature through the Radiative Transfer Equation (RTE). This difference is commonly referred to as the residual.

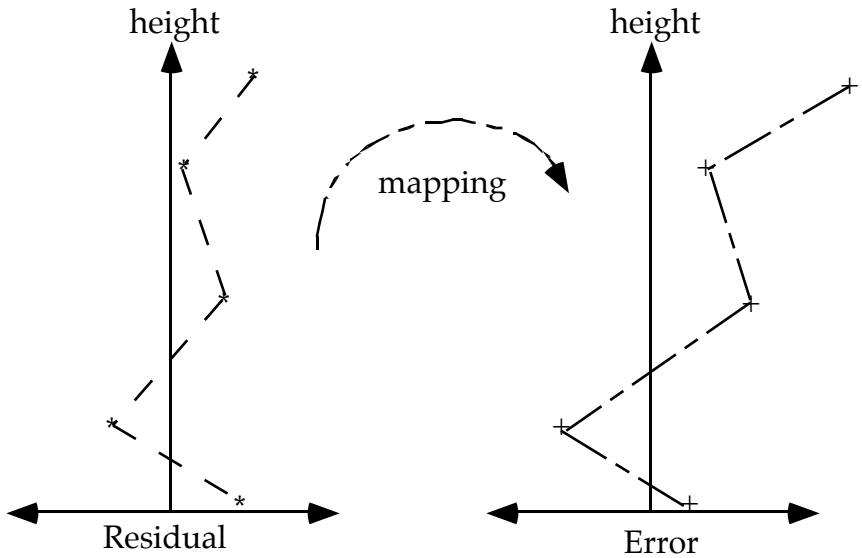

$$\Delta T_b = f(\Delta I) = f\left(\int \frac{\partial B}{\partial T} \Delta T d\tau\right)$$

FIGURE 7.4.1: RESIDUAL TO ERROR MAPPING

Considering the sources of error, if the residual is within the instrument noise limits, then, ignoring the mathematical questions of uniqueness, the solution is as good as can be expected. If other sources of error dominate—which in our case is either null space error or retrieval error—then no technique can minimize the residuals at the measurement noise threshold and the residuals will, in a statistical sense, exceed the threshold. It is this criterion which will be utilized to characterize the error in the AIRS data sets.

Use of EOFs to Characterize the Relation of Error to Residual

Once brightness temperature residuals and measurement errors are placed on a common space-time grid, one could conceivably generate a regression scheme to predict measurement error from residual. Unfortunately, such a regression would involve many thousands of pairs of numbers from many different atmospheric regimes. It would be far better to apply separate regression relations under different conditions. It is also important to know those situations where radiance residual is a poor predictor of measurement error. We can begin to address these problems by reducing the datasets to Empirical Orthogonal Eigenfunctions (EOFs). This technique is a useful method for separating variability in a complicated dataset because the EOFs express statistically dependent space-time variability as a set of mathematically orthogonal structures. They also compress a high-dimensional dataset into a limited number of dominant modes. The EOFs will be the starting point for subsequent analysis.

The basic methodology for calculating EOFs and their use in examining the relationship between residual brightness temperature and measurement error will be described. EOFs are simply the eigenvalues of error covariance matrices. One can imagine a time-varying set of maps of a quantity; the time covariance of this quantity forms a square matrix of dimension equal to the total number of spatial gridpoints in the maps.

The EOFs are the eigenmodes of this covariance matrix, and, like the original quantity they form spatial maps. The associated eigenvalues give the fraction of variance embodied in each EOF. The number of EOFs is equal to the number of degrees of freedom in the map, but it is generally true in practice that only the first few modes carry most of the variance. (Preisendorfer [1988] gives significance criteria.) The important characteristics of EOFs are: 1) they are mathematically orthogonal, 2) they completely span the space of measurements used to generate them, and 3) they generally compress information into a few data structures.

There is also a direct relationship between the EOFs and the original quantity. In the case of residual temperatures, a map can be reconstructed at time t from the residual temperature EOFs $\varphi(x)$ via

$$\Delta T(x,t) = \sum_i a_i(t)\varphi_i(x) \tag{7.4.1}$$

where i represents eigenmode number and x is a general spatial coordinate; here a_i (t) is the projection of the map onto the EOF at time t, i. e. the inner product between the map at time t and the i-th EOF φ_i. In practice the sum in (7.4.1) would be calculated over only the first few, significant modes. It is important to note that there is only one value of $a_i(t)$ for each time t and mode number i and it is the same for each gridpoint in the map.

In this context we are also interested in the EOFs of measurement error, σ. Maps of this quantity can be expanded in terms of its own EOFs $\chi_i(x)$:

$$\sigma(x,t) = \sum_i b_i(t)\chi_i(x) \tag{7.4.2}$$

Again, the χ_i are orthogonal and completely span the space of observation σ, and the b's are the projection of maps onto the EOFs.

Note that the two sets of coefficients φ and χ are not necessarily orthogonal to one another; the amount to which they are linearly dependent is a measure of their statistical correlation. The main purpose of this approach is to examine how well the variations in measurement error $\sigma(x,t)$ are characterized by radiance residuals $\Delta T(x,t)$, or, the degree of statistical correlation between the two quantities. One measure is

$$\hat{\sigma}(t) = \sum_i \hat{b}_i(t)\chi_i(x) \tag{7.4.3}$$

where $\hat{b}_i = \sum_n c_{ni}a_n(t)$. If ΔT is a perfect predictor of σ then $\hat{\sigma}$ should be exactly equal to σ and $\hat{b}_i \equiv b_i$; if ΔT has no relationship to σ, then $\hat{\sigma}$ and σ will be uncorrelated. The real relationship between ΔT and σ is somewhere between these two extremes. Importantly, estimation of statistical dependence is done as a set of objective algebraic manipulations [Preisendorfer (1988); Barnett *et al.* (1981; 1987)].

Metric Verification

The basic tool we will use to verify the EOF quality of the relationship defined in (7.4.3) is the cross validation technique [chapters 8 and 9 of Preisendorfer (1988), and illustrated in Barnett *et al.* (1981; 1987)]. The method can be described as follows. Remove an independent sample and construct the model in eq. 7.4.3 on the remaining N-1 samples. Use this model and estimate $\hat{\sigma}$ according to the removed (independent) data sample. Repeat the procedure, holding out successive independent data samples which

result in new models according to eq. 7.4.3 and obtaining, at each step, an independent estimate of $\hat{\sigma}$. The end result is N independent estimates of $\hat{\sigma}$. These can be 'skill scored' with respect to the observed σ and the significance of the solution in 7.4.3 relative to, say, a simulated white or red noise process.

7.5. Software Exception Handling (Lee)

In the following discussion, all exceptions will be coded and passed along with the level 2 data stream.

Failure	Level 2 Retrieval Action
AIRS/AMSU/HSB full data dropout	Reinitialize and restart retrieval upon encountering renewed data stream. Extent of re-initialization depends upon the duration of the data dropout.
AIRS/AMSU/HSB partial data dropout	Branch to partial retrieval depending on what is available to software AMSU only MW-only Temperature Retrievals HSB only pass AIRS only pass AMSU/AIRS Temperature/Moisture Retrieval AMSU/HSB MW-only Temperature/Moisture Retrievals HSB/AIRS pass
AIRS/AMSU/HSB invalid data	Depending upon severity of invalid data: Ignore offending AIRS footprint data in retrieval and continue Ignore offending HSB footprint data in retrieval and continue Skip entire retrieval for corresponding AMSU footprint
MW-only Retrieval Failure	Set relevant flag(s) Set failed retrieval profile(s) to climatology and proceed
First Cloud-Clearing Failure	Set relevant flag(s) Branch to Second Cloud Clearing stage
First Retrieval Failure	Set relevant flag(s) Set failed retrieval profile(s) to MW-only and proceed
Second Cloud-Clearing Failure	Set relevant flag(s) Output remains that from First Retrieval
Second Retrieval Failure	Set relevant flag Output remains that from First Retrieval

TABLE 7.5.1 EXCEPTION HANDLING ON LEVEL 2 RETRIEVAL FAILURE

References

Aumann, H. H., and M.T. Chahine, 1976: An infrared multi-detector spectrometer for remote sensing of temperature profiles in the presence of clouds, *Appl. Opt.*, **15**, 2091-2094.

Aumann, H. H., and R. Pagano, 1994: The Atmospheric Infrared Sounder on EOS. *Opt. Eng.*, **32**, 776-784.

Backus, G., and F. Gilbert, 1970: Uniqueness in the inversion of inaccurate gross earth data. *Phil. Trans. Royal Soc. London*, **A266**, 123-192.

Barnett, T. P., R. W. Preisendorfer, L. M. Goldstein, and K. Hasselmann, 1981: Significance tests for regression model hierarchies, *J. Phys. Oceanogr.*, **11**(8), 1150-54.

Barnett, T.P. and R. Preisendorfer, 1987: Origins and Levels of Monthly and Seasonal Forecast Skill for United States Surface Air Temperatures determined by Canonical Correlation Analysis, *Monthly Weather Review*, **115**, 1825-1850.

Bauer, A., Godon, M., Carlier, J., and Ma, Q., Water Vapor Absorption in the Atmospheric Window at 239 GHz, *J. Quant. Spectrosc. Radiat. Transfer*, **53**(4), pp. 411-423 (1995).

Bauer, A., Godon, M., Carlier, J., Ma, Q., and R.H. Tipping, Absorption by H20 and H20-N2 Mixtures at 153 GHz, *J. Quant. Spectrosc. Radiat. Transfer*, **50**, pp. 463-475 (1993).

Bauer, A., Godon, M., Kheddar, M., and Hartmann, J.M., Temperature and Perturber Dependences of Water Vapor Line-Broadening. Experiments at 183 GHz; Calculations Below 1000 GHz, *J. Quant. Spectrosc. Radiat. Transfer*, **41**, pp. 49-54 (1989).

Briancon, A. C., 1986: "Estimation and modeling of multidimensional non-stationary stochastic processes: application to the remote sensing of atmospheric temperature fields," Ph.D. thesis, Mass. Inst. of Tech.

Chahine, M. T., 1968: Determination of the temperature profile in an atmosphere from its outgoing radiance. *J. Optic. Soc. Amer.*, **58**, 1634-1637.

Chahine, M. T., 1970: Inverse problems in radiative transfer: determination of atmospheric parameters, *J. Atmos. Sci* **, 27**, 960-967.

Chahine, M. T., 1977: Remote sounding cloudy atmospheres. II. Multiple cloud formations. *J. Atmos. Sci.*, **34**, 744-757.

Chahine, M. T., 1982: Remote sounding of cloud parameters. *J. Atmos. Sci.*, **39**, 159-170.

Chahine, M. T., N.L. Evans, V. Gilbert, and R. Haskins, 1984: Requirements for a passive IR advanced moisture and temperature sounder. *Appl. Opts.*, **23**, 979-989.

Chahine, M. T. and J. Susskind, 1989: Fundamentals of the GLA physical retrieval method. *Report on the Joint ECMWF/EUMETSAT Workshop on the Use of Satellite Data in Operational Weather Prediction:* 1989-1993. Vol. 1, 271-300. T. Hollingsworth, Editor.

Chedin, A., N. A. Scott, C. Wahiche, and P. Moulinier, 1985: The improved initialisation inversion method: A high resolution physical method for temperature retrievals from the TIROS-N series. *J. Clim. Appl. Meteor.*, **24**, 128-143.

Chéruy, F., N.A. Scott, R. Armante, B. Tournier, and A. Chedin, 1995: Contribution to the development of radiative transfer models for high spectral resolution observations in the infrared, *J. Quant. Spectrosc. Radiat. Transfer*, **53**, 6, 597-611

Crone, L.J., L.M. McMillin, and D.S. Crosby, 1996: Constrained Regression in Satellite Meteorology. (Accepted for publication in *J. Appl. Meteor*.)

Cuomo, V., R. Rizzi, and C. Serio, 1993: An objective and optimal estimation approach to cloud-clearing for infrared sounder measurements. *Int. J. of Rem. Sensing*, **14**, 729-743.

Derber and Wu, 1996*: Proceedings of the 11th AMS Conference on Numerical Weather prediction*, Norfolk, VA, August 19-23, pp 236-237.

Edwards, D.P., 1992: Genln2: A general line-by-line atmospheric transmittance and radiance model. NCAR technical note 367+STR, National Center for Atmospheric Research.

Eyre, J.R. and H.M. Woolf. 1988: Transmittance of atmospheric gases in the microwave region: a fast model. *Appl.Opt*., 27(15):3244--3249.

Eyre, J. R., 1989a: Inversion of cloudy satellite sounding radiances by non linear optimal estimation. I: Theory and simulation for TOVS. *Q. J. R. Meteorol. Soc.* , **115**, 1001-1026.

Eyre, J. R., 1989b: Inversion of cloudy satellite sounding radiances by nonlinear optimal estimation. II: Application to TOVS data. *Q. J. R. Meteorol. Soc.*, **115**, 1027-1037.

Eyre, J. R., 1990: The information content of data from satellite sounding systems: A simulation study. *Q. J. R. Meteorol. Soc.*, **116**, 401-434.

Fleming, H.F. and L.M McMillin, 1977: Atmospheric transmittance of an absorbing gas 2. Applied Optics, 16:1366

Fleming, H.F. and M.D. Goldberg, and D.S. Crosby, 1986: Minimum variance simultaneous retrieval of temperature and water vapor from radiance measurements, Proc. Second Conference on Satellite Meteorology, Williamsburg, Amer. Met. Soc., 20-23.

Godon, M., Carlier, J. and Bauer, A.,1992: Laboratory Studies of Water Vapor Absorption in the Atmospheric Window at 213 GHz, *J. Quant. Spectrosc. Radiat. Transfer*, **47**(4), pp. 275-285.

Grody, N. C., and Gruber, A and Shen, W. C., 1980 Atmospheric Water Content over the Tropical Pacific Derived from the Nimbus-6 Scanning Microwave spectrometer. *J. Appl. Meteo.*, **19**, 986-996.

Grody, N. C., 1988: "Surface Identification Using Satellite Microwave Radiometers," *IEEE Trans. Geosci. and Remote Sensing*, vol. 26, 850-859.

Halem, M., M. Ghil, R. Atlas, J. Susskind, W. Quirk, 1978: The GISS sounding temperature impact test. *NASA Tech. Memo. 78063*: 2.9-2.82.

Hanel, R. A., B. J. Conrath, D. E. Jennings, and R. E. Samuelson, 1992: Exploration of the solar system by infrared remote sensing. *Cambridge University Press*, Cambridge, Great Britain.

Hannon,S, L.Larrabee Strow, and W.Wallace McMillan, 1996: Atmospheric infrared fast transmittance models: {A} comparison of two approaches. In *Proceedings of SPIE Conference 2830, Optical Spectroscopic Techniques and Instrumentation for Atmospheric and Space Research II.*

Haskins, R.D., R.M. Goody, and L. Chen, 1996: A statistical method for testing a GCM with spectrally-resolved satellite data, Submitted to J. Geophy. Res.

Holben, B.N., T.F. Eck, I. Slutsker, D. Tanre, J.P. Buis, A. Setzer, E. Vermote, J.A. Reagan, Y. J. Kaufman, T. Nakajimi, and F. Lavenu, 1996: Multi-band automatic sun and sky scanning radiometer system for measurement of aerosols, accepted for publication *Rem. Sens. Env*.

Husson, N., B. Bonnet, and N. A. Scott, Management and study of spectroscopic information: The GEISA program, *Journal of Quantitative Spectroscopy and Radiative Transfer*, **48**, 509, 1992.

Janssen, M.A. (ed.), 1993: *Atmospheric Remote Sensing by Microwave Radiometry*, Chap. 1, New York: Wiley.

Kaplan, L.D., 1959: Inferences of atmospheric structures fromsatellite remote radiation measurements, *J. Opt. Soc.Am*., Vol. **49**, pp 1004-1004

Kaplan, L. D., M. T. Chahine, J. Susskind, and J. E. Searl, 1977: Spectral band passes for a high precision satellite sounder. *Appl. Opt.*, **16**, 322-325.

Kuo, C. C., D. H. Staelin and P. W. Rosenkranz, 1994: "Statistical Iterative Scheme for Estimating Atmospheric Relative Humidity Profiles," *IEEE Trans. Geosci. and Remote Sensing* ,vol. 32, 254-260.

Liebe, H.J., Gimmestad, G.G., Calculation of Clear Air EHF Refractivity, *Radio Science*, **13**(2), pp. 245-251 (1978).

Liebe, H.J., Gimmestad, G.G., Hopponen, J.D., Atmospheric Oxygen Microwave Spectrum-Experiment versus Theory, *IEEE Trans. on Ant. and Prop.*, **AP-25**(3), pp. 327-335 (1977).

Liebe, H.J., Hufford, G.A., and Manabe, T., A Model for the Complex Permittivity of Water at Frequencies Below 1 THz, *Int. J. of Infrared and Mill. Waves,* **12**(7), pp. 659-675 (1991).

Liebe, H.J., Rosenkranz, P.W., and Hufford, G.A., Atmospheric 60-GHz Oxygen Spectrum: New Laboratory Measurement and Line Parameters, *J. Quant. Spectrosc. Radiat. Transfer*, **48**(5/6), pp. 629-643 (1992).

Liebe, H.J., MPM-An Atmospheric Millimeter-Wave Propagation Model, *Int. J. of Infr. and Milli. Waves*, **10**(6), (1989).

Liebe, H.J., and Layton, D.H., Millimeter-Wave Properties of the Atmosphere: Laboratory Studies and Propagation Modeling, NTIA Report 87-224, October 1987.

Liebe, H.J., Thompson, M.C. Jr., and Dillon, T.A., Dispersion Studies of the 22 GHz Water Vapor Line Shape, *J. Quant. Spectrosc. Radiat. Transfer*, **9**, pp. 31-47 (1969).

Liebe, H.J. and Dillon, T.A., Accurate Foreign-Gas-Broadening Parameters of the 22-GHz H20 Line from Refraction Spectroscopy, *J. Chem. Phys*., **50**(2), pp. 727-732 (1969).

Llewellyn-Jones, D.T., P.J. Minnett, R.W. Sanders, and A.M. Zavody, 1984: Satellite multi-channel infrared measurements of sea-surface temperature of the N.E. Atlantic Ocean using AVHRR/2. *Quart. J. Roy. Meteor. Soc*., **100**, 613-631.

McMillin, L. M., 1971: A Method of determining surface temperatures from measurements of spectral radiances at two wavelengths. Ph. D. dissertation, Iowa State Univ. Ames, IA, 1971.

McMillin, L.M. and H.E. Fleming, 1976: Atmospheric transmittance of an absorbing gas: a computationally fast and accurate transmittance model for absorbing gases with constant mixing ratios in inhomogeneous atmospheres. *Appl.Opt*., 15(2):358--363,

McMillin, L.M. and H.E. Fleming, 1977: Atmospheric transmittance of an absorbing gas. 2: A computationally fast and accurate transmittance model for slant paths at different zenith angles. *Appl.Opt*., 16(5):1366--1370.

McMillin, L.M., H.E. Fleming, and M.L. Hill, 1979: Atmospheric transmittance of an absorbing gas. 3: A computationally fast and accurate transmittance model for absorbing gases with variable mixing ratios. *Appl.Opt*., 18(10):1600--1606.

McMillin, L.M. , L.J. Crone, M.D. Goldberg, and T.J. Kleespies, 1995: Atmospheric transmittance of an absorbing gas 4. *Appl.Opt*., 34:6274.

McMillin, L.M., L.J. Crone, and T.J. Kleespies, 1995: Atmospheric transmittance of an absorbing gas 5. *Appl.Opt*., 34:8396.

McMillin, L. M. and Dean, C. A., 1982: Evaluation of a New Operational Technique for producing clear radiances. *J. Appl. Meteo.*, **21**, 1005-1014.

McMillin, L.M., L.J. Crone, and D.S. Crosby, 1989: Adjusting Satellite Radiances by Regression with an Orthogonal Transformation to a Prior Estimate, J. Appl. Meteor, 28, 969-975.

McMillin, L. M 1991: Evaluationi of a Classification Method for Retrieving Atmospheric Temperatures from Satellite Measurements. *J. Appl. Meteo.*, **30**, 432-446.

Oman, S.D., 1982: Shrinking Towards Subspaces in Multiple Regression, Technometrics, 24, 307-311.

Phillips, N., J. Susskind, and L. McMillin, 1988: Results of a joint NOAA/NASA sounder simulation study. *J. Atmos. Ocean. Tech.*, **5**, 44-56.

Poynter, R.L. and Pickett, H.M., Submillimeter, Millimeter, and Microwave Spectral Line Catalog, *Applied Optics*, **24**(14), pp. 2235-2240 (1985).

Preisendorfer, R.W., Principal Component Analysis in Meteorology and Oceanography, ed. Curtis D. Mobely, Elsevier, 1988.

Reuter, D., J. Susskind, and A. Pursch, 1988: First guess dependence of a physically based set of temperature-humidity retrievals from HIRS2/MSU data. *J. Atmos. Ocean. Tech.*, **5**, 70-83.

Rodgers, C. D., 1976: Retrieval of atmospheric temperature and composition from remote measurements of thermal radiation. *Rev. Geophys. and Space Phys.*, **14**, 609-624.

Rodgers, C. D., 1990: Characterization and error analysis of profiles retrieved from remote sounding measurements. *J. Geophys. Res.*, **95**, 5582-5595.

Rosenkranz, P.W., A Rapid Atmospheric Transmittance Algorithm for Microwave Sounding Channels, *IEEE Trans. on Geo. and Remote Sensing*, **33**(5) pp. 1135-1140 (1995).

Rosenkranz, P.W., Absorption of Microwaves by Atmospheric Gases, ch. 2 in Atmospheric Remote Sensing by Microwave Radiometry, (M.A. Janssen, ed.) New York: Wiley (1993).

Rothman, L.S., R.R. Gamache, R.H. Tipping, C.P. Rinsland, M.A.H. Smith, D.C Benner, V.Malathy Devi, J.M. Flaud, C.Camy-Peyret, A.Perrin, A.Goldman, S.T. Massie, L.R. Brown, and R.A. Toth The Hitran Molecular Database: Editions of 1991 and 1992,*J. Quant. Spectrosc. Radiat. Transfer*, **48**(5/6), pp. 469-507 (1992).

Rudman, S.D. R.W. Saunders, C.G. Kilsby, and P.J. Minnett, 1994: Water vapor continuum absorption in mid-latitudes: aircraft measurements and model comparisons. *Quart. J. Roy. Meteor. Soc.*, **120**, 795-807.

Schluessel, P., H.-Y. Shin, W.J.Emery, and H. Grassl, 1987: Comparison of satellite-derived sea-surface temperature with in-situ measurements. *J. Geophys. Res.*, **92**, 2859-2874.

Scott, N. A., and A. Chedin, A fast line by line method for atmospheric absorption computations: the Automatized Atmospheric Absorption Atlas, 4A, *J. Appl. Meteor.*, **20**, 801-812, 1981.

Smith, W. L., 1968: An improved method for calculating tropospheric temperature and moisture from satellite radiometer measurements. *Mon. Wea. Rev.*, **96**, 387-396.

Smith, W. L., and Woolf, H. M., 1976: The Use of Eigenvectors of Statistical Covariances Matrices for Interpreting Satellite Sounding Radiometer Observations. *J. Atmos. Sci*., **33** 1127-1140

Smith, W. L., and Platt, C.R.M., 1978:Comparison of satellite-deduced cloud heights with indications from radiosonde and ground-based laser measurements. *J. Appl. Met.*, **17**, 1796-1802.

Smith, W.L., Woolf, H.M., Hayden, C.M., Wark, D.Q., and McMillin, L.M.,1979: The TIROS-N Operational Vertical Sounder, Bull. Amer. Meteor.Soc. 60 1177.

Smith, W.L., R.O. Knuteson, H.E. Revercomb, F.A. Best, R. Dedecker, H.B. Howell, M. Woolf, 1995: Cirrus cloud properties derived from high sprectal resolution infrared spectrometry during FIRS II. Part I: The High Resolution Interferometric Sounder (HIS) systems. *J. Atmos. Sci*., **52**, 4238-4245.

Smith, W.L., H.E. Revercomb, R.O. Knuteson, W. Feltz, H.B. Howell, W.P. Menzel, N.R. Nalli, O. Brown, J. Brown, P. Minnett, W. McKeown,1996: Observations of the infrared radiative properties of the ocean -- implications for the measurement of sea surface temperature via satellite remote sensing. *Bull Amer. Meteor*. Soc, **77**, 41-51.

Staelin, D, H., Barrett, A.H., Rosenkranz, P.W., Barath, F.T., Johnston, E.J., Waters, J. W., Wouters, A., and Lenior, W.B., 1975a: The scanning microwave scpectrometer (SCAMS) experiment. PP 59-86 in *The Nimnus-6 Users Guide*. Goddard Space Flight Center, Greenbelt.

Staelin, D, H., Cassel, A. L., Kunzi, K. F., Pettyjohn, R. L., Poon, R. K. L. and Rosenkranz, P. W., 1975b: Microwave Atmospheric Temperature Sounding: Effects of Clouds on the Nimbus 5 Satellite Data. *J. Atmos. Sci*., **32** 1970-1976

Strong, A.E. and E.P. McLain, 1984: Improved ocean surface temperature from space -- Comparison with drifting buoys. *Bull Amer. Meteor. Soc*., **85**, 138-142.

Strow, LL, 1993: The measurement of global carbon monoxide using the Atmospheric InfraRed Sounder (AIRS). In A.Chedin, M.T. Chahine, and N.A. Scott, editors, *High Spectral Resolution Infrared Remote Sensing for Earth's Weather and ClimatE Studies*, pages 351--362. Berlin: Springer Verlag.

Strow,L.L., D.C. Tobin, and S.E. Hannon, 1994: A compilation of first-order line-mixing coefficients for CO_2 Q-branches. *Journal of Quantitative Spectroscopy and Radiative Transfer*, **52**:281.

Sundqvist, H., E. Berge and J.E. Kristjansson, 1989: "Condensation and cloud studies with a mesoscale numerical prediction model," *Mon. Wea. Rev.*, vol. 117, 1641-1657.

Susskind, J., J. Rosenfield, and D. Reuter, 1983: An accurate radiative transfer model for use in the direct physical inversion of HIRS and MSU temperature sounding data. *J. Geophys. Res.*, **88**, 8550-8568.

Susskind, J., J. Rosenfield, D. Reuter, M. T., Chahine, 1984: Remote sensing of weather and climate parameters from HIRS2/MSU on TIROS-N. *J. Geophys. Res.*, **89**, 4677-4697.

Susskind, J. and D. Reuter, 1985a: Retrieval of sea-surface temperatures from HIRS2/MSU. *J. Geophys. Res.*, **90C**, 11602-11608.

Susskind, J., D. Reuter, 1985b: Intercomparison of physical and statistical retrievals from simulated HIRS2 and AMTS data. In: Deepak A., Fleming H. E., Chahine, M. T. (eds) Advances in remote sensing retrieval methods. A Deepak, Hampton VA, 641-661.

Susskind, J., 1993: Water vapor and temperature. *Atlas of Satellite Observations Related to Global Change.* Edited by R. J. Gurney, J. L. Foster, and C. L. Parkinson. Cambridge University Press, Cambridge, England, pp. 89-128.

Susskind, J, J. Joiner and M. T. Chahine, 1993: Determination of temperature and moisture profiles in a cloudy atmosphere using AIRS/AMSU. NATO ASI Series, Vol. 19. High spectral resolution infrared remote sensing for earth's weather and climate studies. Springer Verlag Berlin Heidelberg. pp. 149-161. A. Chedin, M. T. Chahine, and N. A. Scott (Editors).

Susskind, J., J. Joiner, and C. D. Barnet, 1995: Determination of atmospheric and surface parameters from simulated AIRS/AMSU sounding data: Retrieval and Cloud Clearing Methodology. Submitted to *Advances in Space Research*.

Susskind, J., C. D. Barnet, and J. Blaisdell 1996: Determination of atmospheric and surface parameters from simulated AIRS/AMSU sounding data Part II: Cloud Clearing Methodology. Submitted to J. Atmos. Ocean. Tech.

Strong, A.E. and E.P. McClain, 1984: Improved ocean surface temperatures from space -- comparison with drifting buoys. *Bull. Amer. Meteor. Soc.*, **85**, 138-142.

Tobin, D.C., 1996a*: Infrared Spectral Lineshapes of Water Vapor and Carbon Dioxide*. PhD thesis University of Maryland Baltimore County.

Tobin, D. C., L. L. Strow, W. J. Lafferty, and W. B. Olson, Experimental investigation of the self- and N_2-broadened continuum within the ν_2 band or water vapor, *Applied Optics*, **35**, 4724-4734, 1996b.

Twomey, S., 1963: On the numerical solution of the Fredholm integral equations of the first kind by inversion of the linear system produced by quadrature. *J. Assoc. Comp. Mach.*, **10**, 79-101.

Uddstrom, M.J. and L.M. McMillin, 1994a: System noise in the NESDIS TOVS forward model. part I: specification. *J. Appl. Meteor.* **33**, 919-938.

Uddstrom, M.J. and L.M. McMillin, 1994b: System noise in the NESDIS TOVS forward model. part II: consequences. *J. Appl. Meteor.* **33**, 939-947.

Wan, Zhengming and J. Dozier, 1996: a generalized split-window algorithm for retrieving land surface temperature from space. *IEEE Trans. On Geosci. And Rem. Sens*., **34**, 892-905.

Wark, D.Q. and H.E. Fleming, 1966: Indirect measurements of atmospheric temperature profiles from satellites: I. Introduction, *Monthly Weather Review*, **94**.

Wark, D.Q. and Hillery, D.T, 1969: Atmospheric temperature: A sucessful test of remote probing, *Science*, **165**, 1256-1258.

Wilheit, T.T., 1990: "An algorithm for retrieving water vapor profiles in clear and cloudy atmospheres from 183 GHz radiometric measurements: Simulation studies," *J. App. Meteor.*, vol. 29, 508-515.

Wolfe, W. L., 1965: *Handbook of Military Infra-red Technology*, U. S. Goverment Printing Office, Washington, D. C.